STRUCTURAL RELIABILITY OF BRIDGES ELEVATED WITH STEEL PEDESTALS

A Dissertation

by

VAHID BISADI

Submitted to the Office of Graduate Studies of
Texas A&M University
in partial fulfillment of the requirements for the degree of

DOCTOR OF PHILOSOPHY

Approved by:

Co-Chairs of Committee,	Monique Head
	Luca Quadrifoglio
Committee Members,	Paolo Gardoni
	Daren B.H. Cline
Head of Department,	John Niedzwecki

December 2012

Major Subject: Civil Engineering

ABSTRACT

Overheight vehicle impact to bridge decks is a major problem in the transportation networks in the United States. An important factor that causes this problem is inadequate vertical clearance of bridges. Using steel pedestals to elevate bridge decks is an efficient and cost-effective solution for this problem. So far, steel pedestals have been used in the low seismic regions of the United States and therefore, their design has been based on providing enough strength to carry vertical loads and the lateral behavior of bridges elevated with pedestals have not been a major concern. But even in low seismic zones the seismic hazard should not be completely ignored. Also there might be some bridges in medium or high seismic regions that need to be elevated because of the lack of enough vertical clearance and using steel pedestals can be considered as an option for elevating those bridges. To address the mentioned needs, this dissertation proposes a framework to determine the structural reliability of bridges elevated with steel pedestals by developing probabilistic capacity and demand models for the slab-on-girder bridges subjected to lateral loads.

This study first compares the behavior of previously tested pedestals with the behavior of elastomeric bearings in low seismic regions using statistical tests. Then, to provide a general framework, which can be applied to all bridges that are elevated with steel pedestals, this dissertation develops probabilistic capacity and demand models for steel pedestals considering all the aleatory and epistemic uncertainties of the problem. Using the developed probabilistic models along with the available models for other

components of bridges, seismic fragility curves for elevated bridges are obtained and used to determine the structural reliability. Finally, this study uses the developed framework in a decision analysis that helps the engineering community and decision makers to check if the installation of steel pedestals on a specific bridge has financial justification or not. Results show that for a typical two-span slab-on-girder bridge, the use of steel pedestals has financial justification only in low seismic regions and if the societal benefits of elevating the bridge can at least cover the installation cost of pedestals.

DEDICATION

To my wife, my parents and my brother

ACKNOWLEDGEMENTS

I would like to thank Dr. Head and Dr. Gardoni for their help and support. Dr. Head has always been supportive and helpful. She has ensured that I have had good opportunities and experiences to make a solid foundation for my future. Dr. Gardoni has definitely played an important role to improve the quality of my dissertation by providing innovative suggestions and making sure that I'm on the right track during working on my dissertation. I really appreciate all the time that he spent to clarify the concepts of reliability and probabilistic modeling for me. I would also like to thank Dr. Cline. and Dr. Quadrifoglio, for their guidance and support, Dr. Roesset who was in my committee before his retirement and gave me valuable advice about analytical modeling and also my TA mentor, Dr. Jones.

My great and heartfelt thanks go to my wife, Maryam Mardfekri, who has also been my office mate during my PhD studies and always helped me and gave me great suggestions about my research. Also, she has always supported me emotionally and made my life happy. To her, I not only give my thanks but also my love.

Thanks also go to my fellow graduate student, Armin Tabandeh, who has helped me through technical discussions about statistical methods and nonlinear time history analyses.

I want to thank my friends and the faculty and staff of Zachry Department of Civil Engineering for making my time at Texas A&M University a great experience. I

would also like to extend my gratitude to all my friends in Persian Student Association (PSA).

I would like to express my deepest gratitude to my parents and my brother. I acknowledge all the support and encouragement I received from them during my life. My parents have always worked hard to provide a pleasant and happy life for me. My deep appreciation and love is extended to them.

Last but not least, I thank God for whom all this was made possible.

TABLE OF CONTENTS

Page

LIST OF FIGURES

LIST OF TABLES

1. INTRODUCTION

1.1 Background

An important problem within the U.S. transportation network is overheight vehicle collision with bridge decks. According to a survey by Fu et al. (2004) among 29 states, 18 states declared that they consider overheight vehicle collision as a problem in their transportation network. Several cases of overheight vehicle collisions in the United States have been reported (Hartick et al. 1990; Feldman et al. 1998; Fu et al. 2004; Wardhana and Hadipriono 2003), where inadequate vertical clearance of bridges has been identified (Hilton 1973; Hadipriono 1985). There are four types of methods to solve this problem: routing procedures, warning systems, clearance augmentation, and impact absorbers (Sharma et al. 2008). Using steel pedestals to elevate the decks of simply-supported bridges is an efficient and cost-effective clearance augmentation method (Hite et al. 2008). Steel pedestals are short columns that increase the vertical clearance height of bridges. Due to a lack of understanding of the performance of steel pedestals when subject to combined axial and lateral loads, so far, steel pedestals have been used in limited areas of the United States of low seismicity and their design has been based on providing enough strength to carry primarily vertical dead and live loads. Therefore, there is a need to 1) assess the structural reliability of bridges elevated with steel pedestals and subjected to lateral loads and 2) determine whether the addition of steel pedestals is detrimental or beneficial depending on the specifics of the bridge.

Using steel pedestals to elevate bridges is a relatively new approach. Therefore there are very few studies about the structural behavior of steel pedestals and their effect on the lateral response of the elevated bridges. Hite et al. (2008) conducted quasi-static tests on six steel pedestals and presented the hysteretic force-displacement relationships of the tested pedestals. However, the results of the conducted experiments cannot be extended to steel pedestals with other dimensions nor different loading conditions. Therefore, a general framework is required for the fragility estimation of bridges elevated with steel pedestals. Developing fragility estimates for bridges elevated with steel pedestals requires the development of probabilistic capacity and demand models that can capture uncertainties in the material and geometrical properties and lateral loads, which is explored in this dissertation.

As such, this study presents the development of probabilistic models for seismic capacity and demands on simply-supported slab-on-steel-girder bridges elevated with steel pedestals. The proposed models along with the available probabilistic capacity models for the bridge components (such as Choe et al. 2007) can be used in a system reliability analysis to estimate the fragility of bridges elevated with steel pedestals. Following Gadoni et al. (2002, 2003), the probabilistic models are developed starting from common deterministic models and adding correction terms to compensate for the inexactness/bias in the deterministic models. The correction terms are calibrated using experimental data for capacity models and demand data generated from nonlinear time history analyses (NTHAs) of detailed three-dimensional (3D) finite element models for demand models. In order to maximize the information content of the finite number of

NTHAs for developing demand models, an experimental design is used to generate the geometrical and mechanical properties used in the finite element models. Unknown model parameters in the proposed probabilistic demand models are estimated using a Bayesian updating method.

1.2 Research Objectives

The goal of this research is to develop a probabilistic framework for the assessment of the structural reliability of steel pedestals. The anticipated results consist of estimating the ultimate load carrying capacity of steel pedestals considering all failure modes associated with the post-installed unheaded anchor bolts of steel pedestals, assessing the demands on the steel pedestals subject to earthquake load, assessing the structural reliability of the steel pedestals via probabilistic capacity and demand models, and computing the life-cycle costs that aid the decision-making process for elevating bridges. From the framework, the lateral capacity and demand on the steel pedestals will be evaluated and the structural reliability of steel pedestals will be assessed. Probabilistic capacity models for steel pedestals will be based on the capacity of steel pedestal components such as base plate, anchor bolts and base concrete. The capacity models along with demand models will be developed such that engineers can use them easily without running detailed nonlinear time history analyses. Based on the developed capacity and demand models, the structural reliability of steel pedestals will be assessed. To justify the use of steel pedestals, a decision analysis will be conducted for steel

pedestals. The following five specific objectives are considered to develop a framework for reliability assessment and decision analysis for bridges elevated with steel pedestals:

- *Objective 1*: To investigate the seismic effects of elevating bridges with steel pedestals
- *Objective 2*: To develop probabilistic capacity models for steel pedestals used to elevate bridges
- *Objective 3*: To develop probabilistic demand models for bridges elevated with steel pedestals
- *Objective 4*: To assess the structural reliability of steel pedestals
- *Objective 5*: To provide a decision analysis tool to aid the decision–making process for determining elevation of bridges with steel pedestals

Figure 1-1 shows an overview of the research plan in this dissertation. The header of each box in Figure 1-1 shows an objective and the required steps to achieve the objective are provided below the corresponding header.

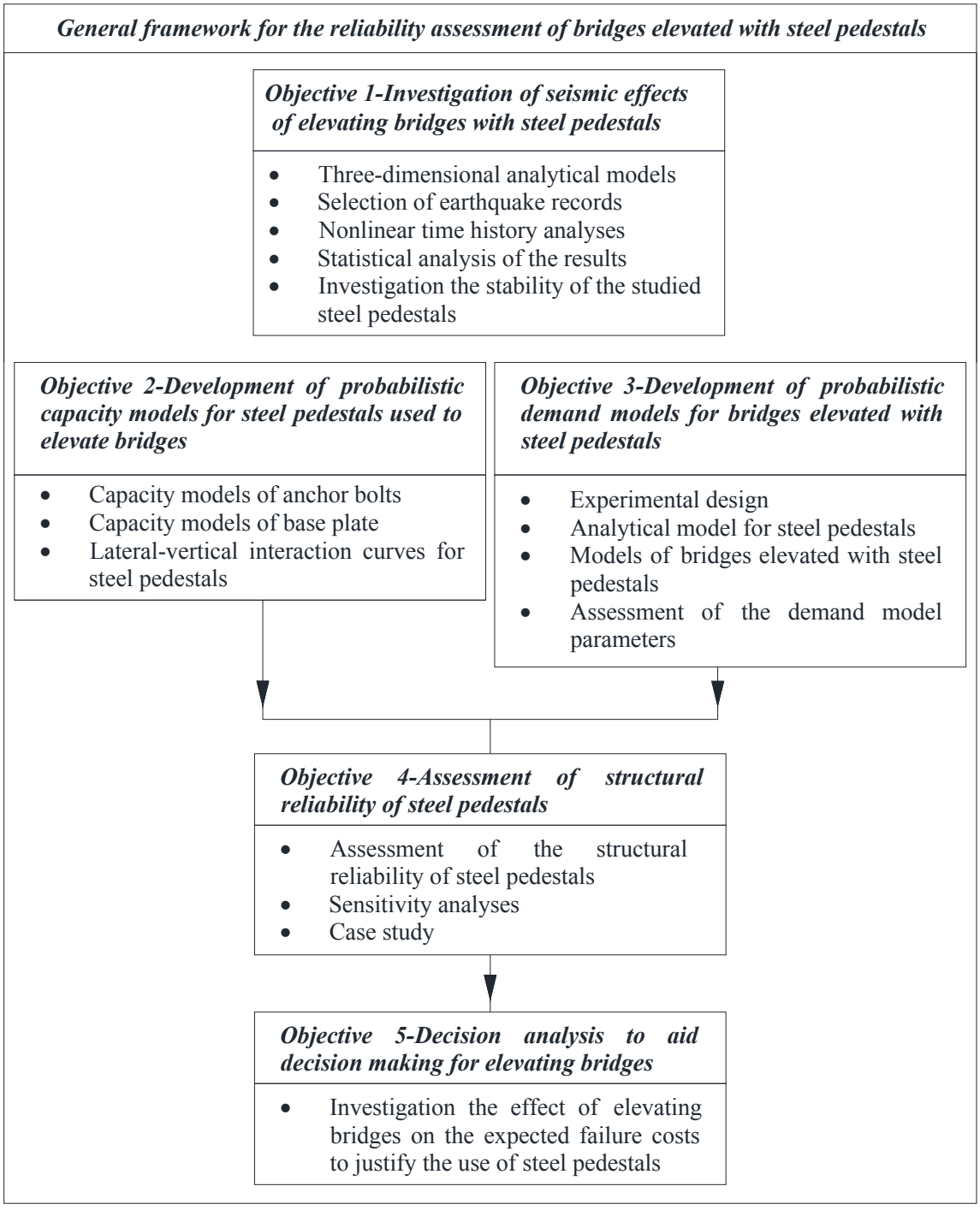

Figure 1-1. Overview of the research plan in this dissertation

1.3 Organization of Dissertation

This dissertation is organized using a section-subsection format. The following five sections discuss the details of research and methods used to achieve the five specific objectives mentioned in the previous subsection. Each section explains an objective and the required steps and conducted research to achieve that objective. The results of these five sections provide a general framework to assess the structural reliability of bridges elevated with steel pedestals. The last section provides conclusions of this research and proposes some recommendations for the future work. Following is a brief overview of each section in this dissertation.

- Section 1 (current section) provides an introduction about the problem, including background, research objectives and organization of dissertation.
- Section 2 investigates the seismic effects of elevating bridges with steel pedestals in the Southeastern United States, where steel pedestals have been used in the past to elevate bridges. In Section 2, the responses of a typical bridge elevated with previously tested steel pedestals are compared to the responses of the same bridge with elastomeric bearings, which are common types of bridge bearings. The results of this section are only valid for the tested pedestals and for the Southeastern United States. More comprehensive models are presented in Sections 3 through 5. Research conducted in Section 2 has been published in the *Engineering Structures*, 33(12) with the title of "Seismic effects of elevating bridges with steel pedestals in the southeastern United States."

- In section 3, probabilistic capacity models are developed for steel pedestals used to elevate bridges. All the failure modes of base plate and anchor bolts including tensile and shear modes of failure and their interaction are considered in developing capacity models. Error terms are added to the available deterministic models and their mean and standard deviation are estimated by comparing the outputs of the deterministic models with experimental data. This work has been published in the *Journal of Structural Engineering ASCE*, 137(12) with the title of "Probabilistic capacity models and fragility estimates for steel pedestals used to elevate bridges."
- In section 4, probabilistic demand models are developed for bridges elevated with steel pedestals by adding correction and error terms to deterministic models. Correction terms are selected from candidate explanatory functions that are thought to be influential on the responses. Virtual data are used as the required data to develop probabilistic models and an experimental design is employed to maximize the information content of the virtual data. Model parameters are estimated using Bayesian updating method. Fragility of a typical two-span bridge using developed demand models in this section and capacity models in section 3 is estimated. This work has been summarized in a journal paper entitled "Probabilistic seismic demand models and fragility estimates for bridges elevated with steel pedestals" and submitted to *Journal of Structural Engineering ASCE*.
- Section 5 provides a decision analysis framework for elevating bridges using steel pedestals. The probability of failure of bridges is computed due to vehicular impact and earthquake loads as function of the pedestal height in different regions of the

United States. The optimum height of pedestals is then defined as the height that minimizes the probability of failure. Comparison between the expected costs of failure before and after bridge elevation shows that if the elevation of a bridge in a specific region has financial justification or not. This work has been summarized in a journal paper entitled "Decision analysis for elevating bridge decks with steel pedestals" and submitted to *Structure and Infrastructure Engineering*.

- The conclusion of this dissertation is provided in Section 6 along with the unique contributions from this work as well as some suggestions for the future work.

2. SEISMIC EFFECTS OF ELEVATING BRIDGES WITH STEEL PEDESTALS*

2.1 Introduction

While steel pedestals have been used recently in the southeastern United States to increase the vertical clearance of bridges, their effects on the seismic responses of bridges in that region are still unknown. Steel pedestals resemble short columns that are used as a cost-effective means to elevate bridges in order to decrease the likelihood of overheight vehicle collisions to bridges. Figure 2-1 shows a bridge in Georgia elevated with steel pedestals.

Figure 2-1. A bridge in Georgia elevated with steel pedestals

However, the mechanism of transferring inertial loads in steel pedestals is similar to steel rocker bearings, which have revealed poor performance during earthquakes

* Reprinted with permission from "Seismic effects of elevating bridges with steel pedestals in the southeastern United States." by Vahid Bisadi, Monique Head and Daren B.H. Cline, 2011, *Engineering Structures*, 33(12), 3279-3289, Copyright 2011 by Elsevier Ltd.

(Douglas 1979; Mander et al. 1996; DesRoches et al. 2000, 2003; Buckle et al. 2006), thereby raising concerns as to the seismic performance of steel pedestals given their height and connectivity to bent caps via post-installed unheaded, unhooked anchor bolts that are embedded into drilled holes filled with grout. Therefore, there is a need to investigate the effects of adding steel pedestals to existing bridges, which changes the lateral stiffness, on the structural responses of the bridge during earthquakes since no analytical study is available to date. Hite et al. (2008) conducted six quasistatic reversed cyclic experimental tests on bridge steel pedestals to obtain the hysteretic behavior that is used in the analytical model developed herein.

This section investigates the elevated bridge responses during earthquakes to find the effects of the replacement of elastomeric bearings with steel pedestals. To evaluate the seismic response of bridges elevated with steel pedestals, an analytical study is conducted that uses a finite element (FE) model developed in Open System for Earthquake Engineering Simulation (OpenSees). The nonlinear response of bridges via nonlinear time-history analyses is investigated. The load–displacement relationships from experimental tests (Hite et al. 2008) are used to define the pedestal stiffness and hysteretic behavior in the FE model. This study considers a typical multi-span, slab-on-girder bridge as a representative of the southeastern United States bridges and compares the responses of the studied bridge in four cases. In one case elastomeric bearings that are the commonly used bridge bearings are used in the model. The bridge responses in this case are considered as the bridge responses before the elevation. In the other cases, three types of previously tested steel pedestals by Hite et al. (2008), are used as bridge

bearings in the model and bridge responses are compared to the first case. Also, the bridge responses with different steel pedestals are compared to each other. This study uses 100 artificially generated earthquakes for five different locations in the southeastern region of the United States since the occurrence of earthquakes is still probable even in low seismic regions like the southeastern United States. For example, based on AASHTO (2010) seismic hazard maps, the horizontal peak ground acceleration of an earthquake with a return period of 1000 years in different parts of Georgia is between 0.03g and 0.12g, Alabama is between 0.03g and 0.1g, and South Carolina is between 0.09g and 0.5g.

A statistical effects model is considered for the resulting data from nonlinear time-history analyses given the massive output produced from the computation of 800 total cases run. The comparison between the bridge responses is conducted using Tukey's Honest Significant Difference (HSD) test to show any statistically significant differences in bridge responses, which help identify cases where the addition of steel pedestals may not be favorable. Tukey's test is a statistical test that is used for the comparison between two groups, for example between the responses of a bridge with elastomeric bearings and the responses of the same bridge with steel pedestals subject to a set of ground motions. Information about Tukey's HSD test is available in multiple comparison textbooks such as Hsu (1996).

In this section, the geometrical and mechanical properties of the studied steel pedestals are presented and then the details of the FE model and modeling assumptions are discussed. After that, the generation of artificial earthquake records is briefly

discussed. Then the fitted statistical model on the data is presented and based on that the seismic performances of the bridge after elevation with the studied steel pedestals are compared to its performance before elevation (with elastomeric bearings) using statistical significant difference tests. Finally, demand forces on steel pedestals are compared to their capacity considering their strength and stability criteria.

2.2 Properties of the Studied Steel Pedestals

The performances of three types of steel pedestals are investigated: one short and two tall steel pedestals that have been used to elevate bridges (Hite et al. 2008). These pedestals are shown in Figure 2-2. The short steel pedestals have a height of 500 mm and W200 × 46.1 steel profile. It will be denoted by ‘‘S’’ in this dissertation. The tall steel pedestals have a height of 850mmand built-up steel profiles (with an area of 9800 mm^2), and will be denoted by ‘‘T1’’ and ‘‘T2’’ as illustrated in Figure 2-2. The direction of steel pedestals is considered in a manner that the web of the steel profile of the pedestal is parallel to the longitudinal axis of the bridge. This is the direction of installation that usually is selected in practice as shown in Figure 2-1. These steel pedestals are anchored to the cap beams or abutments with 32 mm stainless steel stud anchor bolts having a minimum yield strength of 210 MPa. The mechanism of transferring loads from steel pedestals to the stud anchor bolts in S and T1 pedestals are through A36 L-shaped (L100 × 100 × 12 mm) angles that are welded to the base plate of the pedestals as shown in Figure 2-3. T2 pedestals do not have angles attached to their base plate, but rather the load is transferred by the anchor bolts themselves, which are within the base plate as

shown in Figure 2-2. The other properties of this type are similar to those of T1. Detailed information about the properties of each type of studied pedestals in this dissertation and their response to quasi-static lateral forces is available in Hite et al. (2008).

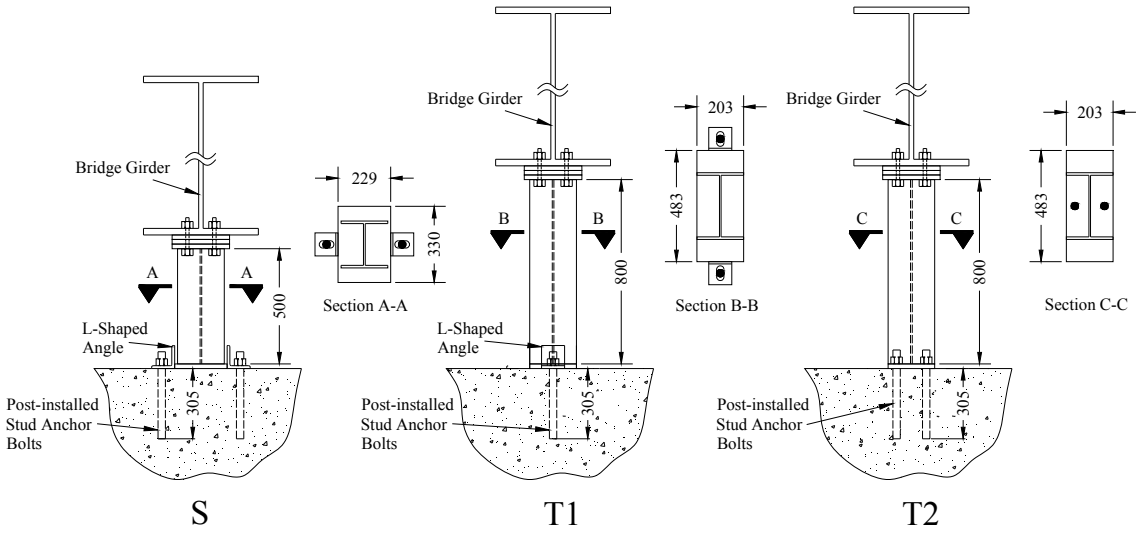

Figure 2-2. Three types of steel pedestals studied in section 2

Figure 2-3. L-shaped angles welded to the short pedestal (S) base plate (anchor bolt nut not shown)

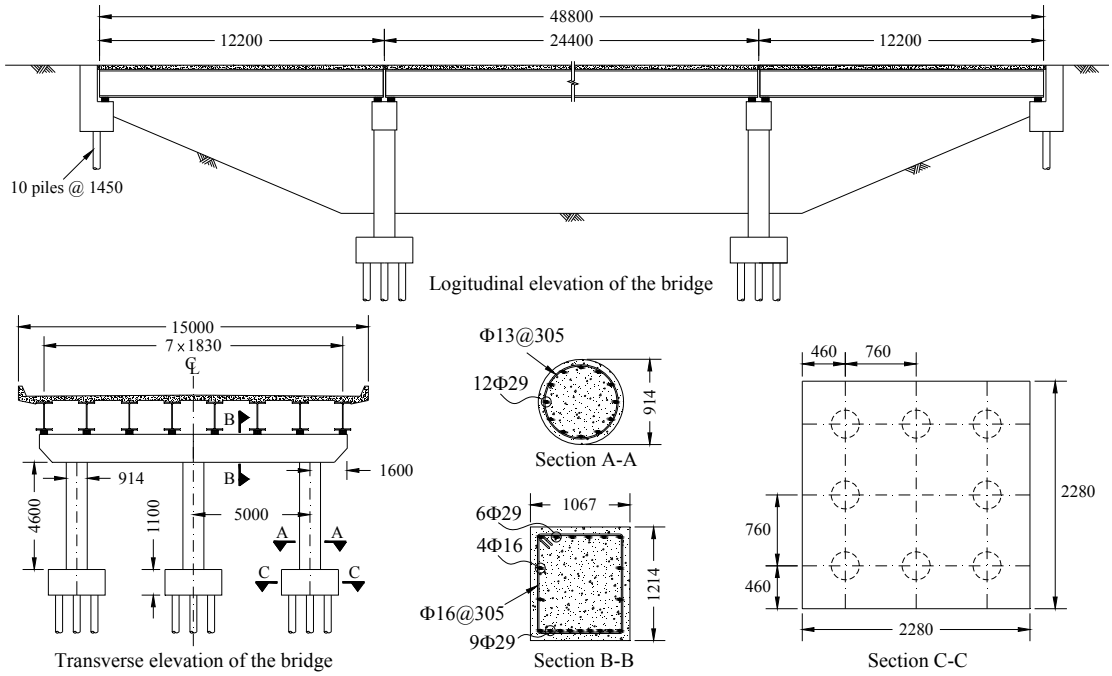

Figure 2-4. Geometric properties of the considered typical three-span bridge in the southeastern United States

2.3 Three-Dimensional Analytical Modeling

2.3.1 Description of the Representative Bridge

Steel pedestals can be used to elevate bridges with various geometries. For the evaluation of the seismic performance of steel pedestals in the southeastern region of the United States, a bridge geometry is needed that can be considered as being representative of bridges in this region. This study uses an unskewed three span slab-on-girder bridge shown in Figure 2-4 for this purpose. Based on a statistical analysis on the bridges in the central and southeastern parts of the United States by Nielson and DesRoches (2006), this bridge can be considered as a representative of bridges in those regions. The end spans of the bridge have length 12.2 m and the middle span has length 24.4 m. The width of the bridge is 15 m and the deck consists of a 180mm concrete slab

placed over eight steel girders. The bridge has two bents, where each of them consists of a rectangular cap beam and three circular columns with 1% longitudinal reinforcement. There are 10 piles under each abutment and 8 piles under each column bent.

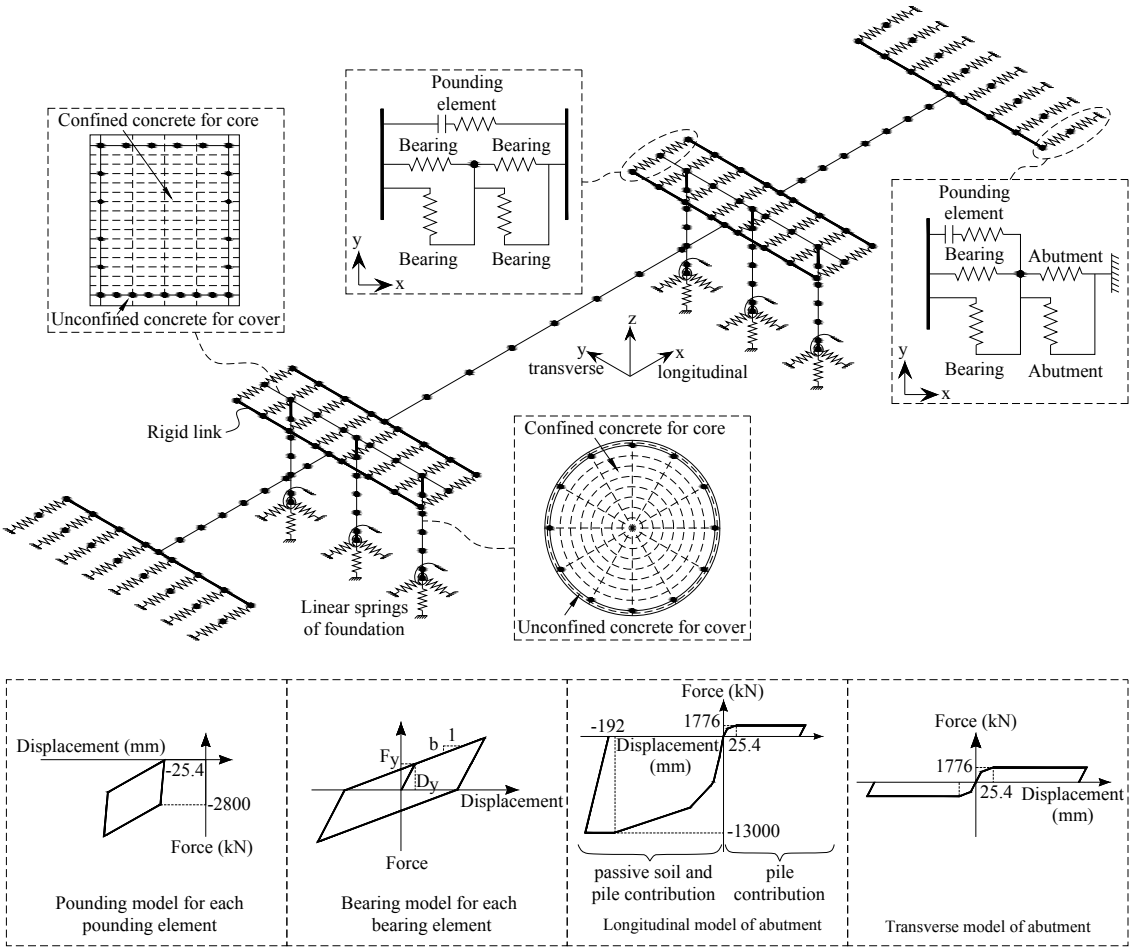

Figure 2-5. Three-dimensional nonlinear model of the studied bridge modeled in OpenSees

2.3.2 Modeling of Bridge Components

Figure 2-5 illustrates the three-dimensional model of the bridge created in OpenSees. In this model, decks are modeled using equivalent linear beam–column elements and their masses are concentrated at the nodes along the decks. Rigid links are added to the ends of equivalent deck beams to properly connect them to the bent cap beam nodes through bearing springs and also to account for in-plane rotation of the deck. Bent cap beams and columns are modeled using displacement beam–column elements with fiber sections. Unconfined concrete properties are assigned to the fibers in the cover area and confined concrete in the core area of the section. Following Mander et al. (1988), a confinement effectiveness coefficient is obtained equal to 1.07 and 1.15 for columns and bent cap beams of the studied bridge, respectively. A contact element proposed by Muthukumar (2003) that considers the hysteretic energy loss is used to model pounding between decks and between abutments and decks. This contact element is composed of a gap element representing the expansion joint and a bilinear spring to capture the energy dissipation and other effects during the impact. Considering a contact element to model pounding is essential in nonlinear analyses of bridges because it directly affects the forces transferred from superstructure to substructure.

This study uses six linear springs in six degrees of freedom to model bent foundations, a trilinear model implemented by Choi (2002) to model the lateral behavior of piles at abutments and a quadrilinear model developed by Nielson (2005) to model the behavior of passive soil. The initial lateral stiffness of piles is considered equal to 7 kN/mm/pile (Caltrans 2006) and their vertical stiffness is assumed to be 175 kN/mm/pile

(Choi 2002). These models are shown in Figure 2-5. In the models of abutments, passive soil and piles are considered in the longitudinal direction and only piles in the transverse direction. The stiffness of the wing walls is conservatively neglected in the model.

2.3.3 Modeling of Bearings

Two types of bearings (i.e., elastomeric bearings for the bridge before elevation and steel pedestals for the bridge after elevation) are studied in this study and their performances are compared.

2.3.3.1 Modeling of Elastomeric Bearings

Following Kelly (1998) and Naeim and Kelly (1999), bilinear models as shown in Figure 2-5 represent elastomeric bearings in this study. In this figure F_y, D_y and b are yield strength, yield displacement and strain hardening ratio of the bearing, respectively. Table 2-1 shows the considered values of these parameters at the middle and center spans. Dimensions of elastomeric bearings are obtained based on the AASHTO LRFD Bridge Design Specifications (2010) and their stiffnesses are computed given the designed dimensions.

Table 2-1. Properties of elastomeric bearings considered in the models

Elastomeric bearings (E)	Dimensions (mm)	D_y (mm) †	F_y (kN) †	b †
End span	300×200×100	10	10.5	0.33
Center span	450×300×150	15	23.7	0.33

† D_y, F_y and b are yield displacement, yield strength and strain hardening ratio of the bearing.

2.3.3.2 Modeling of Steel Pedestals

The nonlinear force–displacement relationship of steel pedestals depends on many factors such as the geometry of the pedestal and details of its connection to the base and to the bridge girder. This study uses a bilinear hysteretic model (as shown in Figure 2-5 for bearings) based on the experimental results of the quasistatic tests conducted by Hite et al. (2008). To this end, the hysteretic models used to represent steel pedestals loosely encompass the point at which the anchorage to concrete is expected to degrade. This is important to note since failure in the anchorage or its surrounding concrete is not part of the study in this section and the anchorage to concrete is not explicitly modeled. Possible modes of failure such as anchor failure in steel pedestals will be studied in the next section. This section focuses on the overall seismic performance of steel pedestals based on the force–displacement relationships obtained from experimental tests. A sample of bilinear models that are fitted to experimental results of T2 pedestals in the transverse direction is shown in Figure 2-6. Similar bilinear models are used for the other pedestal types. The values of yield strength, yield displacement and strain hardening ratio of the three types of steel pedestals are shown in Table 2-2.

Table 2-2. Properties of steel pedestals considered in the models

Steel pedestal type	Direction	D_y (mm) †	F_y (kN) †	b †
Short (S)	Longitudinal	5.20	26.0	0.16
	Transverse	6.20	31.0	0.16
Tall (T1)	Longitudinal	2.35	18.0	0.3
	Transverse	6.55	32.7	0.36
Tall (T2)	Longitudinal	1.65	19.8	0.15
	Transverse	9.90	49.5	0.36

† D_y, F_y and b are yield displacement, yield strength and strain hardening ratio of the bearing.

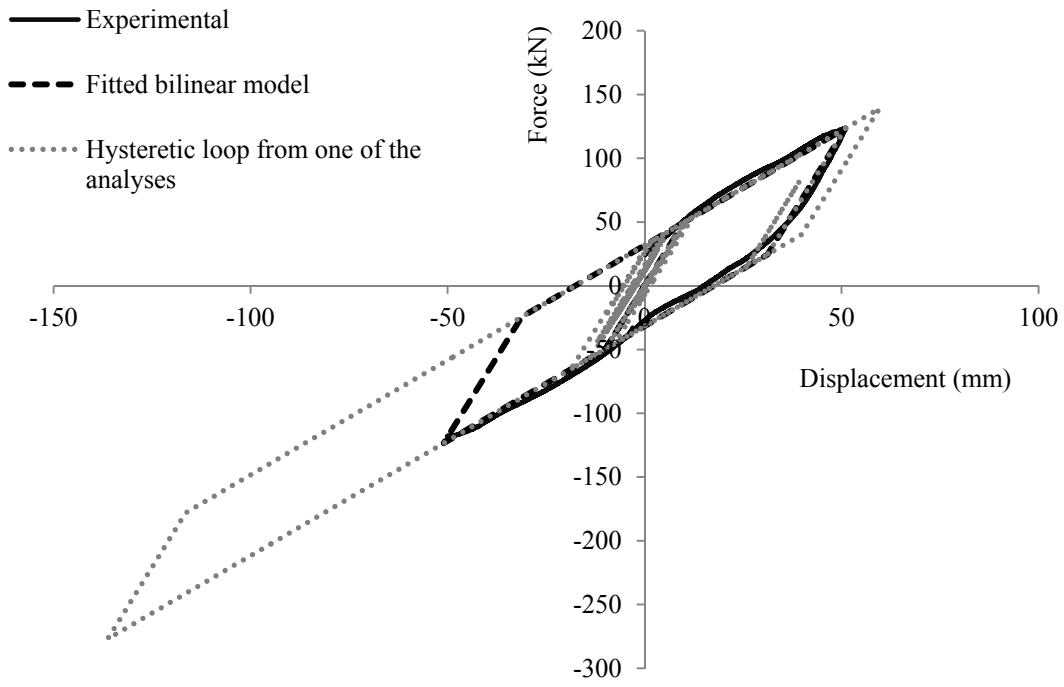

Figure 2-6. Analytical and experimental force–displacement relationship for the T2 steel pedestals in transverse direction

2.4 Nonlinear Time History Analyses

Nonlinear time-history analyses in the OpenSees finite element package are used to determine various responses of the studied bridge, namely the maxima of deck displacement, abutment force, column shear and moment in both longitudinal and transverse directions, cap beam shear and moment, and pounding force. Ground motion records are applied to the model and the analyses are repeated for each type of bearing.

The artificial ground motions were generated by Fernandez (2007) for five different locations of the southeastern United States. The locations are Bartow, Liberty and Lowndes counties in Georgia, Fort Payne, Alabama and Charleston, South Carolina.

Two hazard levels of 2% and 10% probability of exceedance in 50 years (corresponding to the return period of 475 and 2475, respectively) are selected for the analyses. Fernandez (2007) simulated 1000 response spectra for each hazard level in each location and then selected 10 at random to obtain time histories. Figure 2-7 shows the mean curve of the 10 selected response spectra and Table 2-3 shows the maximum and minimum PGA of the selected ground motions for each location. Figure 2-8 shows samples of artificial time history records used in this study.

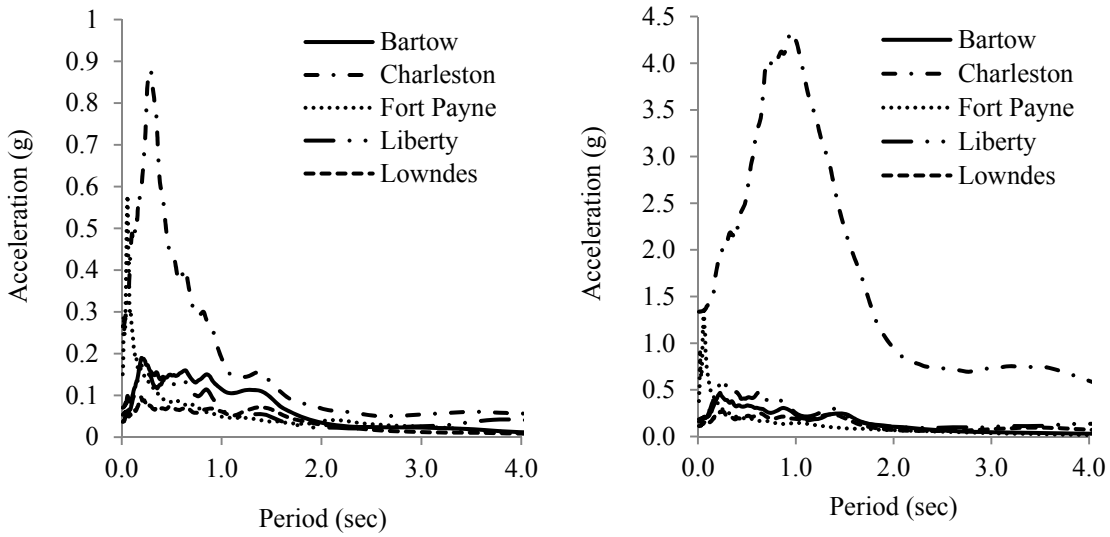

Figure 2-7. Mean response spectra of ground motions used in the nonlinear time-history analyses: (a) earthquakes with return period of 475 years; and (b) earthquakes with return period of 2475 years

Table 2-3. Maximum and minimum values of the PGA of applied ground motions

Location	Return Period of 475 years		Return Period of 2475 years	
	min. PGA	max. PGA	min. PGA	max. PGA
Bartow	0.052g	0.099g	0.094g	0.233g
Liberty	0.016g	0.078g	0.059g	0.280g
Lowndes	0.012g	0.053g	0.046g	0.204g
Fort Payne	0.082g	0.178g	0.147g	0.670g
Charleston	0.165g	0.430g	1.010g	1.730g

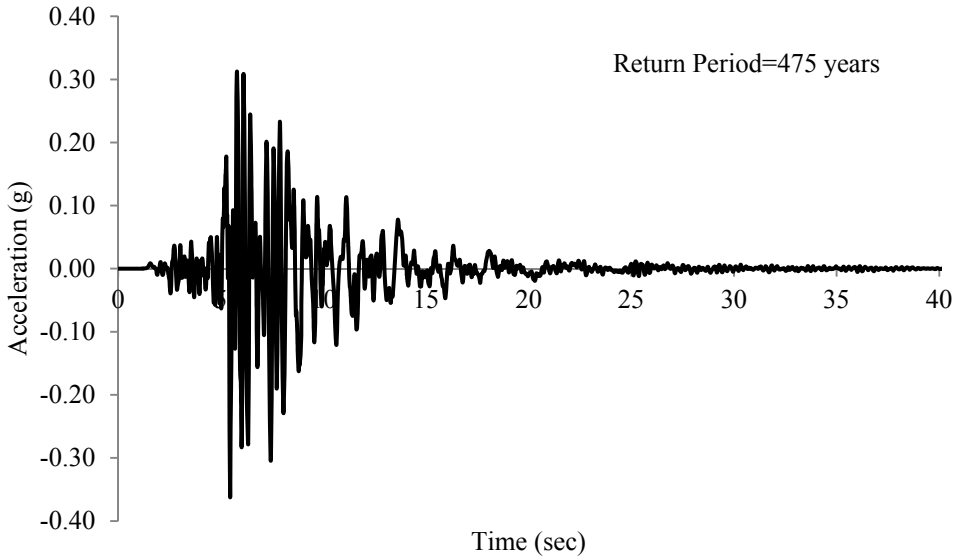

(a)

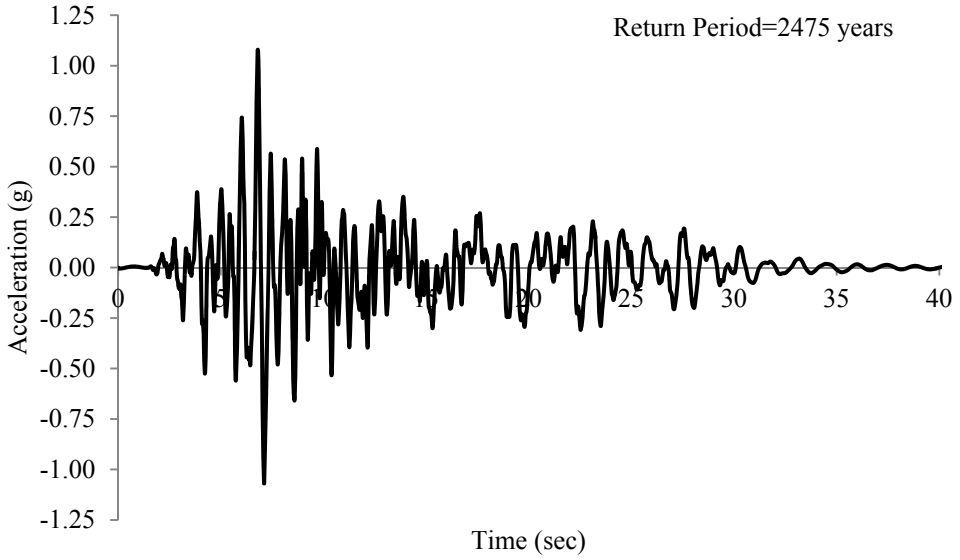

(b)

Figure 2-8. Samples of artificial time-history records used in this study: (a) return period of 475 years for Charleston; and (b) return period of 2475 years for Charleston

Table 2-4. Effects considered in the statistical model and their levels

Effect	Type of effect	Levels
Bearing type	fixed	Elastomeric Bearing (E), Short Pedestal (S), Tall Pedestal (T1), Tall Pedestal (T2)
Location	fixed	Bartow, Liberty, Lowndes, Fort Payne, Charleston
Earthquake return period	fixed	475 Years, 2475 Years
Simulation	random	1,..,10

2.5 Statistical Analysis of the Results

2.5.1 Effects Model

This section of the dissertation considers four types of bearings, five locations, two return periods of earthquakes, two directions of applying ground motions on the studied bridge (longitudinal and transverse directions) and 10 simulations with different artificial earthquake records for each combination of bearing types, locations, return period and direction of earthquake. Therefore the total number of simulations is 800. Regarding the large amount of data in this study, it is imperative to conduct a statistical analysis of the results to compare the performance of elastomeric bearings to steel pedestals and the performance of different types of studied steel pedestals. For this purpose, a statistical "effects model" in JMP software (SAS Jmp) is used separately for each response variable of the bridge. General information about effects models can be found in statistical textbooks such as Montgomery and Runger (2006). Bearing type, location, and earthquake return period are considered to be fixed effects in the model along with their possible interactions. Because the ground motion records have been selected at random from a suite of earthquake records for each location and hazard level, a random effect

(called simulation) is added to the model in which location and hazard level are nested. Table 2-4 shows the effects included in the model and the levels of each effect and Figure 2-9 shows an overview of the statistical model used in this study. As Figure 2-9 shows, location and return period are the nested in earthquake record effect, which is considered a random effect in this study. Location has five and return period has two levels. Bearing type is another effect in the model that has four levels and it is considered as fixed model in the effects model.

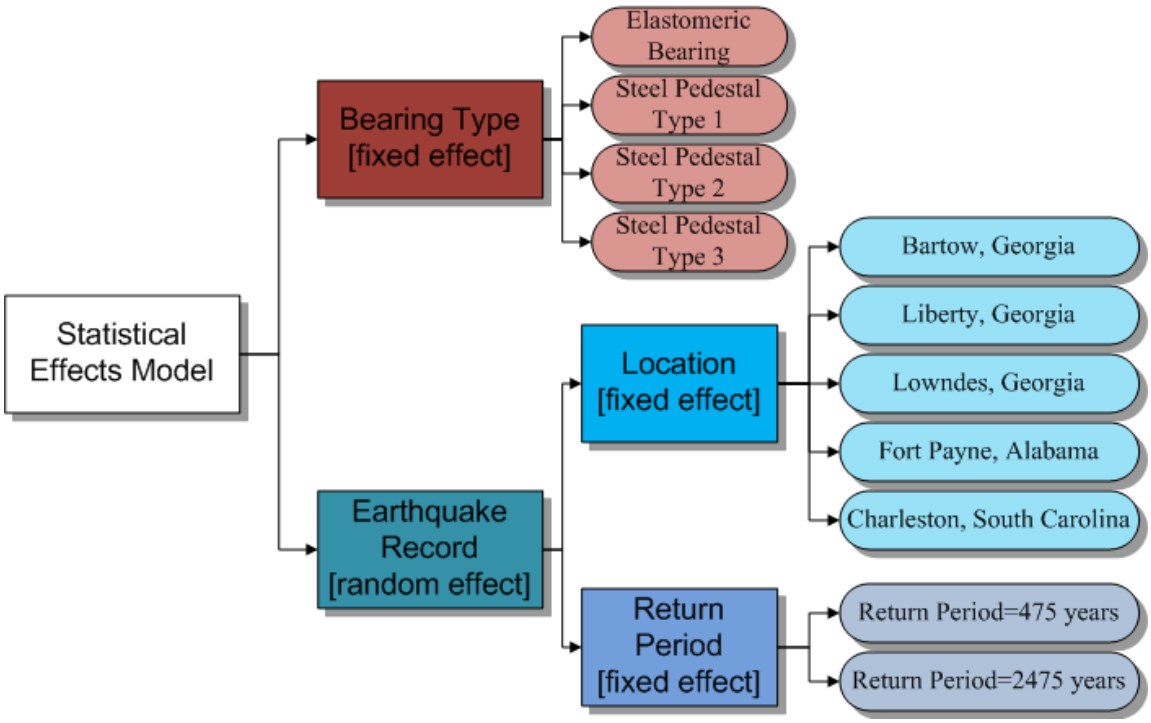

Figure 2-9. An overview of the statistical effects model used in this study

2.5.2 Comparing Least Squares Means by Tukey's HSD Test

Figure 2-10 shows the least squares means of variables computed based on the statistical models. The least squares means are estimates of the average response among all possible simulations and across the locations and return periods in the experiment. Figure 2-10 provides a visual aid to compare the results. For example, Figure 2-10 shows that the mean of longitudinal deck displacement of the studied bridge with the considered short pedestal is more than the mean of the deck displacement with the considered tall steel pedestals. Since there are limited data points, it has to be confirmed that the difference between the responses is significant enough before jumping to conclusions about the observations. Therefore, a statistical test is needed to check if the difference between the same response of the studied bridge with different bearings is significant or not. Statistical tests provide procedures to draw conclusions based on the statistics of the data rather than just compare the values in Figure 2-10. To compare the means of responses based on available data, Tukey's HSD Test with level of significance, α_s, equal to 0.05 is used in this research. Tukey's HSD Test is a procedure for multiple comparisons in which α_s is the chance that any type I error occurs. Tukey's Test corrects the increase in the probability of making a type I error when multiple comparisons are made.

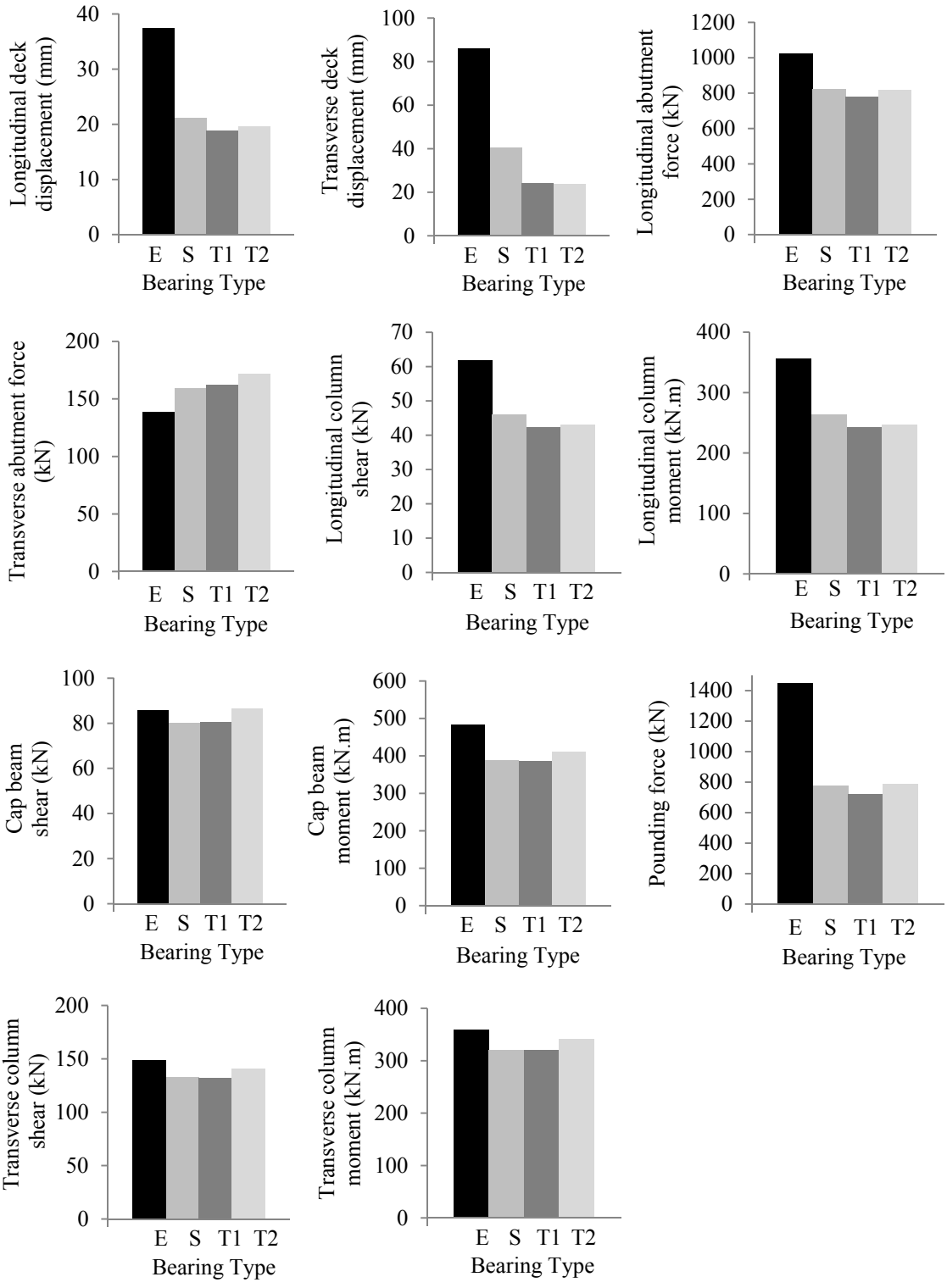

Figure 2-10. Least squares mean values of bridge responses. (Elastomeric bearing, S-short steel pedestal, T1-tall steel pedestal type 1, T2-tall steel pedestal type 2)

For the purpose of variance stabilization, Tukey's HSD Test is applied to the means of the square root of the responses. This transformation is used to ensure the homoscedasticity assumption of the test that states the model variance is independent of variables. Whether comparing the means of the original responses or of the transformed responses, Tukey's HSD Test is used to indicate which conditions tend to have larger/smaller response values. The results of multiple comparisons for various bridge responses are shown in Table 2-5. In this table, capital letters A, B, C and D are used to signify the difference between the responses. Sharing a letter between two groups shows that there is no statistically significant evidence of a difference between the observed mean (square root of) responses in those two groups at the 0.05 level. For example, sharing letter C for longitudinal displacement in tall steel pedestals (T1 and T2) means that there is no statistically significant evidence of a difference between the mean square root of longitudinal displacements of two types of tall pedestals. But because steel pedestals do not have a shared letter with the elastomeric bearings, it can be concluded that elastomeric bearings generally have different longitudinal displacements than steel pedestals. Another example is the results of Tukey's HSD Test for pounding force in Table 2-5. Sharing letter B between three types of steel pedestals show that there is not any statistically significant evidence of a difference in pounding force of the studied bridge when different steel pedestals are used (despite the corresponding mean values in Figure 2-10 being different). It should be noted that capital letters in Table 2-5 are used just to show the lack of a significant difference between responses and do not have any other meaning. If there is significant difference between two responses in Table 2-5,

Figure 2-10 helps to identify which is larger and which is smaller by comparing their least squares means.

Table 2-5. Results of Tukey's HSD Test on the square root of responses for comparison performance of bridge bearings

Response	Elastomeric Bearing (E)	Short Pedestal (S)	Tall Pedestal (T1)	Tall Pedestal (T2)
Longitudinal displacement	A	B	C	C
Transverse displacement	A	B	C	C
Longitudinal abutment force	A	A B	B	A B
Transverse abutment force	C	B	B	A
Longitudinal column shear	A	B	C	C
Transverse column shear	A	B	B	A
Longitudinal column moment	A	B	C	C
Transverse column moment	A	B	B	A
Cap beam moment	A	C	C	B
Cap beam shear	A B	C	B C	A
Pounding force	A	B	B	B

2.5.3 Results of the Statistical Analyses

Table 2-5 shows that elastomeric bearings do not share any letter with steel pedestals for longitudinal and transverse deck displacements, longitudinal shear and moment in columns, cap beam moment and pounding force. Also, Figure 2-10 shows that the means of those responses are larger for elastomeric bearings than steel pedestals. Therefore, it can be concluded that elevating the studied bridge with any of the steel pedestal types studied in this dissertation decreases longitudinal and transverse deck displacements, longitudinal shear and moment in columns, cap beam moment and pounding force. The reduction of force demands in the longitudinal direction arises from the additional stiffness of steel pedestals compared to elastomeric bearings. This additional stiffness

helps reduce the pounding force, which in turn, reduces the other force demands in the longitudinal direction. In the transverse direction, elevating the bridge leads to an increase in the abutment force, which is the result of its increased stiffness. This is concluded from Table 2-5, where elastomeric bearings do not share letter C with steel pedestals, which have letters A and B.

Comparison of steel pedestals in pairs show that the two types of studied tall steel pedestals (T1 and T2) are more effective in decreasing longitudinal shear and moment in columns and also in decreasing transverse displacements than the studied short pedestal (S). It is inferred from Table 2-5, where the studied tall pedestals have letter C for those responses but the studied short pedestal have letter B. It should be noted that the failure of pedestals due to instability or lack of strength are not included in these results but are investigated in the next subsection.

The interaction terms in the statistical models show how the effects of each factor can depend on different levels of the other factors. In this study, despite statistical significance, the magnitudes of the interactions tend to be small, except in the cases shown in Figures 2-11 and 2-12. These figures present the interaction of bearing type with earthquake return period and with location, respectively, for three response variables. Because the mean plots for different levels of return period in Figure 2-11 and for different levels of location in Figure 2-12 are not parallel, the effect of bearing type on the response variables shown in those figures is not the same for different return periods and different locations. Considering that earthquakes in Charleston tend to be larger than earthquakes in the other locations, it is apparent in Figures 2-11 and 2-12 that

using steel pedestals helps to decrease the pounding force and transverse displacement more in large earthquakes than it does in small earthquakes. Large earthquakes in this study are referred to as those with a return period of 2475 years and wherever the comparisons are among locations, earthquakes related to the Charleston area are considered as large earthquakes. Figures 2-11 and 2-12 also show that using steel pedestals decreases the longitudinal abutment force only in large earthquakes. In the previous paragraph, it was concluded that the two types of tall steel pedestals (T1 and T2) are more effective than the short pedestal (S) in decreasing transverse displacement. Figures 2-11 and 2-12 show this effect in more detail and reveal that the decrease in transverse deck displacement occurs only in large earthquakes while in small earthquakes there is not a clear difference in the performance of short and tall pedestals.

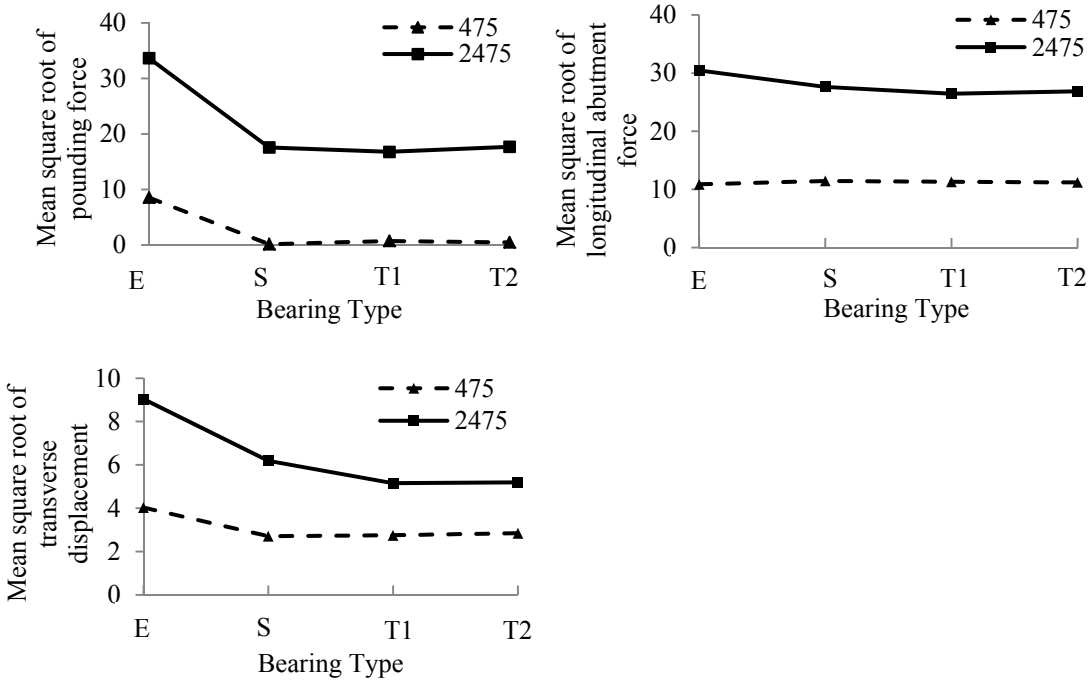

Figure 2-11. Mean plots of square root of those responses in which there is interaction between the return period of earthquake and bearing type

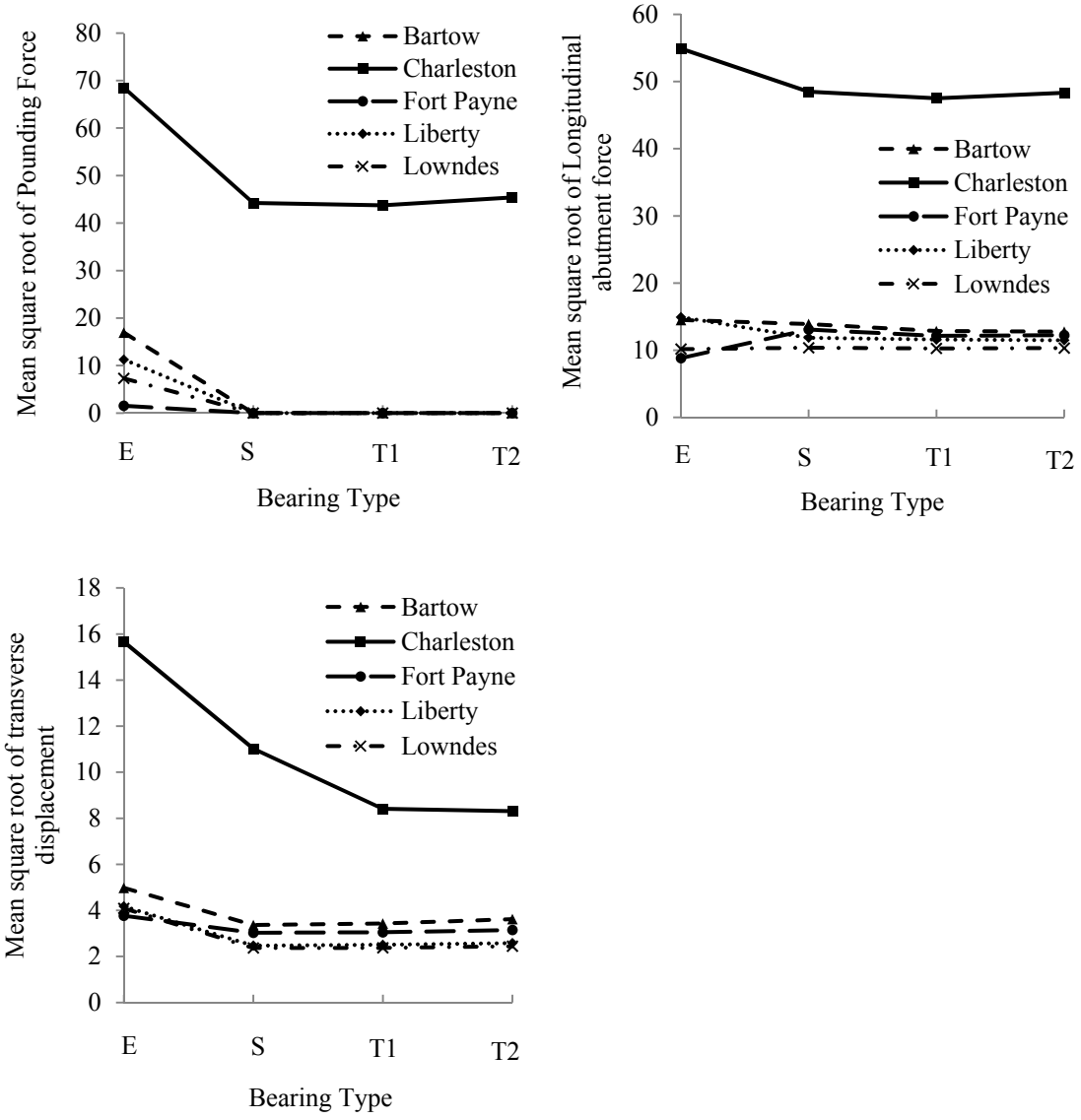

Figure 2-12. Mean plots of square root of those responses in which there is interaction between location and bearing type

2.6 Seismic Force Demand vs. Capacity of Steel Pedestals

The results of the previous section show the influence of elevating bridges with steel pedestals on the seismic responses by considering the stiffness and force–displacement relationship of steel pedestals in the bridge model. But in addition to the steel pedestal

stiffness and force–displacement relationship, the capacity to withstand seismic forces is important in the evaluation of the seismic behavior. In this subsection, the lateral force capacity of steel pedestals is estimated and the seismic demands are compared with estimated force capacity. Two criteria of strength and stability are of interest for the estimation of the lateral force capacity of steel pedestals. Figure 2-13 shows the forces in the studied short steel pedestal (S) in the longitudinal direction.

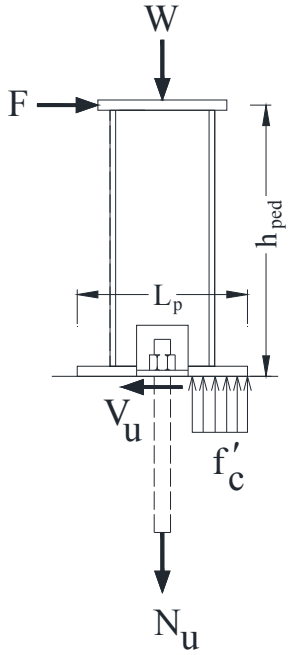

Figure 2-13. Applied forces on short steel pedestal

Based on the equilibrium equations in this figure, Eqs. (2-1) and (2-2) are obtained as the stability and strength criteria for the short steel pedestal in the longitudinal direction, respectively.

$$F \le \frac{(W + N_u)\left(L_p - \frac{W + N_u}{f_c^{'} B_p}\right)}{2h_{ped}} \tag{2-1}$$

$$F \le V_u \tag{2-2}$$

where W=the gravity load; N_u= the tensile capacity of anchor bolts; L_p= length of the base plate; B_p = the width of the base plate, $f_c^{'}$ is the ultimate compressive stress in concrete; h_{ped}= the height of the pedestal; and V_u= the shear capacity of anchor bolts. Four failure modes of steel rupture, concrete cone breakout, pullout and splitting failure are considered for the estimation of the tensile capacity of anchor bolts. Also three failure modes of steel failure, concrete edge breakout and concrete pry-out are considered for the estimation of the shear capacity of anchor bolts. Details about the mechanisms of these failures and formulas to calculate anchor capacity in each of them are provided by Eligehausen et al. (2006). The stability and strength criteria for the other studied cases in this study are obtained similarly. In all the studied steel pedestals, stability criteria are more critical than strength criteria when determining the lateral force capacity of the steel pedestal. Figure 2-14 shows the seismic demand and capacity of the steel pedestals. In this figure, box-whisker plots show the seismic demands in the studied ground motions and horizontal dotted lines show the capacity of the pedestals based on the stability criteria. On each box for demand, the central mark represents the median, the edges of the box show the 25th and 75th percentiles, the whiskers extend to the most extreme data points and outliers are plotted individually by plus signs.

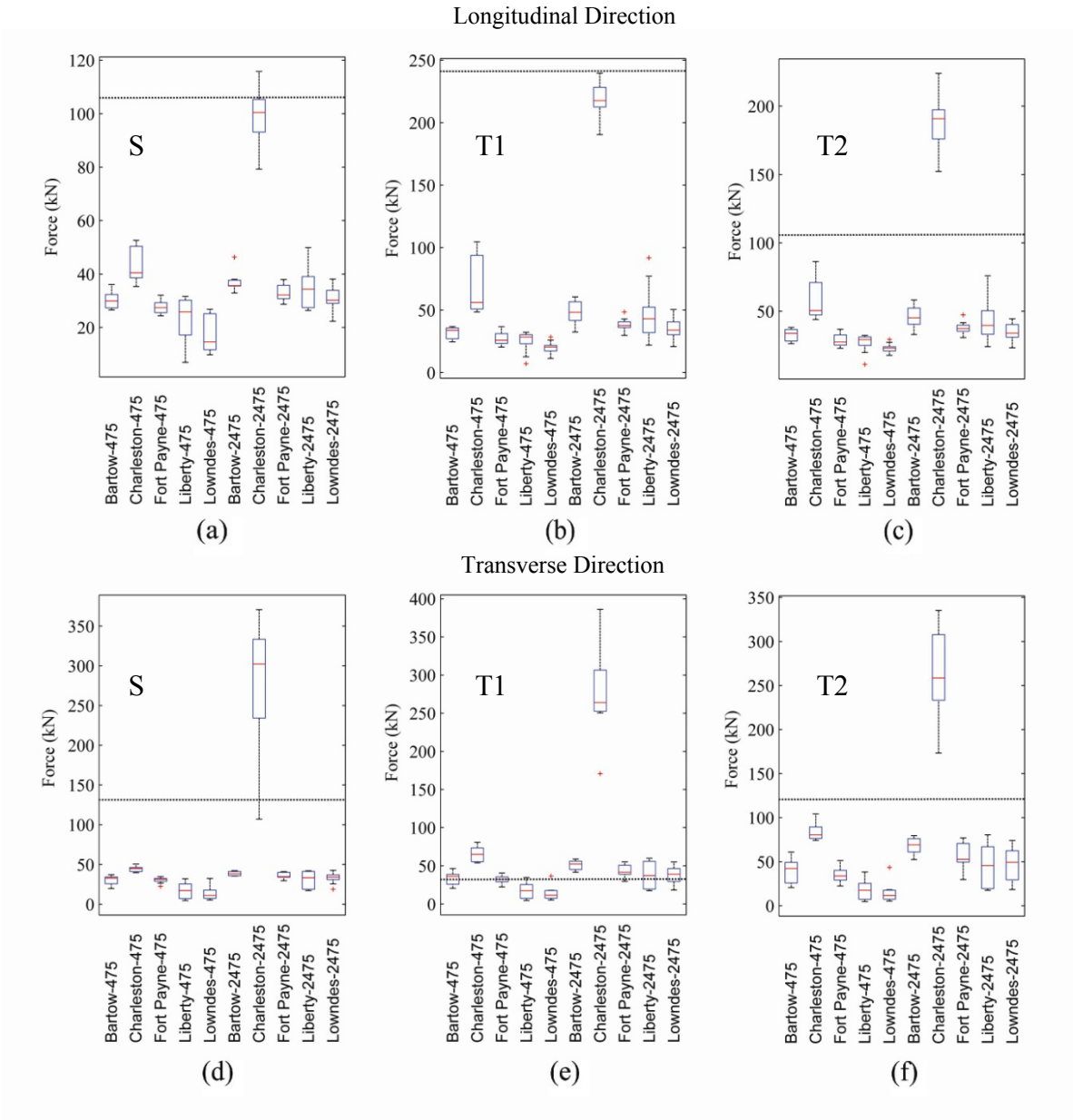

Figure 2-14. Comparison between seismic force demands and capacities of steel pedestals: (a) S in longitudinal direction; (b) T1 in longitudinal direction; (c) T2 in longitudinal direction; (d) S in transverse direction; (e) T1 in transverse direction; and (f) T2 in transverse direction

Figure 2-14 reveals that studied steel pedestals have a stability problem in maximum credible earthquakes (with a return period of 2475 years) generated for Charleston in which the PGA of ground motions are higher than other studied locations.

Also, T1 steel pedestals have a stability problem in the transverse direction in almost all of the ground motions due to their small resisting lever arm in the transverse direction, resulting from the small width of base plate and the arrangement of anchor bolts (section B–B, Figure 2-2). Therefore, the use of this type of pedestal is not well-suited due to stability problems. Generally, using four anchor bolts at the corners of the base plate similar to what is being used in the column base plates of buildings can increase the lateral force capacity of steel pedestals and decrease their stability problems when installed in bridges.

2.7 Conclusions

This section investigated the seismic performance of three types of steel pedestals used to elevate bridges and compared them to the performance of elastomeric bearings (which were assumed to be used before elevation) in a representative bridge subjected to 100 artificial ground motions generated for the southeastern parts of the United States. It should be noted that the results of this section are valid only for the southeastern region of the United States and for the studied pedestal types. A general framework that works for all dimensions and geometrical properties will be presented in the next sections. The fitted bilinear models for experimental force–displacement relationships were used in a bridge model created in OpenSees to evaluate the seismic performance of steel pedestals. Then statistical effects models were employed to process the data, and Tukey's HSD Test was used to compare the performance of bearings. Also, the lateral force capacity of

the pedestals was evaluated and compared to the seismic demands. The findings, which are valid for the case study bridge analyzed, are as follows:

- Elevating the studied bridge with the steel pedestals reduced most of the demands such as longitudinal and transverse deck displacements, longitudinal shear and moment in columns, cap beam moment and pounding force.
- The most important effect was the reduction in pounding force that comes from stiffening the bridge when replacing elastomeric bearings with steel pedestals. This is the main reason for the reduction in longitudinal demands such as the longitudinal abutment force.
- Elevating the studied bridge with steel pedestals had some unfavorable effects, too, such as increasing the transverse abutment force.
- Studied steel pedestals showed a stability problem in large earthquakes (such as Charleston earthquakes with a return period of 2475 years). T1 pedestals (see Figure 2-2) showed a stability problem in the transverse direction even in small earthquakes. So, the use of this type of pedestal is not well-suited.
- Using the studied steel pedestals helped to decrease pounding force and transverse displacement more in large earthquakes than in small earthquakes but it should be noted that in the large earthquakes instability may occur.
- In large earthquakes the two types of studied tall steel pedestals, T1 and T2, were more effective in decreasing transverse displacements than the short pedestals but all of them may become unstable in large earthquakes (as was observed in the Charleston 2475 return period simulations.)

- The two types of studied tall steel pedestals (T1 and T2) were more effective in decreasing longitudinal shear and moment in columns and also in decreasing transverse displacements than the short pedestal (S). The scope of this study was limited to the three types of typical steel pedestals used in the southeastern United States. Further experimental and analytical studies are still needed for pedestals with other geometrical properties and locations.

3. PROBABILISTIC CAPACITY MODELS FOR STEEL PEDESTALS USED TO ELEVATE BRIDGES*

3.1 Introduction

Previous section investigated the seismic effects of elevating bridges with steel bridges and compared their responses with elastomeric bearings. The results of section 2 are valid for the tested pedestals by Hite et al. (2008) and for the Southeastern United States. Those results cannot be extended to steel pedestals with different properties and different locations. Therefore, an analytical method is needed so that engineers can evaluate the failure probability of steel pedestals with various geometrical and mechanical properties subjected to different lateral load levels. This section provides the probabilistic capacity models for the steel pedestals used to elevate bridges.

Figure 3-1 shows a steel pedestal with post-installed anchor bolts that are used to attach the pedestal to the bent cap beam or abutment of a bridge. Usually two anchor bolts are used in the steel pedestals to carry inertial loads but using four bolts (two bolts in each side as shown in Figure 3-1) is recommended in this section because in this case the pedestal has resisting lever arms in both longitudinal and transverse directions and is able to carry the lateral load in both directions. This section presents findings for the lateral load capacity and vulnerability of steel pedestals with four anchor bolts. However, the proposed procedure can also be applied to the steel pedestals with two

* Reprinted with permission from "Probabilistic capacity models and fragility estimates for steel pedestals used to elevate bridges." by Vahid Bisadi, Paolo Gardoni and Monique Head, 2011, *ASCE Journal of Structural Engineering*, 137(12), 1583-1592, Copyright 2011 by ASCE.

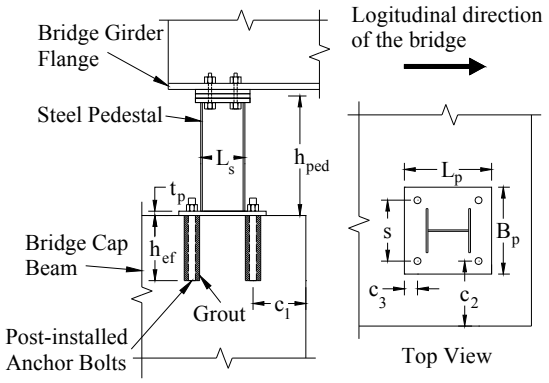

Figure 3-1. Steel pedestal at the corner of a bridge bent beam

anchor bolts in the direction where the pedestal has a resisting lever arm.

The load capacity of the pedestals depends on the capacity of the anchor bolts and the capacity of the base plate. Eligehausen et al. (2006) presented a comprehensive literature review about the methods of computing anchor bolt capacity. Also, there is much research about the load carrying capacity of column base plate connections, such as Melchers (1992) and Stamatopoulos and Ermopoulos (1997). However, these investigations focused only on base plates typically used in buildings and did not consider all the failure modes of post-installed anchor bolts used in steel pedestals.

This section shows the development of probabilistic models for the lateral load capacity of steel pedestals in the longitudinal direction of bridge accounting for the failure modes associated with the post-installed unheaded non-expansion anchor bolts (which are typically used in steel pedestals), yielding of the base plate, and compressive failure of the concrete under the pedestal. The lateral capacity of steel pedestals is presented for the case where the lateral load pushes the pedestal toward the inside part of the cap beam (inward capacity) and for the case where the lateral load pushes the

pedestal toward the outside of the cap beam (outward capacity). These two cases are considered separately because some of the parameters such as the concrete covers on the anchor bolts are not the same in both cases. Depending on the values of parameters either of them can govern the capacity of the pedestal. For the lateral capacity of the interior steel pedestals in the transverse direction, the inward load capacity models for the longitudinal direction can be used with the corresponding values for the concrete covers. For the exterior steel pedestals in transverse direction, inward and outward capacities have to be estimated separately following the method proposed in this dissertation for the longitudinal direction.

The probabilistic capacity models in this study are constructed based on available deterministic methods for computing the load carrying capacity of anchor bolts and base plates. The proposed capacity models consider the prevailing uncertainties including statistical uncertainty and model errors due to inaccuracy in the model form or missing variables. The developed probabilistic models are of value to the engineering community to assess the lateral load capacity and failure probability of existing bridges elevated with steel pedestals. It should be noted that this section focuses on the probabilistic capacity models of steel pedestals and all the fragility estimates presented in this section are conditioned on the demand. There are lots of uncertainties in the demand on the steel pedestals, which are considered in developing the probabilistic demand models for bridges elevated with steel pedestals in the next section.

This section has six subsections. After the introduction, the failure modes of different components of steel pedestals and the variables that can affect them are

discussed and probabilistic capacity models for them are presented. Next, a procedure is developed to find lateral-vertical interaction curves for steel pedestals. The fourth subsection describes probability of failure versus lateral and vertical loads on the pedestal. Then the fragility for an example steel pedestal using developed capacity models is estimated and the sensitivity of the results to changes in the mean value and coefficient of variation of random variables is investigated. Finally, the last subsection presents some conclusions.

3.2 Probabilistic Capacity Model of Steel Pedestals Subjected to Lateral Loads

The load carrying capacity of steel pedestals depends on the capacity of anchor bolts, yielding capacity of base plate and the compressive capacity of concrete under the pedestal. It is assumed that the steel profile of the pedestal and its welded connection to the base plate have enough capacity to carry lateral loads and do not govern the capacity of the pedestal. This assumption is consistent with the experimental results obtained by Hite et al. (2008).

Figure 3-1 illustrates the geometrical variables used in this study, where h_{ef} = embedment length of anchor bolts in concrete (considered as random variable); c_1 = distance between the longitudinal axis of anchor in tension and perpendicular edge of concrete to the lateral load direction (considered as random variable); c_2 = distance between the longitudinal axis of anchor in tension and parallel edge of concrete to the lateral load direction (considered as random variable); c_3 = distance between the longitudinal axis of anchor and perpendicular edge of base plate to the lateral load

direction; h_{ped} = pedestal height; L_s = steel profile dimension parallel to the lateral load; t_p = base plate thickness; L_p = base plate dimension parallel to the lateral load; B_p = base plate dimension perpendicular to the lateral load; and s = distance between the longitudinal axis of anchors perpendicular to the lateral load direction.

3.2.1 Anchor Capacity

Eligehausen et al. (2006) provide a comprehensive study and literature review about the capacity of anchor bolts. According to Eligehausen et al. (2006) and the American Concrete Institute (ACI) (2008), anchor bolts may fail in tension, shear or interaction between tension and shear. When steel pedestals are subjected to lateral loads, both shear and tension forces are available in anchor bolts. As such, discussion about all the probable failure modes of anchor bolts in tension and shear is presented in the following subsections.

3.2.1.1 Anchor Bolt Failure Modes in Tension

There are five anchor bolt failure modes in tension: steel rupture, concrete cone breakout, pullout, concrete side blow-out and splitting failure (ACI 2008). All these modes, except concrete side blow-out that is related to headed anchor bolts are considered in this study. Anchor bolts that are used for bridge steel pedestals in this study are post-installed unheaded anchors and concrete side blow-out is not applicable to them. In this study, the anchor bolts tension capacity, N_u, at the tension side of the steel pedestal is defined as the minimum of the four tension failure mode capacities

$$N_u = \min\left(N_{u,s}, N_{u,c}, N_{u,cp}, N_{u,sp}\right) \tag{3-1}$$

where $N_{u,s}$ = anchor failure load in tension associated with steel rupture; $N_{u,c}$ = anchor failure load in tension associated with concrete cone breakout; $N_{u,cp}$ = anchor failure load in tension associated with pullout failure; and $N_{u,sp}$ = anchor failure load in tension associated with splitting failure.

Steel Rupture

Steel rupture failure mode rarely occurs in anchor bolts and usually other modes of failure happen before (Eligehausen et al. 2006). The following equation computes the failure load for this mode:

$$N_{u,s} = nA_s f_u = n\left(\frac{\pi d^2}{4}\right)\left(\lambda_s f_n\right) \tag{3-2}$$

where n = number of anchors in each side of the pedestal; A_s = cross sectional area of one anchor bolt; f_u = ultimate stress of anchor bolt steel; d = anchor bolt diameter; λ_s = random variable for the ratio of ultimate stress to nominal stress of steel; and f_n = nominal stress of anchor bolt steel. This study uses the random variable λ_s because the ultimate stress of anchor bolt steel usually is about ten to twenty percent more than its nominal stress (Eligehausen et al. 2006). This random variable considers the uncertainty in the material property of steel. No model error terms are considered for steel rupture because the model is based on the principles of mechanics of materials and is assumed to be accurate.

Concrete Cone Breakout

Concrete cone breakout is the most common failure mode of the anchor bolts (Eligehausen et al. 2006). Some methods are available to calculate the failure load of this mode such as the 45 degree cone Method, the Variable Angle Cone (VAC) Method and the Concrete Capacity Design (CCD) Method (Fuchs et al. 1995). The CCD Method is the most common and, according to Farrow et al. (1995), also the most accurate. The following modification of the CCD Method that accounts for the underlying uncertainties is proposed in this study

$$N_{u,c} = \left(14.6 \frac{A_{c,N}}{A_{c,N}^0} \psi_{s,N} \psi_{m,N} h_{ef}^{1.5} f_c'^{0.5} \right) \times \left(\frac{\varepsilon_2 \varepsilon_3 \varepsilon_4}{\varepsilon_1^2} \right) \tag{3-3}$$

$$A_{c,N}^0 = 9 h_{ef}^2 \tag{3-4}$$

$$A_{c,N} = \min \Big[3h_{ef} \left(3h_{ef} + s \right), \left(3h_{ef} + s \right) \left(1.5h_{ef} + c_1 \right), 3h_{ef} \left(1.5h_{ef} + c_2 + s \right), \left(1.5h_{ef} + c_1 \right) \left(1.5h_{ef} + c_2 + s \right) \Big] \tag{3-5}$$

$$\psi_{s,N} = \min \left\{ \left[0.7 + 0.3 \frac{\min(c_1, c_2)}{1.5 h_{ef}} \right], 1 \right\} \tag{3-6}$$

$$\psi_{m,N} = 1 \quad if \quad \frac{z}{h_{ef}} \geq 1.5 \tag{3-7}$$

$$\psi_{m,N} = \frac{2.5}{1 + \frac{z}{h_{ef}}} \quad if \quad \frac{z}{h_{ef}} < 1.5 \tag{3-8}$$

where $A_{c,N}$= projected concrete failure area of anchors under consideration for calculation of strength in tension, limited by the overlap of the individual concrete cones

of adjacent anchors and the edges of the component; $A_{c,N}^{0}$ = projected concrete failure area of a single anchor for calculation of strength in tension if not limited by corner influences, spacing or member thickness; $\psi_{s,N}$ = coefficient for the effect of edge distances; $\psi_{m,N}$ = coefficient for the consideration of helpful effect of compression zone under the pedestal; $f_c^{'}$ = concrete compressive strength (considered as random variable); $\varepsilon_i \quad (i = 1,2,3,4)$ = random variables with the lognormal distribution that capture the model errors; and z = lever arm between the tension force of anchors and compression force in concrete under the pedestal. The value of $A_{c,N}^{0}$ in Eq. (3-4) is computed based on the assumption of a cone shape failure for the concrete around the anchor. However, due to the presence of concrete edges near the anchor, the failure shape is not always a complete cone. Therefore, the ratio $A_{c,N} / A_{c,N}^{0}$ is added to Eq. (3-3). The ratio $A_{c,N} / A_{c,N}^{0}$ in Eq. (3-3) is limited to the number of anchors in tension which is 2 in this study. Coefficients for the effect of load eccentricity and special reinforcement consideration are neglected in Eq. (3-3) because they are not applicable to the studied case. The coefficient $\psi_{m,N}$ should be neglected when tensile anchors are the ones located near the edge of the concrete (Eligehausen et al. 2006) because in this case the compressive anchors do not help to stabilize the concrete cone that is come out from the concrete body around tensile anchors. The coefficient $\psi_{s,N}$ is considered because near the edges of concrete a complete cone cannot form during the failure. Details about the coefficients used in Eqs. (3-3) to (3-8) can be found in Eligehausen et al. (2006).

Table 3-1. Error terms in probabilistic model for steel pedestals

Error term	Applied to	Mean	C.O.V.
ε_1	Concrete cone breakout of anchor in tension	0.96	0.23
ε_2	Concrete cone breakout of anchor in tension	0.96	0.21
ε_3	Concrete cone breakout of anchor in tension	1.04	0.26
ε_4	Concrete cone breakout of anchor in tension	1.10	0.15
ε_5	Splitting failure of anchor in tension	0.95	0.163
ε_6	Steel failure of anchor in shear	1	0.300
ε_7	Concrete edge failure of anchor in shear	0.96	0.165
ε_8	Concrete pry-out of anchor in shear	1	0.300
ε_9	Proposed method to calculate pedestal capacity	1.06	0.175

Note: ε_i, i=1,…,9, have lognormal distributions.

Following Gardoni et al. (2002), model error terms are used in Eq. (3-3). These error terms are considered as random variables in the analyses. Table 3-1 shows the error terms used in the probabilistic capacity models. In this table, ε_1 through ε_4 are multiplicative error terms related to $N_{u,c}^0$, $(A_{c,N} / A_{c,N}^0)N_{u,c}^0$, $\psi_{s,N}N_{u,c}^0$ and $\psi_{m,N}N_{u,c}^0$ respectively, where $N_{u,c}^0 = 14.6 h_{ef}^{1.5} f_c^{'0.5}$. Therefore, the term in the first parenthesis of Eq. (3-3) is modified by a combined error term in the second parenthesis. The mean and coefficient of variation (C.O.V.) of error terms ε_1 through ε_4 are chosen based on the experiments and statistical analyses conducted by Eligehausen et al. (2006).

Pullout

For unheaded grouted anchors, a probabilistic model that considers pullout failure due to bond failure at the steel/grout or at grout/concrete interface is proposed using a uniform bond stress model (Zamora et al. 2003) as follows:

$$N_{u,cp} = n \times \min\left(\tau \pi d h_{ef}, \tau_0 \pi d_0 h_{ef}\right) \tag{3-9}$$

where τ = random variable representing the uniform bond stress between anchor steel and grout at pullout failure; τ_0 = random variable representing the uniform bond stress between grout and concrete at pullout failure; and d_0 = random variable representing the grout hole diameter. The first and second terms in parenthesis show the force due to a uniform bond stress around a cylinder and correspond to steel/grout and grout/concrete bonds, respectively. For completeness, Eq. (3-9) considers bond failure both at the steel/grout and grout/concrete interfaces. However, bond failure between steel and grout is more common than bond failure between grout and concrete. This model is also based on the mechanics of material principles and thus no model error is considered for it.

Splitting Failure

Splitting failure usually occurs with anchors close to an edge of a concrete member with small thickness (Eligehausen et al. 2006). The probability of occurrence of this mode of failure is small for anchor bolts installed in thick concrete members such as the bridge cap beams but not equal to zero, and is assessed as such for completeness in this study. Following deterministic model proposed by Huer and Eligehausen (2007) for splitting failure mode of bonded anchors, Eqs. (3-10) to (3-13) for the probabilistic model of splitting failure load are proposed

$$N_{u,sp} = \left[\frac{\left(s_{cr,sp} + s\right) h_{cap}}{s_{cr,sp}(1.5c_1 + h_{ef})} \psi_{h,sp} \psi_{g,sp} k_p \left(\pi d h_{ef}\right)^{1/2} c_1^{3/7} \left(1.5c_1 + h_{ef}\right)^{1/6} f_c'^{1/2} \right] \times \varepsilon_5 \quad (3\text{-}10)$$

$$\psi_{h,sp} = \left(\frac{1.5c_1 + h_{ef}}{h_{cap}} \right)^{5/6} \quad (3\text{-}11)$$

$$\psi_{g,sp} = \max\left[\sqrt{n} - \left(\sqrt{n} - 1\right)\sqrt{\frac{s}{s_{cr,sp}}}, 1\right] \tag{3-12}$$

$$s_{cr,sp} = \min\left(5c_1^{2/3}d^{1/3}, 32d\right) \tag{3-13}$$

where $s_{cr,sp}$ = distance for calculating projected area of anchors; $\psi_{h,sp}$, $\psi_{g,sp}$ = modification coefficients; k_p = product factor; h_{cap} = cap beam thickness; and ε_5 = model error term. Factor $\psi_{g,sp}$ considers the larger load bearing area for two tensile anchors in comparison to a single anchor and factor $\psi_{h,sp}$ is a modification factor to modify the effect of concrete member height. The mean and C.O.V. of ε_5 is selected based on the experiments and finite element analyses conducted by Huer and Eligehausen (2007) and are shown in Table 3-1.

3.2.1.2 Anchor Bolt Failure Modes in Shear

Three shear failure modes are referenced in ACI (2008). The modes are steel failure, concrete edge breakout and concrete pry-out. In this study, the anchor bolts shear capacity, V_u, at the tension side of the steel pedestal is defined as the minimum of the three shear failure mode capacities

$$V_u = \min\left(V_{u,s}, V_{u,c}, V_{u,cp}\right) \tag{3-14}$$

$V_{u,s}$ = anchor failure load in shear associated with steel rupture; $V_{u,c}$ = anchor failure load in shear associated with concrete cone breakout; and $V_{u,cp}$ = anchor failure load in shear associated with concrete pry-out.

Steel Failure

Steel failure mode occurs in anchors with enough cover and embedment length. Following the deterministic model in Eligehausen et al. (2006) and ACI (2008), the following probabilistic capacity model for calculation of failure load in this mode is proposed

$$V_{u,s} = \left[n\mu \frac{\pi d^2}{4} \left(\lambda_s f_n \right) \right] \times \varepsilon_6 \tag{3-15}$$

where μ = 0.6 for post-installed anchors; and ε_6 = model error term. Since I did not have access to the corresponding experimental results, reasonable values for the mean and standard deviation of ε_6 were assumed as shown in Table 3-1.

Concrete Edge Failure

Concrete edge failure is associated with anchors near the free edge of the concrete subjected to a shear force perpendicular to the edge. At this mode of failure, a semi-conical fracture surface is developed originating from the anchor toward the free surface of the concrete at the near edge. Muratli et al. (2004), Eligehausen et al. (2006) and ACI (2008) have proposed deterministic formulas to compute the failure load of this mode. Following Eligehausen et al. (2006) that gives more convenient deterministic model for anchors with diameters more than 25mm (which are typically used in steel pedestals), Eqs. (3-15) to (3-20) are proposed in this dissertation as probabilistic model for concrete edge failure

$$V_{u,c} = \left[3.0 \frac{A_{c,V}}{A_{c,V}{}^{0}} \psi_{s,V} \psi_{h,V} d^{0.1\left(\frac{l_f}{c_1}\right)^{0.5}} l_f^{0.1\left(\frac{d}{c_1}\right)^{0.2}} f_c'^{0.5} c_1^{1.5} \right] \times \varepsilon_7 \tag{3-16}$$

$$A_{c,V}{}^{0} = 4.5 c_1^{2} \tag{3-17}$$

$$A_{c,V} = \min\left(1.5c_1, h_{cap}\right) \times \min\left\{\left(3c_1 + s\right), \left(1.5c_1 + c_2 + s\right)\right\} \tag{3-18}$$

$$l_f = \min\left(h_{ef}, 8d\right) \tag{3-19}$$

$$\psi_{s,V} = \min\left\{\left(0.7 + 0.3\frac{c_2}{1.5c_1}\right), 1\right\} \tag{3-20}$$

$$\psi_{h,V} = \max\left\{\left(1.5\frac{c_1}{h_{cap}}\right)^{0.5}, 1\right\} \tag{3-21}$$

where $A_{c,V}$ = projected concrete failure area of anchors under consideration for calculation of strength in shear, limited by the overlap of the individual concrete cones of adjacent anchors and the edges of the component; $A_{c,V}^{0}$ = projected concrete failure area of a single anchor for calculation of strength in shear if not limited by corner influences, spacing or member thickness; $\psi_{s,V}$ = coefficient for the effect of edge distances; $\psi_{h,V}$ = coefficient for the effect of concrete component thickness; ε_7 = model error term; and l_f = effective load transfer length. The formula for $A_{c,V}^{0}$ in Eq. (3-17) is obtained by assuming a half-pyramid for the failure surface of a single anchor. Furthermore, the ratio $A_{c,V} / A_{c,V}^{0}$ captures the effects of the edges that prevent the development of a full half-pyramid. The mean and coefficient of variation (C.O.V.) of

the error term ε_7 are chosen based on the experiments and statistical analyses conducted by Eligehausen et al. (2006) and are shown in Table 3-1.

Concrete Pry-out

Concrete pry-out occurs when the surface concrete near the bolt crushes. According to Eligehausen et al. (2006), the failure load in this mode is considered as twice the concrete cone breakout capacity in tension. The following probabilistic model for this mode of failure is used

$$V_{u,cp} = \left(2.0 N_{u,c}\right) \times \varepsilon_8 \tag{3-22}$$

where ε_8 = model error term. Since I did not have access to the corresponding experimental results, reasonable values for the mean and standard deviation of ε_8 were assumed as shown in Table 3-1.

3.2.1.3 Shear-Tension Interaction

Anchor bolts of steel pedestals in bridges subjected to lateral loads carry shear and axial forces simultaneously. The interaction between shear and tension has the following general relationship (Eligehausen et al. 2006)

$$\left(\frac{N}{N_u}\right)^q + \left(\frac{V}{V_u}\right)^q = 1 \tag{3-23}$$

where N =tension force in anchor bolt; V =shear force in anchor bolt; and q =exponent of interaction equation.

A variety of recommendations for the exponent q is available in the literature varying from 1 (Cook and Klinger 1989) to 2 (Shaik and Whayong 1985). But $q = 5/3$ is the mostly accepted value (McMackin et al. 1973; Meinheit and Heidbrink 1985). This study considers q as a random variable to include the effect of uncertainty in this parameter.

3.2.2 Base Plate Yielding

Yielding of the base plate is another mode of failure for the whole system of the steel pedestal. When the lateral load is applied on the pedestal, the base plate steel may yield at the edge of steel profile of the pedestal. Eligehausen and Fichtner (2007) have investigated the stiffness requirements for base plates. The plastic moment capacity of the base plate is computed based on the equations of mechanics of materials as follows

$$M_{pl} = f_{py} \frac{B_p t_p^2}{4} \tag{3-24}$$

where f_{py} = yield stress of base plate steel.

3.3 Lateral-Vertical Load Interaction Curves for Steel Pedestals

For determination of the lateral and vertical load capacity of a bridge steel pedestal, a method is needed by which the load capacity of the pedestal can be obtained based on the capacity of the pedestal components, i.e., anchor bolts, base plate and base concrete. The method proposed by Stamatopoulos and Ermopoulos (1997) for obtaining the interaction curves of column base-plate connections is applicable for this purpose. Other

methods such as the one proposed by Penserini and Colson (1989) or EC3 method (Melchers 1992) are available but comparisons of these methods with experimental results by Stamatopoulos and Ermopoulos (1997) show that their method gives more realistic results than others.

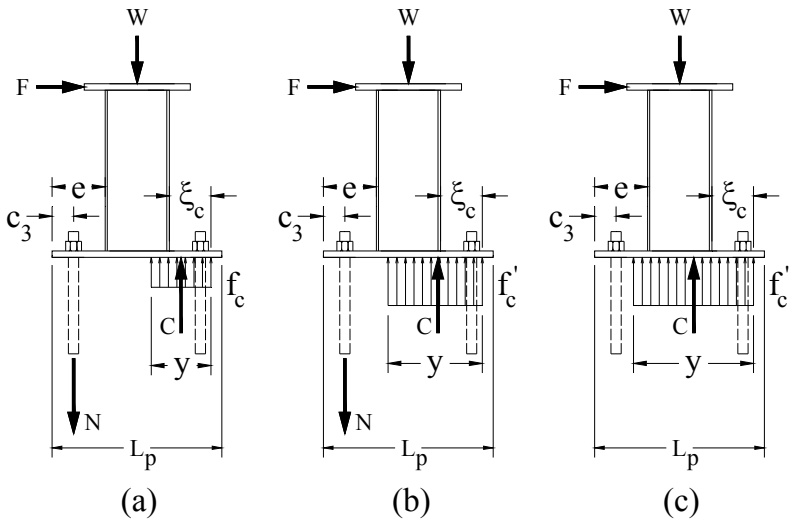

Figure 3-2. Failure modes of steel pedestals: (a) Failure Mode 1 due to large F and small W; (b) Failure Mode 2 due to large F and large W; and (c) Failure Mode 3 due to small F and large W

This dissertation modifies the method by Stamatopoulos and Ermopoulos (1997) to make it applicable to post-installed anchors for bridge steel pedestals. Three failure modes are considered for the steel pedestal as shown in Figure 3-2. Mode 1 occurs when the lateral force is large and vertical force is much less than pedestal vertical load capacity. In this mode compression stress in concrete under the pedestal is less than ultimate compressive stress of concrete. Mode 2 is associated to the cases where the applied vertical force on the pedestal is considerable and the lateral force is also large. In

this case, the concrete stress is equal to the ultimate compressive stress of concrete. Finally, mode 3 occurs in cases where the vertical load on the pedestal is large. No tensile load is in anchor bolts in the third mode and the failure occurs by a plastic mechanism in base plate or compression failure of the concrete. The difference between the first and second mode of failure is the concrete stress that is estimated under the base plate. The difference between second and third mode of failure is the presence of tensile force within the anchor bolts in the second mode.

Following Stamatopoulos and Ermopoulos (1997), a cantilever effective length is considered for the cantilever parts of the base plate at the edges, which is shown by ξ_c in Figure 3-2. This is the length of the base plate in its cantilever part where there is nonzero stress under the base plate. It is determined based on the plastic moment capacity of the base plate assuming an equivalent rectangular stress distribution instead of complicated real stress distribution under the base plate. The cantilever effective length is computed from Eq. (3-25).

$$\xi_c = t_p \sqrt{\frac{f_{py}}{2 f_c}} \tag{3-25}$$

where f_c = concrete stress under the pedestal.

The first failure mode of Figure 3-2 is different from the first failure mode proposed by Stamatopoulos and Ermopoulos (1997). They used a triangular stress distribution under the base plate in the first mode that contradicts the assumption for calculating cantilever effective length.

The maximum tensile force in the anchor bolts is the minimum of the force that leads to anchor failure and the force that cause a plastic failure mechanism at tension side of the base plate. The anchor tensile failure load considering shear-tension interaction is computed from Eq. (3-23) as follows

$$N_a = \left[1 - \left(\frac{V}{V_u}\right)^q\right]^{1/q} N_u \tag{3-26}$$

and the anchor tensile force that causes a plastic failure mechanism in the base plate is computed as follows (Stamatopoulos and Ermopoulos 1997)

$$N_p = \frac{f_{py} B_p t_p^{\,2}}{4\left(e - c_3\right)} \tag{3-27}$$

where e = distance between the edge of profile and the edge of base plate.

Thus, the tensile load of the anchors at failure modes 1 and 2 is found from Eq. (3-28).

$$N_{\max} = \min\left(N_a, N_p\right) \tag{3-28}$$

Stamatopoulos and Ermopoulos (1997) considered column base plates with cast in place anchors. Therefore, yielding of steel was considered as the only failure mechanism of the anchors. The embedment length of cast in place anchors and their end hooks are such that the other modes of failure can be neglected. However, for steel pedestals with post installed anchor bolts with limited length, there is no hook at the end of the anchors. Therefore, the other modes of failure of the anchor bolts have to be also considered. In this study, all possible modes of failure are considered in Eq. (3-26). The flowchart presented in Figure 3-3 shows the steps for calculating the lateral-vertical load

interaction curve for steel pedestals, where α = random variable that represents the fraction of the lateral load that is transferred to the anchor bolts in tension side of the base plate; F_a = assumed value for the lateral capacity of steel pedestal; F_c = calculated value for the lateral capacity of steel pedestal ; and ε = acceptable tolerance. Parameters $W_{\max}$ and Δ_{cr} are computed from Eqs. (3-29) and (3-30), respectively.

$$W_{\max} = f_c^{'} B_p \left[L_p - 2\left(e - \xi_{cu}\right) \right] \tag{3-29}$$

$$\Delta_{cr} = \left[L_p - c_3 - \left(e - \xi_{cu}\right) \right]^2 - \frac{W}{f_c^{'} B_p} \left[L_p + 2\left(\frac{F h_{ped}}{W} - c_3 \right) \right] \tag{3-30}$$

where Δ_{cr} = a parameter that shows the failure mode 3 occurs when its value is less than zero; $W_{\max}$ = maximum tolerable vertical force by steel pedestal; ξ_{cu} = effective cantilever length of base plate when concrete stress is equal to $f_c^{'}$; and W = vertical load demand. Details about the derivation of Δ_{cr} can be found in Stamatopoulos and Ermopoulos (1997).

Described procedure gives the lateral load capacity of the steel pedestal for any value of vertical load. This procedure is applicable to find the lateral load capacity of the pedestal when the applied load is inward. In this case, the load is applied such that the steel pedestal is pushed toward the center of the cap beam, the anchor bolts near the edge are in tension, and the anchor bolts far from the edge are in compression. With this arrangement of tension and compression anchors, coefficient $\psi_{m,N}$ should be neglected in Eq. (3-3) (Eligehausen et al. 2006). In the case of an outward load where the load pushes the steel pedestal toward outside of the cap beam, the arrangement of tension and

compression anchors are reverse to the inward case and coefficient $\psi_{m,N}$ should be determined as a function of the lever arm between compression and tension forces under the pedestal. Since this lever arm is a function of the parameter y in Figure 3-2, an additional iterative loop should be added to the mentioned procedure when the applied load is outward.

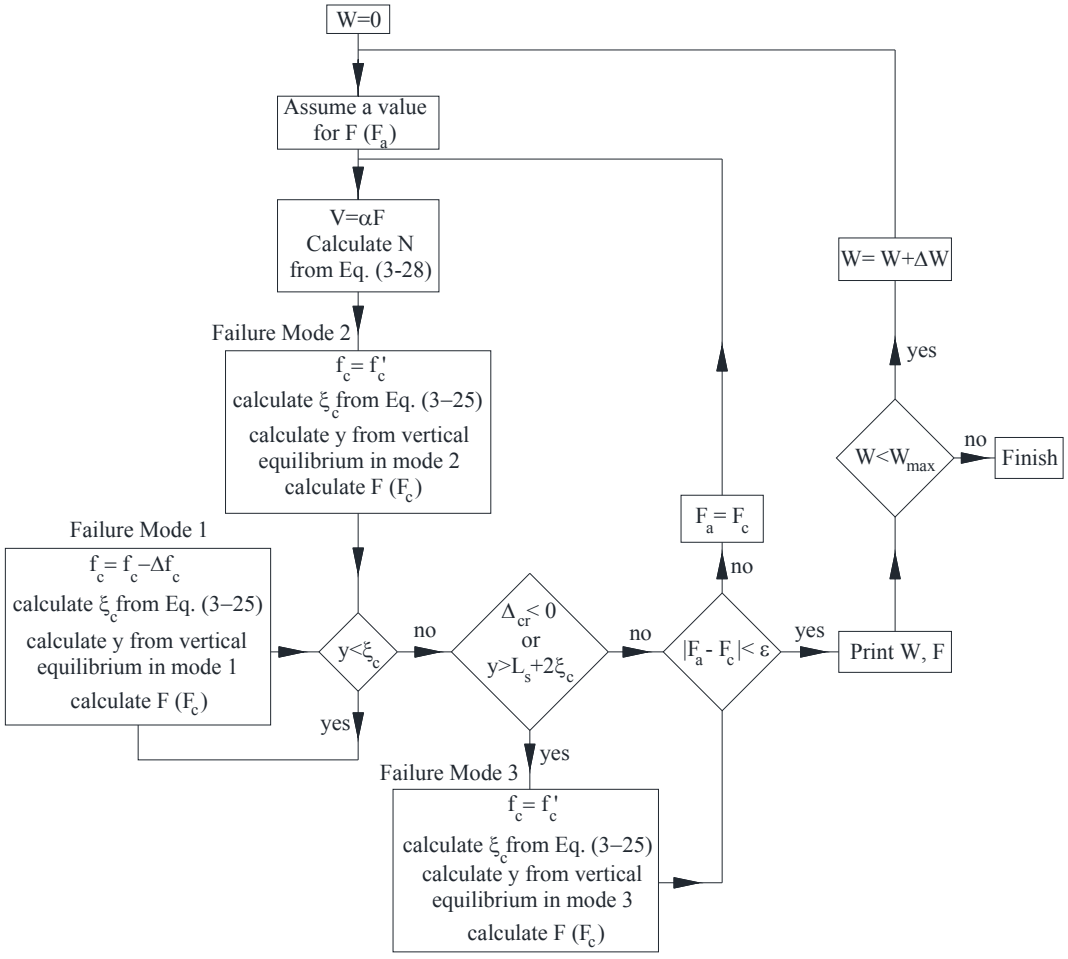

Figure 3-3. Flowchart for calculation of lateral-vertical load interaction curve for steel pedestal

Considering the error term ε_9 in Table 3-1 is for covering error in the described procedure for finding the lateral load capacity of the steel pedestals. Applying the procedure illustrated in Figure 3-3 for the specimens tested by Dewolf and Sarisley (1980) and Thambiratnam and Paramasivam (1986) shows that the error term ε_9 has a mean equal to 1.06 and coefficient of variation equal to 0.175. Hence, the probabilistic model of the lateral load capacity of the pedestal is presented in this study as follows

$$F_c = F \times \varepsilon_9 \tag{3-31}$$

where F = lateral capacity obtained from the procedure illustrated in Figure3-3.

3.4 Probability of Failure versus Lateral and Vertical Loads

Based on the conventional notation in reliability theory (Ditlevsen and Madsen, 1996), a limit state function g(.) is defined such that g(.)≤0 represent the failure of steel pedestal. Using the probabilistic model for steel pedestal capacity described in Eq. (3-31), the limit state function is written in the following form.

$$g\left(\mathbf{x}, F_D, W_D\right) = F_C\left(\mathbf{x}, W_D\right) - F_D \tag{3-32}$$

where $\mathbf{x}$ = vector of random variables; F_D = lateral force demand; W_D = vertical force demand; and $F_C(\mathbf{x}, W_D)$ = probabilistic lateral load capacity of the steel pedestal computed from Eq. (3-31). A conditional probability of failure given the values of F_D and W_D is obtained as follows

$$P\left[g\left(F_D, W_D, \mathbf{x}\right) \le 0 \mid F_D, W_D\right] \tag{3-33}$$

and the generalized reliability index related to this probability is computed as

$$\beta\left(F_D, W_D, \mathbf{x}\right) = \Phi^{-1}\left\{1 - P\left[g\left(F_D, W_D, \mathbf{x}\right) \le 0 \mid F_D, W_D\right]\right\} \tag{3-34}$$

where $\Phi^{-1}\{.\}$ denotes the inverse of the standard normal cumulative probability. Figure 3-4 shows a conceptual diagram of the fragility of bridge steel pedestals evaluated in this study versus lateral and vertical forces applied on them. Figure 3-4 shows that at a specified vertical load, failure probability of steel pedestal increases as lateral load increases. At a specified lateral load, as the vertical load increases the failure probability of the steel pedestal decreases at first and increases after reaching a minimum point.

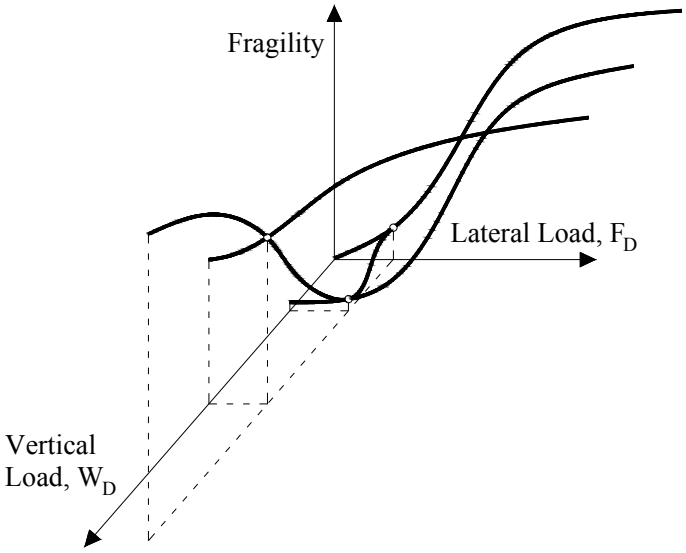

Figure 3-4. Conceptual diagram for the fragility of bridge steel pedestals

3.5 Probability of Failure for an Example Steel Pedestal

The proposed probabilistic models developed in the previous sections are used to compute the probability of failure for any post-installed, unheaded anchor bolts subjected to lateral load and positioned within the base plate of a steel pedestal. The

horizontal and vertical demand forces on the steel pedestals can be the result of any applied loads on the bridge that can produce force demands on the bearings. For example, the lateral load on the pedestal can be due to earthquake loads, braking loads, wind loads. Since this study focuses on the capacity models and all the fragility estimates are conditioned on demands, no details of the demand models are presented in this section. Following the formulation in Gardoni et al. (2003), the presented capacity models in this study can be used in combination with probabilistic demand model to estimate the probability of failure of the pedestal subjected to the corresponding load.

Table 3-2. Deterministic parameters for the example pedestal

Parameter	Unit	Value
d	mm	32
h_{cap}	mm	1200
h_{ped}	mm	500
c_3	mm	60
s	mm	280
L_p	mm	400
B_p	mm	400
t_p	mm	25
L_s	mm	200
f_n	MPa	517

As an example, this section estimates the probability of failure of an example bridge steel pedestal with properties presented in Table 3-2 for given the values of demand forces. The parameters presented in Table 3-2 are considered as deterministic in this example because their values can be easily measured with sufficient accuracy. The uncertainty in the material properties of anchor steel is considered in the parameter λ and therefore f_n is considered as a deterministic parameter. Table 3-3 shows the random variables of the example pedestal along with the considered values of their means and

C.O.V.s, and the considered ranges for their mean value in sensitivity analysis. All the random variables are assumed to be statistically independent in this study. The input variables reflect the actual (potentially deteriorated) state of the system. Mean values and C.O.V.s for the steel/grout and grout/concrete bond stresses are selected as reported by Zamora et al. (2003) and Subramanian and Cook (2004) for the specimens from nine types of grouts.

Table 3-3. Random variables in probabilistic model for the example pedestal

Random Variable	Unit	Distribution	Mean	C.O.V.	Range of the mean in sensitivity analysis
d_0	mm	Lognormal	70	0.1	40-100
h_{ef}	mm	Lognormal	300	0.1	100-500
f'_c	MPa	Lognormal	25	0.2	15-50
f_{py}	MPa	Lognormal	240	0.05	200-500
τ	MPa	Lognormal	18.4	0.27	5-25
τ_0	MPa	Lognormal	8.1	0.3	3-12
λ_s	----	Lognormal	1.15	0.05	----
c_1	mm	Lognormal	270	0.1	50-500 (inward load) 350-800 (outward load)
c_2	mm	Lognormal	500	0.1	50-950
q	----	Lognormal	5/3	0.1	1-2
α	----	Beta [0,1]	0.5	0.25	0-1

Figure 3-5 shows the point estimate of the interaction curves for the example steel pedestal computed using the mean values of all random variables. For the outward load case the mean value for the parameter c_1 = 550 mm and the other parameters are the same as shown in Tables 3-2 and 3-3. Figure 3-5 shows that for the mean value of random variables, anchor bolt capacity controls the capacity of the example steel

pedestal when the lateral load is applied inward. When the applied load is outward, base plate capacity controls the capacity of the example pedestal. This situation may change for different geometrical values and mechanical properties. When the pedestal is subject to cyclic loads such as earthquake forces, the smallest value of inward capacity, outward capacity and base plate capacity governs the capacity of steel pedestal. For the example pedestal considered in this study, the inward load capacity governs its capacity subjected to cyclic loads but the outward load capacity and base plate capacity may govern in the other cases and thus all of those capacities should be checked to find the smallest one.

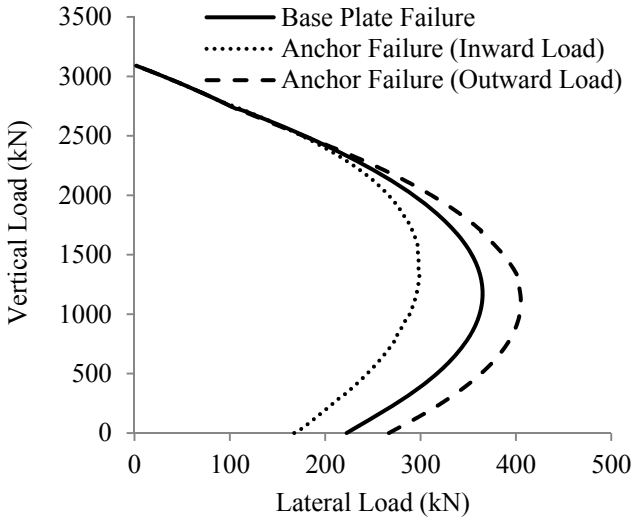

Figure 3-5. Point estimation of interaction curves for the example steel pedestal at mean values

Figure 3-6 shows the contour lines for the fragility of the example bridge steel pedestal that is the result of conducting Monte Carlo simulations with different vertical and horizontal loads with the target coefficient of variation of the failure probability estimate of 0.001. In typical simply supported bridges, the vertical forces on bearings are

usually fall within the bottom part of the Figure 3-6. Therefore, for the studied example pedestal, increasing the vertical load on the bridge decreases the failure probability of the pedestal.

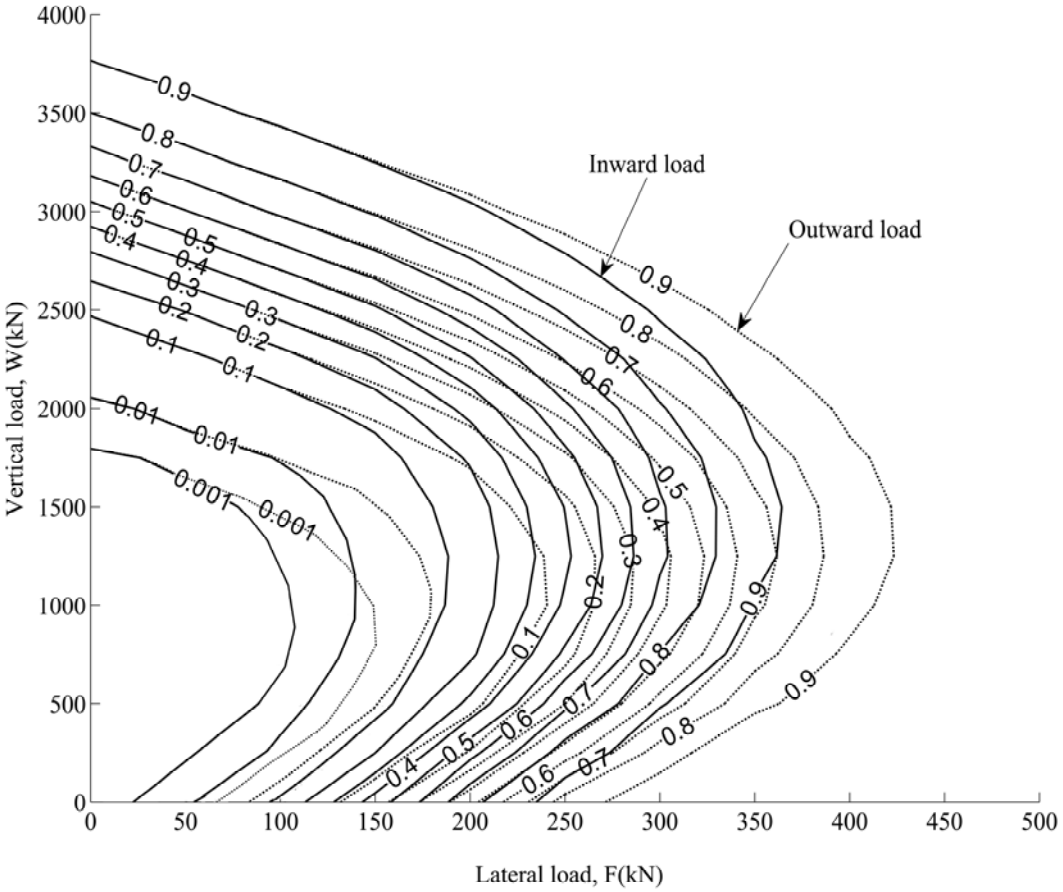

Figure 3-6. Contour lines for the fragility of the example steel pedestal

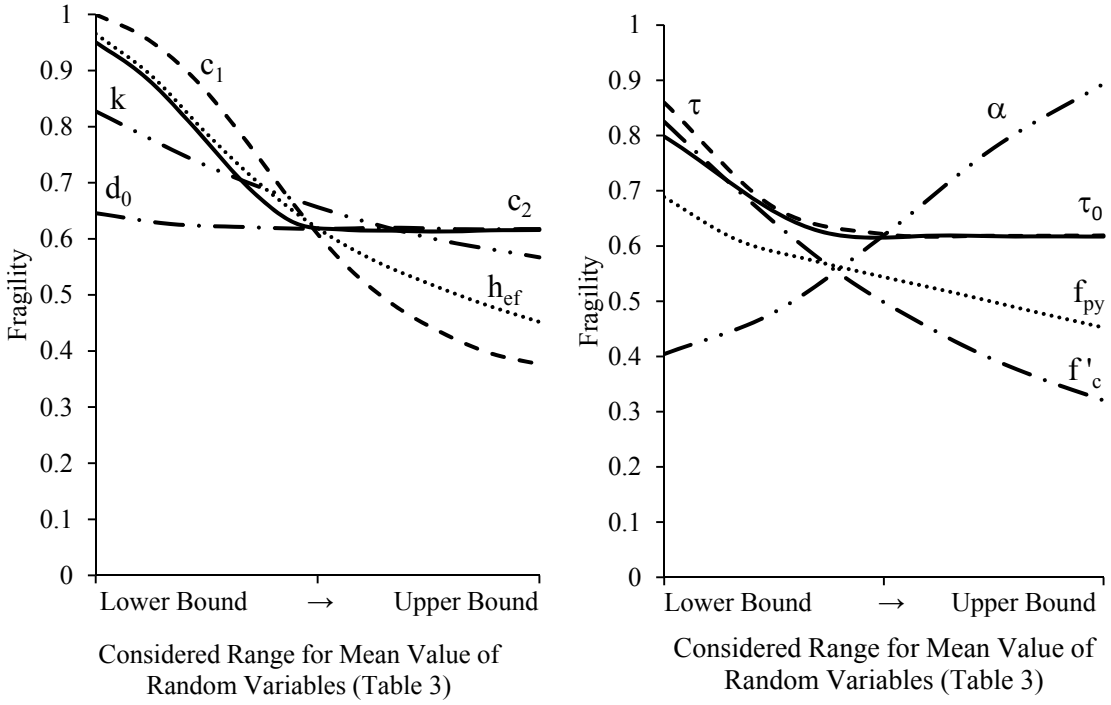

Figure 3-7. Results of the sensitivity to mean analysis for the inward load (W_D=200kN, F_D=200kN)

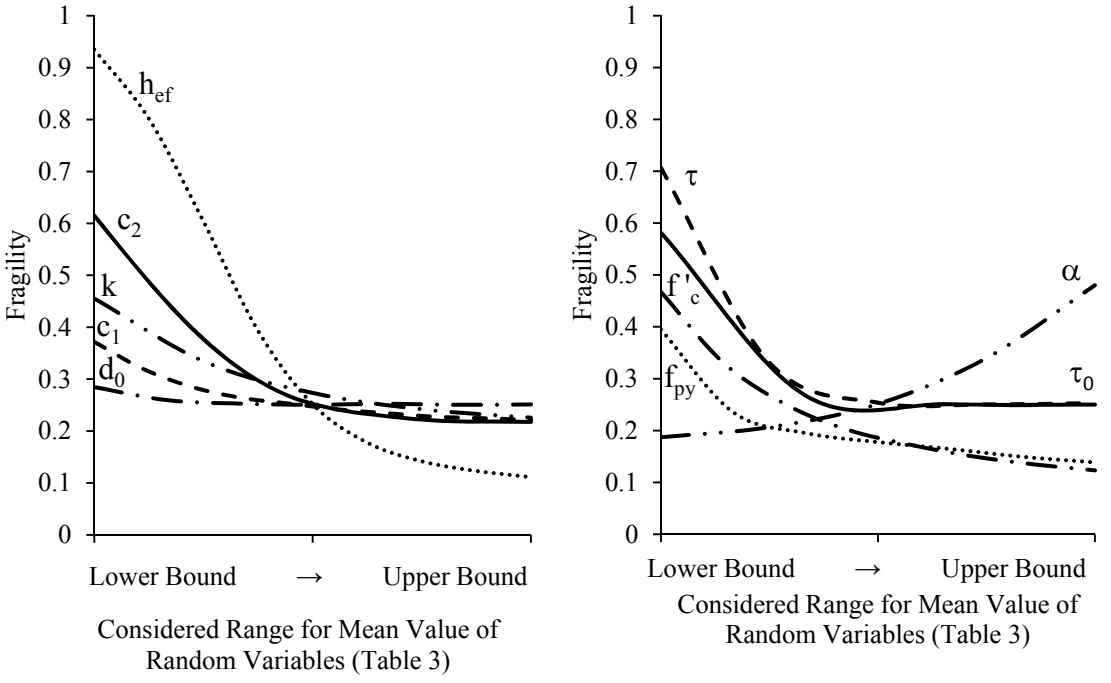

Figure 3-8. Results of the sensitivity to mean analysis for the outward load (W_D=200kN, F_D=200kN)

3.6 Sensitivity Analysis for the Example Steel Pedestal

Because of the discontinuity in the capacity models of components such as the capacity model for concrete cone breakout of anchor bolts, the limit state function for the steel pedestal system is not continuous. Therefore, First Order Reliability Method (FORM) is not applicable to estimate probability of failure of steel pedestals and Monte Carlo simulation should be used for this purpose. Thus, conventional importance and sensitivity analysis, which are based on FORM, could not be conducted for bridge steel pedestals. To investigate the effect of random variables on the failure probability in this study, mean values and C.O.V. of random variables are varied within a practical range of each random variable. Table 3-3 shows the range considered for the mean of each random variable. The C.O.V.s of random variables in the sensitivity analysis to C.O.V. is considered between 0 and 1. For each random variable, the sensitivity of fragility to changes in the mean of that random variable is investigated by changing the mean value over the considered range and calculating fragility by Monte Carlo simulation while the mean of the other random variables are constant. The same method is used to study the sensitivity of probability of failure to the C.O.V. of each random variable. The results of the sensitivity analysis to the means of random variables are shown in Figure 3-7 for the case of inward load and in Figure 3-8 for the case of outward load. A force amount of 200kN is considered for both the lateral and vertical forces in sensitivity analysis.

Figures 3-7 and 3-8 reveal that the sensitivity of steel pedestal fragility to the means of $f_c^{'}$, h_{ef} and α are more than other means for both inward and outward lateral load cases. Mean values of c_1 and c_2 are also effective parameters especially when the

mean value of these parameters take small values. The mean of d_0 does not seem to have an important effect on the fragility. The fragility is sensitive to the means of τ and τ_0 if they have small values, otherwise the fragility is not sensitive to them. Increasing the mean of q reduces the fragility but its effect is less than c_1 and h_{ef}. Figures 3-7 and 3-8 also reveal that the mean of f_{py} is not as effective as the mean of $f_c^{'}$ on the results.

To summarize, increasing $f_c^{'}$, h_{ef} and c_1 are recommended as the most effective ways to decrease the probability of failure of the studied steel pedestal. However, since steel pedestals are usually used in existing bridges, $f_c^{'}$ is known and not changeable.

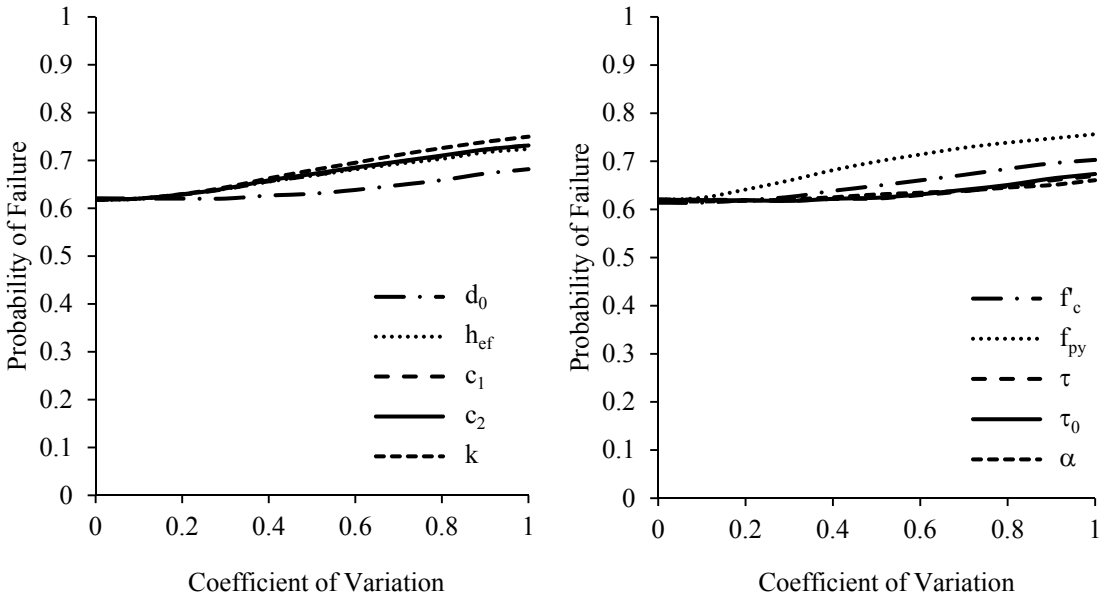

Figure 3-9. Results of the sensitivity to C.O.V. analysis for the inward load (W_D=200kN, F_D=200kN)

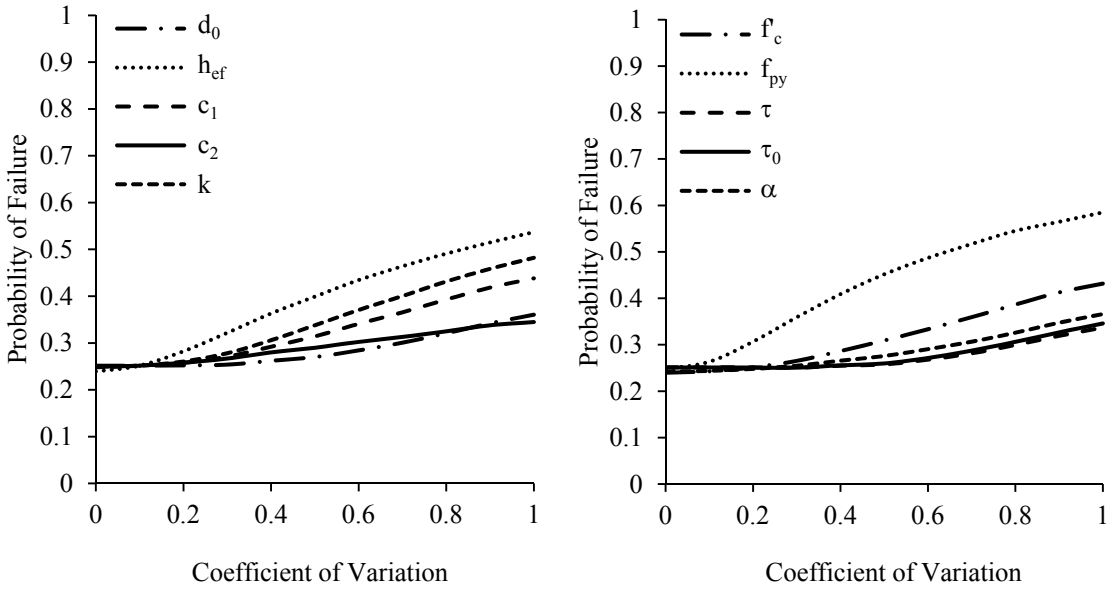

Figure 3-10. Results of the sensitivity to C.O.V. analysis for the outward load (W_D=200kN, F_D=200kN)

The results of the sensitivity analysis to the C.O.V.s of random variables are shown in Figures 3-9 and 3-10. The results of the sensitivity analysis to C.O.V.s of random variables show that for the studied example steel pedestal, the probability of failure is more sensitive to the variation of the C.O.V of f_{py}. The sensitivity of the outward capacity to the variation of C.O.V.s of random variables is more than the sensitivity of the inward capacity.

3.7 Summary and Conclusions

Steel pedestals are efficient tools to elevate bridges. Steel pedestals are composed of steel profiles that are attached to the bent beam or abutment using a base plate and anchor bolts. Currently, there are deterministic models in literature for the capacities of

steel pedestal components such as anchor bolts but there is no probabilistic model available for estimation the lateral load capacity of the steel pedestals as a whole system. This section presented probabilistic capacity models for the lateral load capacity of bridge steel pedestals. Available methods for the calculation of anchor bolt capacity and base plate connection were used and terms considering model errors added to consider inaccuracy of the models. Fragility curves for an example bridge steel pedestal with typical geometrical and mechanical properties using the proposed capacity models were developed and the sensitivity of the results to the mean value of random variables was investigated. Compressive strength of concrete under the pedestal, embedment length of anchor bolts and distribution of lateral force on the pedestal anchors were found to be the most effective random variables for the studied example steel pedestal. Increasing the embedment length and cover of anchor bolts was observed as the most effective ways to decrease the probability of failure of the studied example steel pedestal given force demands. In this section, the fragility estimations were conditioned on demands. Next section develops probabilistic demand models for bridge elevated with steel pedestals.

4. PROBABILISTIC DEMAND MODELS AND FRAGILITY ESTIMATES FOR BRIDGES ELEVATED WITH STEEL PEDESTALS*

4.1 Introduction

To estimate the fragility of bridges elevated with steel pedestals, probabilistic demand models are also required rather than the probabilistic capacity models developed in the previous section. Probabilistic demand models consider the aleatory uncertainties inherent in the loads on the bridge and epistemic uncertainties in the deterministic models that estimate the loads. A probabilistic model developing framework proposed by Gardoni et al. (2002, 2003) is employed for developing demand models. The probabilistic models are developed by adding correction terms to commonly used deterministic models. Correction terms are selected from a set of candidate explanatory functions. An error term is also added to the models that represents the randomness in the models. Bayesian updating method is used to estimate models parameters. Required data for the Bayesian updating process for estimating parameters are generated using detailed 3D nonlinear time history analyses (NTHAs) on a set of bridge configurations. Bridge configurations are selected using an experimental design to maximize the information content of the data.

The next subsection describes the NTHAs and the experimental design used to compute the seismic demand on bridges elevated with steel pedestals. Next, the

* Reprinted with permission from "Probabilistic seismic demand models and fragility estimates for bridges elevated with steel pedestals." by Vahid Bisadi, Paolo Gardoni and Monique Head, 2012, *ASCE Journal of Structural Engineering*, Accepted for publication, Copyright 2012 by ASCE.

proposed probabilistic demand models are developed. Finally, a formulation to compute fragility estimates is presented along with an illustration.

4.2 Seismic Demands on Elevated Bridges with Steel Pedestals

In order to develop probabilistic demand models for bridges elevated with steel pedestals, accurate demands from experimental tests or detailed finite element models are required. Since there are no results available from experimental tests on the seismic response of elevated bridges with steel pedestals, this study uses the results of the NTHAs on detailed 3D finite element models of bridges to develop proposed probabilistic models. This section describes the details of the finite element models used in this study and the experimental design used to generate the bridge configurations and select earthquake records used in the NTHAs.

4.2.1 Analytical Modeling

This study uses detailed 3D finite element models created in the Open System for Earthquake Engineering Simulation (OpenSees) to obtain seismic demands on bridges elevated with steel pedestals and uses those demands to develop the probabilistic models. Figure 4-1 shows the finite element model used in this study. All the nonlinearities are considered explicitly in the abutments, columns and pounding elements, as explained in further details next. The bridge decks are expected to remain elastic during the earthquake loadings and therefore are modeled with equivalent elastic beam-column elements. Rigid links at each end of the decks connect the decks to the

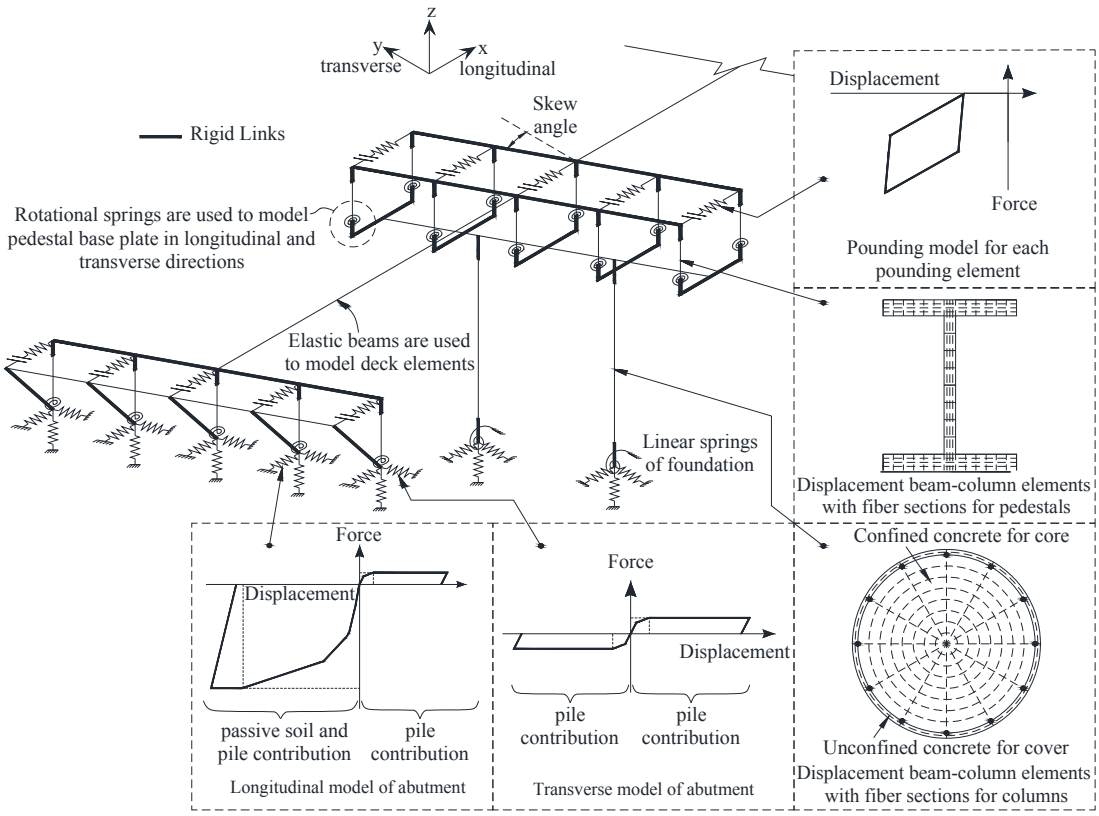

Figure 4-1. Detailed 3-D nonlinear finite element model in OpenSees

pedestals. Rigid links are also used to model the width of the cap beam, the back wall of the abutments and the distance from the bottom edge of the cap beam to its neutral axis. The bent foundations are modeled with translational and rotational linear springs. The stiffnesses of the springs are calculated based on the shear wave velocities that are considered for the models in the experimental design. The abutment model considers the contribution of the abutment backfill and piles in the longitudinal direction and only of the piles in the transverse direction. The abutment piles are modeled using a trilinear model developed by Choi (2002), and the abutment backfill is modeled using a quadrilinear model developed by Nielson and DesRoches (2006). Caltrans' (2006)

recommendations are the basis of initial stiffness values in both of those models. To model the pounding between decks and between abutments and decks, an analytical model of pounding based on Hertz Law developed by Muthukumar and DesRoches (2006) is used. This model uses a nonlinear hysteresis damper that considers the energy dissipation during the impact and can be simplified to an applicable model in OpenSees by using a gap element and a bilinear hysteretic model in series. Displacement beam-column elements with fiber sections are used to model columns and bent cap beams. Confinement effectiveness coefficients for the core areas of the columns and bent cap beams are computed based on the theoretical model developed by Mander et al. (1988) for confined concrete. Pedestals are modeled using displacement beam-column elements with fiber sections. The base plate and anchor bolts used to attach the pedestal to the cap beam or abutment are modeled using rotational springs in longitudinal and transverse directions. The stiffnesses of the rotational springs are computed based on the following formula provided by Wald et al. (2001)

$$K_r = \frac{Ez^2 t_p}{\xi} \tag{4-1}$$

where K_r = the rotational stiffness of the base plate; E = the modulus of elasticity of steel; z = the lever arm between the anchor tensile forces and concrete compressive force under the pedestal; t_p = thickness of the base plate; ξ = coefficient varying between 10 and 20. The comparison presented in Table 4-1 between the rotational stiffness produced by Eq. (4-1) and the rotational stiffness of three sample pedestals tested by Hite et al. (2008) shows that Eq. (4-1) generates good approximations of the rotational

stiffness of pedestal bases. It is assumed that the base plate of pedestals is fixed in translational degrees of freedom. The sliding of the pedestals observed by Hite et al. (2008) is not captured in this study. Determining the analytical force-displacement relationship for sliding of the base plate of pedestals requires further experimental tests.

Table 4-1. Comparison between the rotational stiffness from Eq. (4-1) and experimental results

	Rotational stiffness (kN.m/rad)	
Sample No.	Experiment	Eq. (4-1)
1	1250	1500
2	5534	6175
3	3612	3179

4.2.2 Experimental Design

This study conducts an experimental design to maximize the information content of the NTHAs and minimize the cost associated with running 3D nonlinear analyses. In the experimental design, the structural configurations are selected to cover the possible bridges that could realistically be elevated with steel pedestals. Similarly, the ground motion records are selected to cover a broad but realistic range of seismic excitations.

4.2.2.1 Structural Configurations

This dissertation uses a Latin hypercube sampling technique (McKay et al. 1979), which is a space-filling method, to generate the bridge configurations used in the analyses. Table 4-2 shows the ranges of the basic geometrical and mechanical properties used in the experimental design. All other geometrical and mechanical properties can be computed based on the basic properties. The ranges in Table 4-2 are selected such that

all realistic simply supported bridges that can be elevated with steel pedestals fit in the ranges. Therefore, the developed demand model is a general model that can be applied to all the bridges with geometrical and mechanical properties that fit within the ranges given in Table 4-2. In this study, 200 models of simply-supported bridges are generated from the experimental design.

Table 4-2. Geometrical and mechanical properties used in the experimental design

Property	Unit	Symbol	Range
Number of spans	-	N_s	1,2,3,4,5,6
Average span length	m	L	10-50
Distance between beams	m	S_b	1-4
Diameter of columns	m	D_c	0.7-2
Bridge width	m	W_b	8-30
Column height	m	h_c	3-6
Span length ratio	-	r_s	1-2
Bent cap depth	m	h_{cap}	$[0.75D_c, 1.5D_c]$
Soil Type (USGS)	-	ST	A,B,C,D
Abutment longitudinal soil stiffness	kN/mm/m	K_{al}	3-40
Abutment pile stiffness	kN/mm/pile	K_{pile}	5-10
Additional bridge dead load	%	b_m	0-100
Skew angle	°	α_b	0-60
Concrete compressive strength	MPa	f'_c	20-55
Reinforcement yield strength	MPa	f_{ry}	300-655
Girder steel yield strength	MPa	f_{by}	200-400
Gap in expansion joints	mm	L_{gap}	25-150
Longitudinal reinforcement ratio in columns	%	ρ	1-4
Transverse reinforcement ratio in columns	%	ρ_s	0.1-1.1
Column spiral pitch	mm	s_{sp}	70-400
Pedestal height	mm	h_{ped}	300-1000
Pedestal and base plate steel yield strength	MPa	f_{py}	200-400
Distance from pedestal edge to base plate edge	mm	e	50-150
Pedestal anchor bolt diameter	mm	d	10-40
Pedestal anchor bolt ultimate strength	MPa	f_u	500-800
Pedestal base plate thickness	mm	t_p	10-40
Stiffness coefficient for the base of the pedestal in Eq. (4-1)	-	ξ	10-20

4.2.2.2 Ground Motion Records

In order to develop a general model, ground motion records for the analyses should be selected such that they can cover the relevant characteristics, such as the frequency content and duration, of the possible earthquakes. This study uses the bin approach proposed by Shome and Cornell (1999) for the selection of ground motion records. The bin approach uses different bins to subdivide ground motions based on earthquake magnitude (M) and distance to the earthquake source (R). Table 4-3 shows the five bins of ground motions used in this study. To capture the variability of earthquake characteristics in each bin, 40 ground motion records are selected from the database of the Pacific Earthquake Engineering Research Center (NGA Database 1999), where half of the earthquakes in each bin are selected from ground motions recorded in sites with hard soil or rock (USGS soil types A and B) and the other half from sites with soft soil (USGS soil types C and D). Selected earthquakes are assigned to the generated bridge models for the nonlinear time history analysis. Paired ground motion records are used in each analysis, where one component of the records is applied in the longitudinal direction of the bridge and one in the transverse direction. The critical excitation angle is not used in this study because earthquakes do not always attack bridges at the critical angle and using it can result in overestimation of the failure probability (Maleki and Bisadi 2006, Bisadi and Head 2011).

In some models, drift values determined by nonlinear time history analyses are relatively large and therefore the results of those analyses cannot be completely trusted. Following Ramamoorthy et al. (2006, 2008) and Bai et al. (2011), a 5% drift in columns

is selected as the threshold for valid data points. The results of three models in this study are considered as lower bound data. In those cases, the analysis is stopped once one of the bridge columns reaches 5% drift and the drift at that column, which is equal to the threshold, is considered as the lower bound data Type I and the maximum response reached by the other demand variables up to that moment are considered as lower bound data Type II.

Table 4-3. Bins from which ground motions are selected

Bin No.	Bin characteristics	Magnitude	Distance	No. of Records
1	Large magnitude, small distance	M>6.5	13km<R<30km	40
2	Large magnitude, large distance	M>6.5	R>30km	40
3	Small magnitude, small distance	M<6.5	13km<R<30km	40
4	Small magnitude, large distance	M<6.5	R>30km	40
5	Near fault	M>6.5	R<13km	40

See Appendix A for details of ground motion records in each Bin

4.3 Development of Probabilistic Demand Models

This study uses the formulation proposed by Gardoni et al. (2002, 2003) to develop general probabilistic models. The models have the following form

$$D_{ki}\left(\mathbf{x},\boldsymbol{\theta}_{ki},\sigma_{ki}\right)=\hat{d}_{ki}\left(\mathbf{x}\right)+\gamma_{ki}\left(\mathbf{x},\boldsymbol{\theta}_{ki}\right)+\sigma_{ki}\varepsilon_{ki}\quad k=f,\delta,v\quad i=l,t \tag{4-2}$$

where $D_{ki}\left(\mathbf{x},\boldsymbol{\theta}_{ki},\sigma_{ki}\right)$= natural logarithm of normalized demand measure; k = failure mode of interest; f = pedestal force; δ = column drift; v = column shear; i = direction of the demand; l = longitudinal direction; t = transverse direction; $\mathbf{x}$ = vector of random variables such as mechanical and geometrical properties and boundary conditions; $\boldsymbol{\theta}_{ki}$ =vector of unknown model parameters; σ_{ki} = standard deviation of the model error;

$\hat{d}_{ki}(\mathbf{x})$ = natural logarithm of normalized demand predicted by a selected deterministic demand model; $\gamma_{ki}(\mathbf{x},\boldsymbol{\theta}_{ki})$ = correction terms to consider bias inherent in the deterministic demand model; and ε_{ki} = a random variable with zero mean and unit standard deviation. It is noted that D_{fl} and D_{ft} in Eq. (4-2) are natural logarithms of F_D in Eq. (3-32) in longitudinal and transverse directions, respectively.

Eq. (4-2) uses three assumptions: the homoskedasticity assumption, which requires σ_{ki} to be constant (i.e., not dependent on $\mathbf{x}$); the normality assumption, which requires ε_{ki} to follow a normal distribution; and the additivity assumption, which requires an additive model form. Using a suitable variance stabilization transformation usually helps to satisfy these assumptions (Box and Cox 1964). This study uses the natural logarithm as variance stabilization transformation for all the demands.

The correction term $\gamma_{ki}(\mathbf{x},\boldsymbol{\theta}_{ki})$ in Eq. (4-2) can be expressed in term of a set of explanatory functions as

$$\gamma_{ki}(\mathbf{x},\boldsymbol{\theta}_{ki}) = \sum_{m=1}^{p_k} \theta_{kim} h_{kim}(\mathbf{x}) \tag{4-3}$$

where $h_{ki}(\mathbf{x})$ is a suitable set of "explanatory" basis functions and p_k is the number of explanatory functions in each model.

This study considers column failures due to excessive deformation (deformation mode) and shear force (shear mode), and failure of the pedestals due to excessive lateral load. All three modes of failure are considered in both longitudinal and transverse directions.

4.3.1 Deterministic Demand Models

The Modified N2 Method developed by Gardoni et al. (2003) is used as the deterministic model to compute $\hat{d}_{ki}(\mathbf{x})$. Bilinear force-displacement curves are generated for pedestals and columns in both longitudinal and transverse directions. Nonlinear pushover analyses are conducted in the longitudinal and transverse directions. The force-displacement curves for the pedestals at each span in each direction are obtained by plotting the summation of the forces in the pedestals that support the same span versus the relative displacement of the deck to the bent cap in that direction, and then fitting bilinear curves. For the columns, the force-displacement curves are obtained by plotting the summation of the forces in the columns of each bent versus the displacement of the top of the bent and again fitting bilinear curves. Equations developed by Krawinkler and Nassar (1992) for determining the displacements of nonlinear systems are used to predict deformation demands in this dissertation. The spectral accelerations used in the equations are obtained from a design spectrum for the region where bridge is located. After obtaining deformation demands, force demand for each component can be determined using the appropriate bilinear force-displacement curve.

4.3.2 Bayesian Parameter Estimation

Mean and standard deviation of the parameters in Eq. (4-2) can be estimated using a Bayesian approach. The posterior distribution of the model parameters can be written as (Box and Tiao 1992)

$$f(\boldsymbol{\theta}_{ki}, \sigma_{ki}) = \kappa L(\boldsymbol{\theta}_{ki}, \sigma_{ki})\, p(\boldsymbol{\theta}_{ki}, \sigma_{ki}) \tag{4-4}$$

where κ = normalizing factor; $p(\boldsymbol{\theta}_{ki}, \sigma_{ki})$ = prior distribution of $\boldsymbol{\theta}_{ki}$ and σ_{ki}; $L(\boldsymbol{\theta}_{ki}, \sigma_{ki})$ = likelihood function that is proportional to the conditional probability for given values of $\boldsymbol{\theta}_{ki}$ and σ_{ki}. Following Gardoni et al. (2002), the likelihood function in the general case in which equality, lower bound and upper bound data are available can be written as

$$L(\boldsymbol{\theta}_{ki}, \sigma_{ki}) \propto \prod_{failure\,data} \left\{ \frac{1}{\sigma_{ki}} \varphi\left[\frac{\zeta(\boldsymbol{\theta}_{ki})}{\sigma_{ki}} \right] \right\} \times \prod_{lower\,bound\,data} \Phi\left[-\frac{\zeta(\boldsymbol{\theta}_{ki})}{\sigma_{ki}} \right] \times \prod_{upper\,bound\,data} \Phi\left[\frac{\zeta(\boldsymbol{\theta}_{ki})}{\sigma_{ki}} \right] \tag{4-5}$$

where $\varphi(\cdot)$ and $\Phi(\cdot)$, respectively, denote the standard normal probability density and cumulative distribution functions and $\zeta(\boldsymbol{\theta}_{ki})$ is defined as

$$\zeta(\boldsymbol{\theta}_{ki}) = D_{ki}(\mathbf{x}, \boldsymbol{\theta}_{ki}, \sigma_{ki}) - \hat{d}_{ki}(\mathbf{x}) - \gamma_{ki}(\mathbf{x}, \boldsymbol{\theta}_{ki}) \tag{4-6}$$

With the lack of any prior information about model parameters, non-informative prior distributions are used in Eq. (4-4). In this study, failure data and lower bound data are used in Eq. (4-5).

4.3.3 Model Selection

The explanatory functions in Eq. (4-3) are selected from a set of dimensionless candidate explanatory functions shown in Table 4-4. These candidate explanatory functions are created by combining based on principles of physics and mechanics the geometrical and mechanical properties defined in Table 4-2 and the ground motion intensity measures and other properties defined in Table 4-5. The indices *i* and *i*+π/2 are used to define the direction of some of the properties used in the explanatory functions in Table 4-4. Specifically, *i* indicates that the direction of the property is the same as the one of the

Table 4-4. Explanatory functions for demand models in longitudinal and transverse directions

Explanatory function	Formula	Used for
h_1	1	All models
h_2	$Ln(S_a / g)$	All models
h_3	$Ln(S_d / h_c)$	All models
h_4	$Ln(PGA / g)$	All models
h_5	$Ln(PGV \cdot T_n / h_c)$	All models
h_6	$Ln(PGD / h_c)$	All models
h_7	$Ln\left(2\pi PGV / \left(PGA \cdot T_n\right)\right)$	All models
h_8	$Ln\left(2\pi PGD / \left(PGV \cdot T_n\right)\right)$	All models
h_9	η_{sa}	All models
h_{10}	D_{soil}	All models
h_{11}	$tan\ \alpha_b$	All models
h_{12}	N_s	All models
h_{13}	N_{col}	All models
h_{14}	ER	All models
h_{15}	PR	All models
h_{16}	$Ln(r / h)$	All models
h_{17}	$Ln(L_{gap} / L)$	All models
h_{18}	$Ln(z \cos\alpha / W_b)$	All models
h_{19}	L / W_b	All models
h_{20}	$\hat{d}_{f,i}$	Pedestal models
h_{21}	$\hat{d}_{f,i+\pi/2}$	Pedestal models
h_{22}	K_{ped} / K_{base}	Pedestal models
h_{23}	$\hat{d}_{v,i}$	Column models
h_{24}	$\hat{d}_{\delta,i}$	Column models
h_{25}	$\hat{d}_{v,i+\pi/2}$	Column models
h_{26}	$\hat{d}_{\delta,i+\pi/2}$	Column models
h_{27}	K_{col} / K_f	Column models

modeled demand, and $i+\pi/2$ indicates that direction of the property is orthogonal to the direction of the modeled demand. For example, if the demand of interest is in longitudinal direction, those properties that have index i in Table 4-4 are also in the longitudinal direction and the other ones that have index $i+\pi/2$ are in transverse

direction. In Table 4-4, η_{sa} represents the number of standard deviations by which an observed logarithmic spectral acceleration differs from the mean logarithmic spectral acceleration of a ground-motion prediction equation (Baker et al. 2005). Abrahamson-Silva ground-motion prediction equation (Abrahamson and Silva 2008) is used to calculate η_{sa}.

Table 4-5. Intensity measures and other properties used to define candidate explanatory functions

Measure	Description
S_a	Spectral acceleration
S_d	Spectral displacement
PGA	Peak ground acceleration
PGV	Peak ground velocity
PGD	Peak ground displacement
T_n	Natural period of the equivalent SDOF system
η_{sa}	The number of standard deviations by which an observed logarithmic spectral acceleration differs from the mean logarithmic spectral acceleration of a ground-motion prediction equation
D_{soil}	Soil type=0,1,2,3 for soil types A, B, C and D, respectively
N_{col}	Multi-Column Ratio=0 if bents consist of single columns =1 if bents consist of multiple columns
ER	Elastic Ratio=1-(δ/ δ_y) if the SDOF system response is in elastic range =0 otherwise; δ_y is yield drift
PR	Plastic Ratio=(δ/ δ_y)-1 if the SDOF system response is in plastic range =0 otherwise
r_g	Gyration radius of columns and pedestals in column and pedestal models, respectively
h	Pedestal and column height in pedestal and column models, respectively
z_c	Distance of pedestal or column to the center of its corresponding bent or abutment
K_{ped}	Pedestal lateral stiffness
K_{base}	Pedestal base (abutment or bent) lateral stiffness
K_{col}	Bent lateral stiffness
K_f	Foundation lateral stiffness

A model selection process is used to construct accurate and parsimonious demand models that have the minimum number of explanatory functions that are needed to reach a sufficient accuracy. The "best" model with p_k explanatory functions is selected

from a set of candidate models using all possible subsets of explanatory functions that have p_k members. The "best" model is defined as the one that satisfies the selection criteria better than the other models with the same number of explanatory functions. Choosing the value of p_k is then a trade-off between simplicity and accuracy of the model because choosing a larger p_k might result in a more accurate but more complex model. In this dissertation, the adjusted R^2 (Theil 1961), Mallows' C_p (Mallows 1973) and the Corrected Akaike's Information Criterion (AICc) (Hurvich and Tsai 1989) are used as selection criteria. The adjusted R^2 and AICc capture how closely the model fits the data and C_p is used to measure potential overfitting of the data. Additional details and formulas of these model selection criteria can be found in statistical textbooks such as Burnham and Anderson (2002). For a given subset (all possible models that have the same number of explanatory functions), the model with highest adjusted R^2 or lowest C_p and AICc provides the most accurate predictions among all the models in that subset. To choose the number of explanatory functions, p_k, changes in the values of model selection criteria are monitored versus the number of explanatory functions if increasing the number of explanatory functions does not cause a significant improvement in the selection criteria, that number could be selected as p_k. Using the described procedure, the final form of the developed probabilistic demand models are

$$D_{fl}\left(\mathbf{x},\boldsymbol{\Theta}_{fl},\sigma_{fl}\right)=\left(1+\theta_{20\,fl}\right)\hat{d}_{fl}\left(\mathbf{x}\right)+\theta_{1\,fl}+\theta_{3\,fl}\ln\left(S_d/h_c\right)+\theta_{11\,fl}\tan\alpha+\sigma_{fl}\varepsilon_{fl} \qquad (4\text{-}7)$$

$$D_{ft}\left(\mathbf{x},\boldsymbol{\Theta}_{ft},\sigma_{ft}\right)=\left(1+\theta_{20\,ft}\right)\hat{d}_{ft}\left(\mathbf{x}\right)+\theta_{1\,ft}+\theta_{3\,ft}\ln\left(S_d/h_c\right)+\theta_{11\,ft}\tan\alpha+\sigma_{ft}\varepsilon_{ft} \qquad (4\text{-}8)$$

$$D_{vl}\left(\mathbf{x},\boldsymbol{\Theta}_{vl},\sigma_{vl}\right)=\left(1+\theta_{23vl}\right)\hat{d}_{vl}\left(\mathbf{x}\right)+\theta_{1vl}+\theta_{5vl}\ln\left(PGV\cdot T_n/h_c\right)+\theta_{11vl}\tan\alpha+\sigma_{vl}\varepsilon_{vl}$$

(4-9)

$$D_{vt}\left(\mathbf{x},\boldsymbol{\Theta}_{vt},\sigma_{vt}\right)=\left(1+\theta_{23vt}\right)\hat{d}_{vt}\left(\mathbf{x}\right)+\theta_{1vt}+\theta_{5vt}\ln\left(PGV\cdot T_n/h_c\right)+\theta_{13vt}N_{col}+\sigma_{vt}\varepsilon_{vt}$$

(4-10)

$$D_{\delta l}\left(\mathbf{x},\boldsymbol{\Theta}_{\delta l},\sigma_{\delta l}\right)=\left(1+\theta_{24\delta l}\right)\hat{d}_{\delta l}\left(\mathbf{x}\right)+\theta_{1\delta l}+\theta_{4\delta l}\ln\left(PGA/g\right)+\theta_{5\delta l}\ln\left(PGV\cdot T_n/h_c\right)+\theta_{11\delta l}\tan\alpha+\sigma_{\delta l}\varepsilon_{\delta l}$$

(4-11)

$$D_{\delta t}\left(\mathbf{x},\boldsymbol{\Theta}_{\delta t},\sigma_{\delta t}\right)=\left(1+\theta_{24\delta t}\right)\hat{d}_{\delta t}\left(\mathbf{x}\right)+\theta_{1\delta t}+\theta_{4\delta t}\ln\left(PGA/g\right)+\theta_{13\delta t}N_{col}+\theta_{16\delta t}\ln\left(r_g/h_c\right)+\sigma_{\delta t}\varepsilon_{\delta t}$$

(4-12)

Tables 4-6 to 4-11 show the posteriors of parameters for the models in Eqs. (4-7) to (4-12). Tables 4-12 to 4-15 show the correlation coefficients between the error terms in the different models. Figures 4-2 to 4-7 present the predicted data versus the virtual data for the deterministic and probabilistic models. For the probabilistic models, the median predicted is calculated using the point estimates for the posterior of parameters. It should be noted that in Figures 4-2 to 4-7 the demands are normalized but are not in the logarithmic scale to provide a better comparison between deterministic and probabilistic models. Dashed lines in the right charts indicate the ± 1 standard deviation

Table 4-6. Posterior statistics of the parameters in the pedestal longitudinal force model

Parameter	Mean	Standard Deviation	Correlation coefficient				
			θ_{1fl}	θ_{3fl}	θ_{11fl}	θ_{20fl}	σ_{fl}
θ_{1fl}	0.051	0.023	1.00				
θ_{3fl}	0.274	0.008	0.04	1.00			
θ_{11fl}	–0.214	0.013	–0.44	–0.06	1.00		
θ_{20fl}	–0.705	0.008	0.63	–0.67	–0.01	1.00	
σ_{fl}	0.500	0.004	–0.05	0.00	0.06	–0.02	1.00

Table 4-7. Posterior statistics of the parameters in the pedestal transverse force model

Parameter	Mean	Standard Deviation	Correlation coefficient				
			θ_{1ft}	θ_{3ft}	θ_{11ft}	θ_{20ft}	σ_{ft}
θ_{1ft}	–0.713	0.034	1.00				
θ_{3ft}	0.326	0.009	0.02	1.00			
θ_{11ft}	0.500	0.030	–0.53	–0.09	1.00		
θ_{20ft}	–0.754	0.011	0.62	–0.62	0.08	1.00	
σ_{ft}	0.621	0.006	0.01	0.04	0.00	–0.01	1.00

Table 4-8. Posterior statistics of the parameters in the column longitudinal shear model

Parameter	Mean	Standard Deviation	Correlation coefficient				
			θ_{1vl}	θ_{5vl}	θ_{11vl}	θ_{23vl}	σ_{vl}
θ_{1vl}	0.418	0.131	1.00				
θ_{5vl}	0.533	0.025	0.53	1.00			
θ_{11vl}	0.735	0.062	–0.38	0.11	1.00		
θ_{23vl}	–0.743	0.045	0.59	–0.28	–0.24	1.00	
σ_{vl}	0.514	0.018	–0.01	0.02	0.03	–0.02	1.00

Table 4-9. Posterior statistics of the parameters in the column transverse shear model

Parameter	Mean	Standard Deviation	Correlation coefficient				
			θ_{1vt}	θ_{5vt}	θ_{13vt}	θ_{23vt}	σ_{vt}
θ_{1vt}	0.879	0.125	1.00				
θ_{5vt}	0.478	0.027	0.66	1.00			
θ_{13vt}	0.369	0.062	–0.04	0.30	1.00		
θ_{23vt}	–0.668	0.045	0.41	–0.29	0.05	1.00	
σ_{vt}	0.523	0.018	0.14	0.13	–0.01	0.01	1.00

Table 4-10. Posterior statistics of the parameters in the column longitudinal drift model

Parameter	Mean	Standard Deviation	Correlation coefficient					
			$\theta_{1\delta l}$	$\theta_{4\delta l}$	$\theta_{5\delta l}$	$\theta_{11\delta l}$	$\theta_{24\delta l}$	$\sigma_{\delta l}$
$\theta_{1\delta l}$	–1.749	0.117	1.00					
$\theta_{4\delta l}$	0.352	0.040	–0.24	1.00				
$\theta_{5\delta l}$	0.599	0.052	–0.10	–0.42	1.00			
$\theta_{11\delta l}$	0.384	0.052	–0.19	–0.09	–0.08	1.00		
$\theta_{24\delta l}$	–0.776	0.045	0.59	–0.07	–0.79	0.14	1.00	
$\sigma_{\delta l}$	0.439	0.015	0.02	–0.01	0.06	0.00	–0.04	1.00

Table 4-11. Posterior statistics of the parameters in the column transverse drift model

Parameter	Mean	Standard Deviation	Correlation coefficient					
			$\theta_{1\delta t}$	$\theta_{4\delta t}$	$\theta_{13\delta t}$	$\theta_{16\delta t}$	$\theta_{24\delta t}$	$\sigma_{\delta t}$
$\theta_{1\delta t}$	–0.480	0.241	1.00					
$\theta_{4\delta t}$	0.534	0.046	–0.25	1.00				
$\theta_{13\delta t}$	0.560	0.066	0.40	0.07	1.00			
$\theta_{16\delta t}$	0.274	0.071	0.84	–0.10	0.49	1.00		
$\theta_{24\delta t}$	–0.306	0.034	0.62	–0.73	0.21	0.21	1.00	
$\sigma_{\delta t}$	0.509	0.018	0.03	–0.01	–0.01	0.02	0.02	1.00

Table 4-12. Correlation coefficients of error terms for the same pedestal

Error term	Correlation coefficient	
	ε_{fl}	ε_{ft}
ε_{fl}	1.00	
ε_{ft}	0.51	1.00

Table 4-13. Correlation coefficients of error terms for the same column

Error term	Correlation coefficient			
	ε_{vl}	ε_{vt}	$\varepsilon_{\delta l}$	$\varepsilon_{\delta t}$
ε_{vl}	1.00			
ε_{vt}	0.73	1.00		
$\varepsilon_{\delta l}$	0.01	0.03	1.00	
$\varepsilon_{\delta t}$	0.42	0.55	-0.02	1.00

Table 4-14. Correlation coefficients of error terms for different columns or pedestals on the same bent

Error term	Correlation coefficients					
	ε_{fl}	ε_{ft}	ε_{vl}	ε_{vt}	$\varepsilon_{\delta l}$	$\varepsilon_{\delta t}$
ε_{fl}	0.81 (0.72)					
ε_{ft}	0.44 (0.39)	0.56 (0.44)				
ε_{vl}	0.11	–0.09	0.85			
ε_{vt}	0.07	–0.08	0.70	0.92		
$\varepsilon_{\delta l}$	0.04	–0.08	0.02	0.09	0.41	
$\varepsilon_{\delta t}$	0.07	0.03	0.37	0.54	0.12	0.95

Numbers in parenthesis correspond to the case where two pedestals are on the same bent but carry the weight of different decks. (Two pedestals in different rows)

Table 4-15. Correlation coefficients of error terms for different columns or pedestals on different bents

	Correlation coefficients					
Error term	ε_{fl}	ε_{ft}	ε_{vl}	ε_{vt}	$\varepsilon_{\delta l}$	$\varepsilon_{\delta t}$
ε_{fl}	0.73 (0.64)					
ε_{ft}	0.38 (0.31)	0.34 (0.31)				
ε_{vl}	0.14	–0.05	0.71			
ε_{vt}	0.12	–0.04	0.59	0.66		
$\varepsilon_{\delta l}$	0.08	–0.06	0.18	0.10	0.17	
$\varepsilon_{\delta t}$	0.11	0.02	0.40	0.38	0.03	0.57

Numbers in parenthesis correspond to the case that pedestals are not the bearings of the same span.

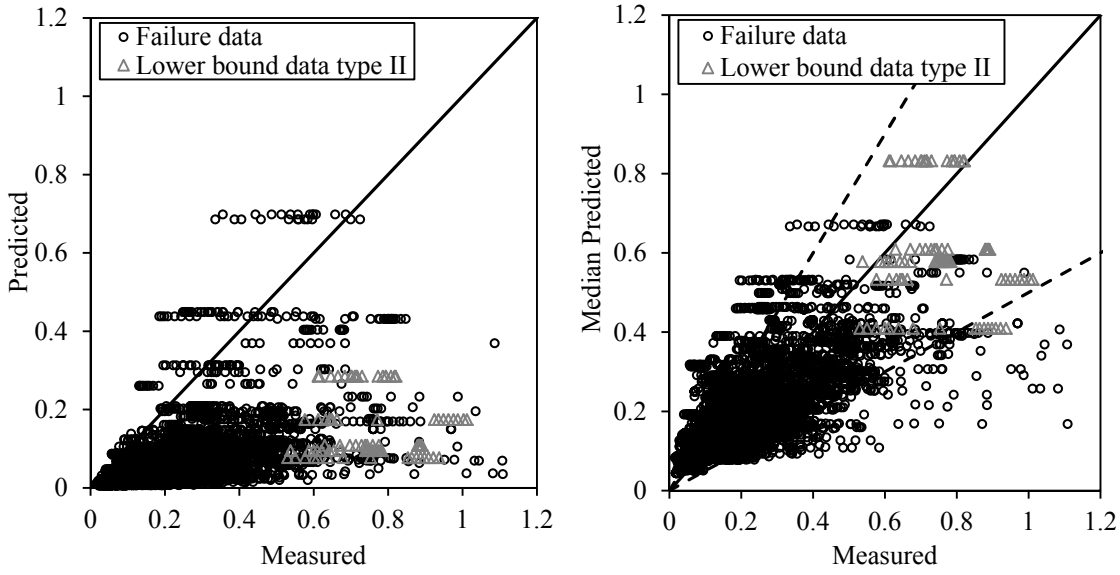

Figure 4-2. Pedestal longitudinal force demands predicted using deterministic (left) and probabilistic (right) models versus measured values from NTHA

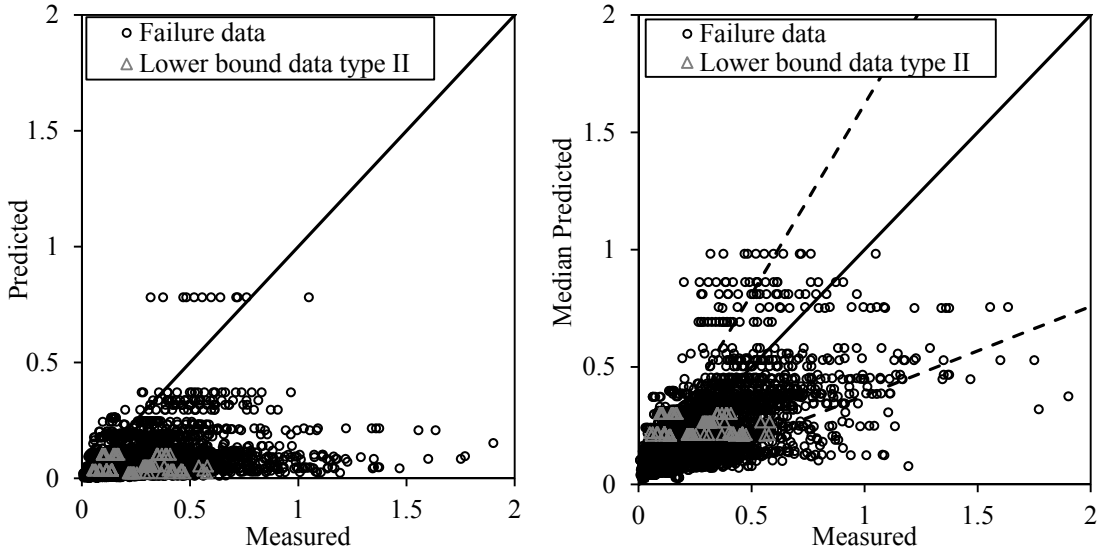

Figure 4-3. Pedestal transverse force demands predicted using deterministic (left) and probabilistic (right) models versus measured values from NTHA

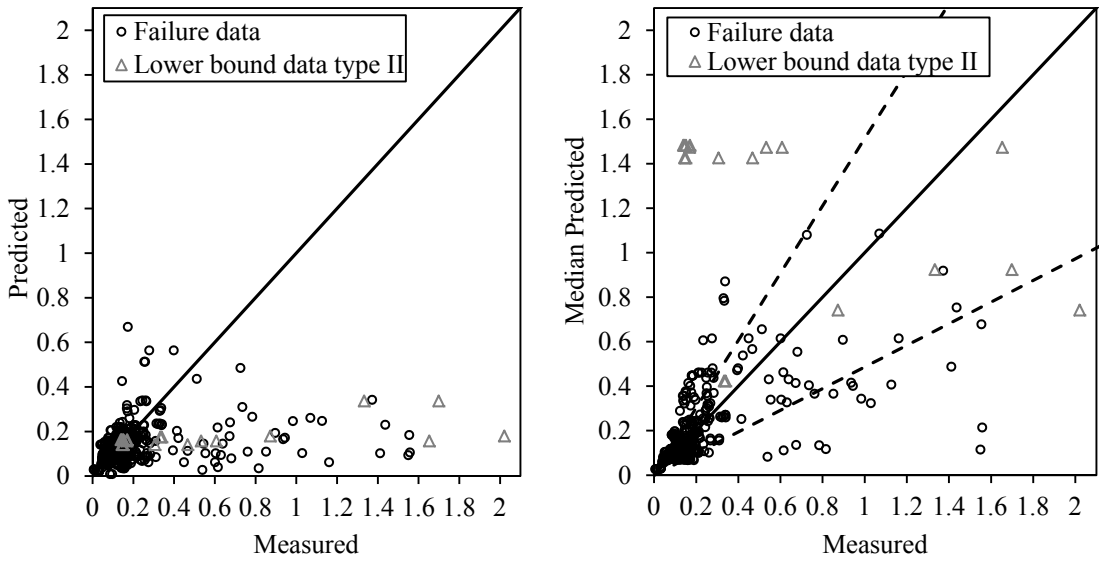

Figure 4-4. Column longitudinal shear demands predicted using deterministic (left) and probabilistic (right) models versus measured values from NTHA

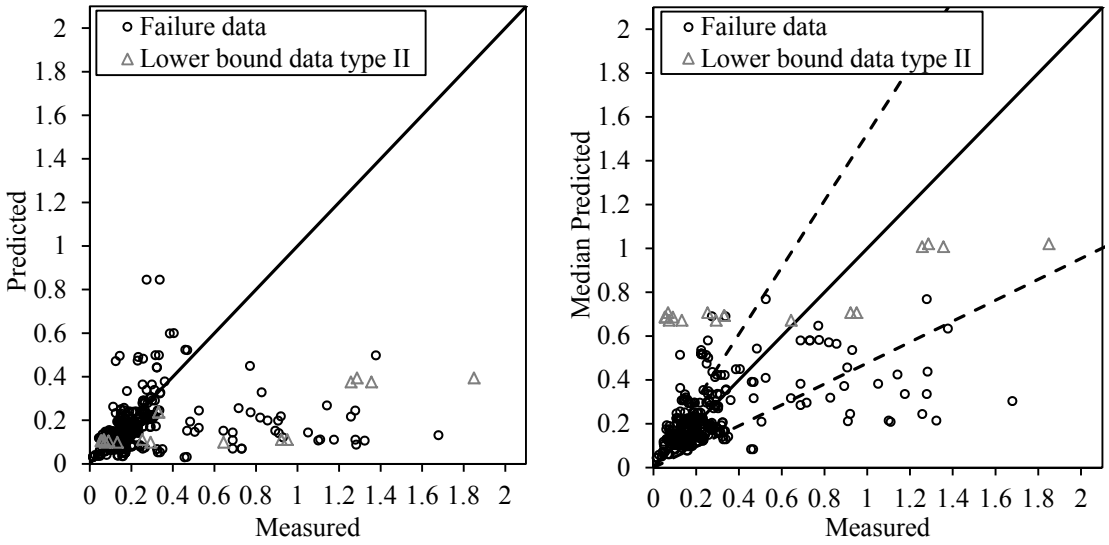

Figure 4-5. Column transverse shear demands predicted using deterministic (left) and probabilistic (right) models versus measured values from NTHA

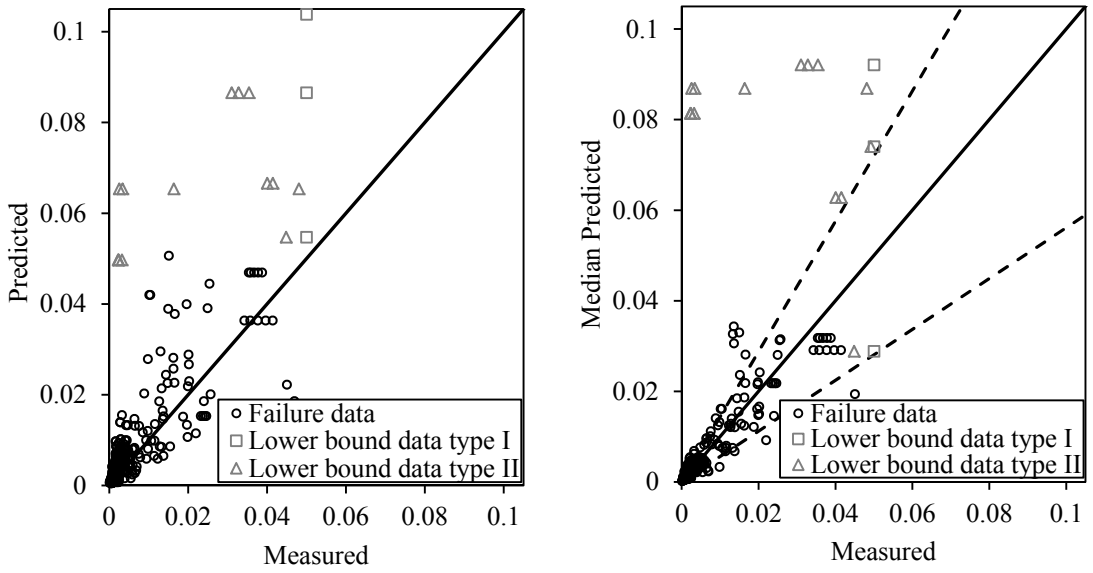

Figure 4-6. Column longitudinal drift demands predicted using deterministic (left) and probabilistic (right) models versus measured values from NTHA

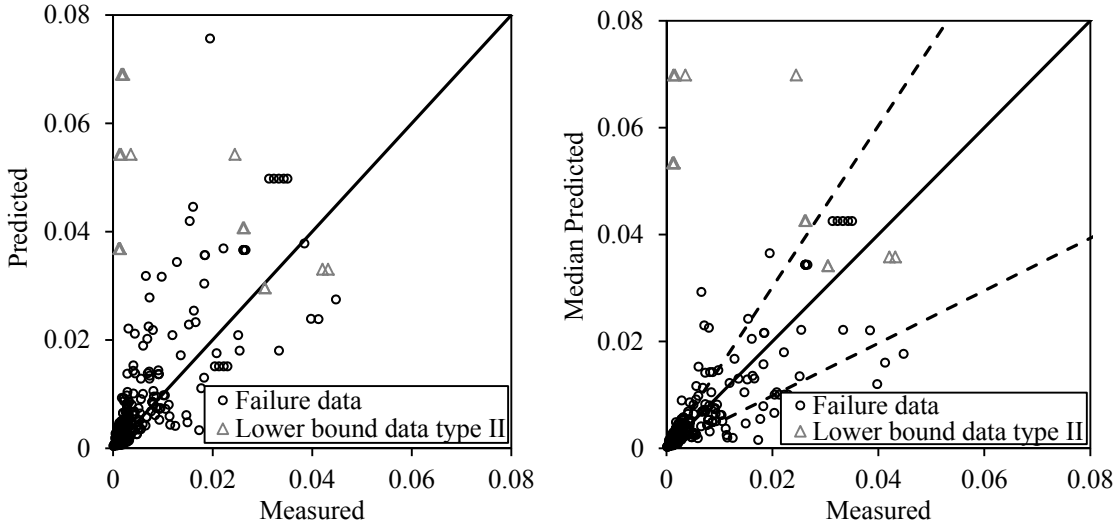

Figure 4-7. Column transverse drift demands predicted using deterministic (left) and probabilistic (right) models versus measured values from NTHA

band. As Figures 4-2 to 4-7 show, the correction terms used in the developed probabilistic models capture the bias in the deterministic model. Table 4-16 compares the mean absolute percentage error (MAPE) in deterministic models and probabilistic models. MAPE is defined as follows for the developed probabilistic models

$$MAPE = \frac{100}{N_s}\left[\sum_{j=1}^{N_s}\left(\left|\frac{\exp(\hat{d}_{ki,j}+\gamma_{ki,j})-\exp(D_{ki,j})}{\exp(\hat{d}_{ki,j}+\gamma_{ki,j})}\right|\right)\right] \tag{4-13}$$

where N_s = sample size. For the deterministic models, MAPE is defined as in Eq. (4-13) but without the correction terms $\gamma_{ki,j}$. The smaller MAPE of developed probabilistic models compared to the corresponding deterministic models reveals that the developed probabilistic models produce better predictions than their corresponding deterministic models.

Table 4-16. Mean absolute percentage errors for deterministic and probabilistic models

	MAPE	
Model	Deterministic	Probabilistic
Longitudinal pedestal force	151.96	44.76
Transverse pedestal force	208.72	68.71
Longitudinal column drift	11.29	6.81
Transverse column drift	10.42	8.23
Longitudinal column shear	122.26	68.21
Transverse column shear	118.00	64.58

4.4 Fragility Estimates

In this dissertation, the fragility of bridges elevated with steel pedestals is defined as the conditional probability that the force demands in the pedestals or the shear or deformation demands in the columns exceed their corresponding capacities for given values of the earthquake intensity measures. The demand quantities of interest are estimated using the probabilistic demand models in Eqs. (4-7) to (4-12). The probabilistic capacity models developed in section 3 are used to predict the pedestal force capacities. The shear and deformation capacities are computed based on the probabilistic capacity models developed by Choe et al. (2007) for single-curvature columns. For the calculation of the deformation capacity of multi-column bents parallel to their plane, in which the columns experience a double-curvature deformation, a simple modification proposed by Zhong et al. (2008) is applied. In the modification, it is assumed that there are inflection points at midheight of the columns, dividing the columns in two equal single-curvature portions of height equal to half of the total

column height. Therefore, the deformation capacity of the double-curvature columns is the sum of the deformation capacities of the two single-curvature portions.

If the vector of random variables, **x**, in Eq. (4-2) is partitioned into a vector of material and geometric variables, **r**, and a vector of earthquakes intensity variables, **s**, the predictive fragility of the bridges system (Gardoni et al. 2002), that considers the uncertainties in the model parameters by treating them as random variables, can be written as

$$\tilde{F}(\mathbf{s}) = P\left[\bigcup_{j=1,\ldots,p}\bigcup_{k=f,\delta,v}\bigcup_{i=l,t}\left\{g_{ki,j}(\mathbf{r},\mathbf{s},\boldsymbol{\Theta}) \le 0 \middle| \mathbf{s}\right\}\right] \tag{4-14}$$

where j=index representing the j[th] component of the bridge system; $\boldsymbol{\Theta} = \left(\boldsymbol{\Theta}_{fl}, \boldsymbol{\Theta}_{ft}, \boldsymbol{\Theta}_{vl}, \boldsymbol{\Theta}_{vt}, \boldsymbol{\Theta}_{\delta l}, \boldsymbol{\Theta}_{\delta t}\right)$;and $g_{ki,j}(\mathbf{r},\mathbf{s},\boldsymbol{\Theta})$ is the limit state function defined as

$$g_{ki,j}(\mathbf{r},\mathbf{s},\boldsymbol{\Theta}) = C_{ki,j}(\mathbf{r}) - D_{ki,j}(\mathbf{r},\mathbf{s},\boldsymbol{\Theta}), \quad j = 1,\ldots,p; k = f,\delta,v; i = l,t \tag{4-15}$$

where $C_{ki,j}(\mathbf{r})$ and $D_{ki,j}(\mathbf{r},\mathbf{s},\boldsymbol{\Theta})$ represent capacity and demand models, respectively.

In general, in cases where several limit states are considered at the same time, sampling analyses such as Importance Sampling have to be carried out to estimate the fragility of the system. Therefore, for the estimation of fragility in Eq. (4-14), Importance Sampling is used.

4.5 Illustration

As an illustration of the proposed approach, this section conducts fragility estimates for a typical two-span bridge elevated with steel pedestals. Figure 4-8 and Table 4-17 show

the configuration and properties of the example bridge. The example bridge is not designed for seismic loads to be representative of typical bridges in Southeastern United States, where the use of steel pedestals as a clearance augmentation method is more common. Importance Sampling is employed to estimate the fragility, where the unknown model parameters in the demand and capacity models are treated as random variables and point estimates of geometrical and material properties (**r**) at their mean values are used in Eq.(4-14). Because the fragilities are estimated for future earthquakes, a design spectrum is used to calculate deterministic demands instead of a real earthquake spectrum from past earthquakes. For a given PGA, the spectral accelerations of the

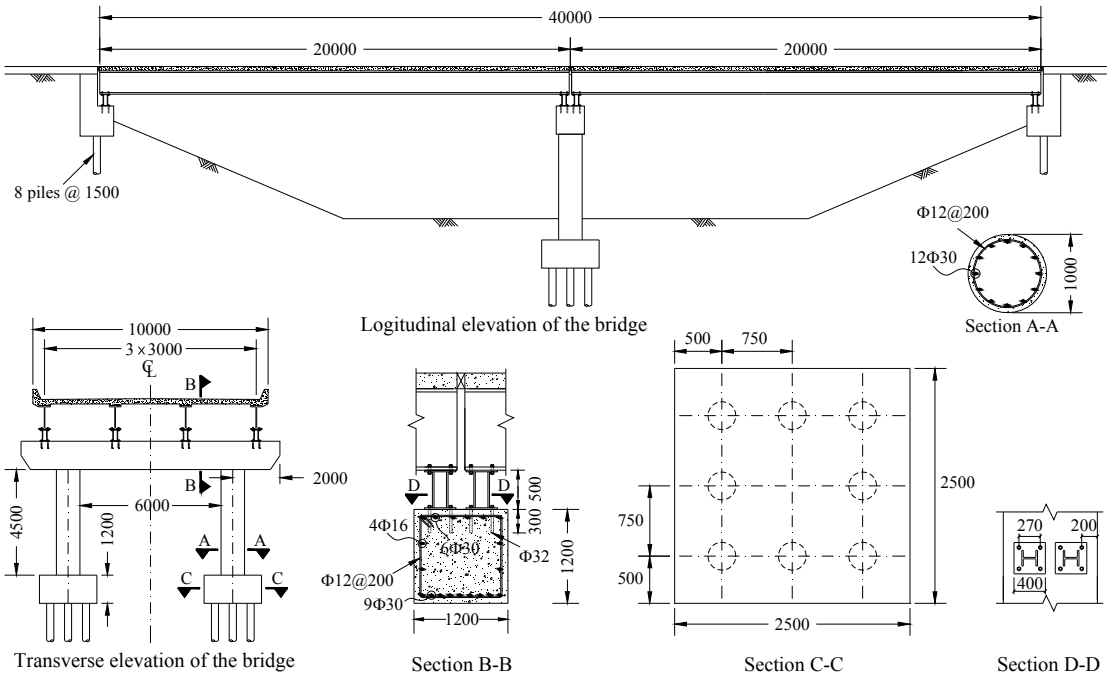

Figure 4-8. Configuration of the studied two-span bridge (Dimensions are in mm)

Table 4-17. Properties of the example bridge

Property	Value	Unit
N_s	2	-
L	20	m
S_b	3.0	m
D_c	1.0	m
W_b	10.0	m
h_c	4.50	m
r_s	1	-
h_{cap}	1.2	m
ST	B	-
K_{al}	20	kN/mm/m
K_{pile}	7.5	kN/mm/pile
β_m	20	%
α_b	0	°
f'_c	25	MPa
f_{ry}	400	MPa
f_{by}	240	MPa
L_{gap}	25	mm
ρ	1.08	%
ρ_s	0.2	%
s_{sp}	300	mm
h_{ped}	500	mm
f_{py}	240	MPa
e	100	mm
d	32	mm
f_u	517	MPa
t_p	25	mm
ξ	20	-

pedestals and columns in each direction are obtained from the design spectrum using the corresponding frequency of the equivalent SDOF system of the pedestals or columns in that direction. Spectral displacement is then computed as $S_d = S_a(T_n / 2\pi)^2$. In this way, fragility curves can be conditioned on only two intensity measures, PGV and PGA. Figure 4-9 shows the design spectrum from AASHTO LRFD Bridge Design Specifications (2010) that is used to calculate deterministic demands. The design

spectrum is a function of two quantities λ_1 and λ_s, which depend on the location of the bridge. To consider the randomness in the site seismology, λ_1 and λ_s are considered as random variables with means equal to 0.73 and 2.2 and standard deviations equal to 0.19 and 0.2, respectively. The values of means and standard deviations are calculated based

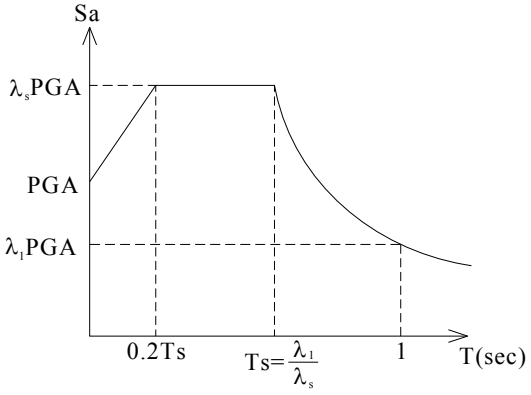

Figure 4-9. AASHTO spectrum used to calculate deterministic demands on the example bridge

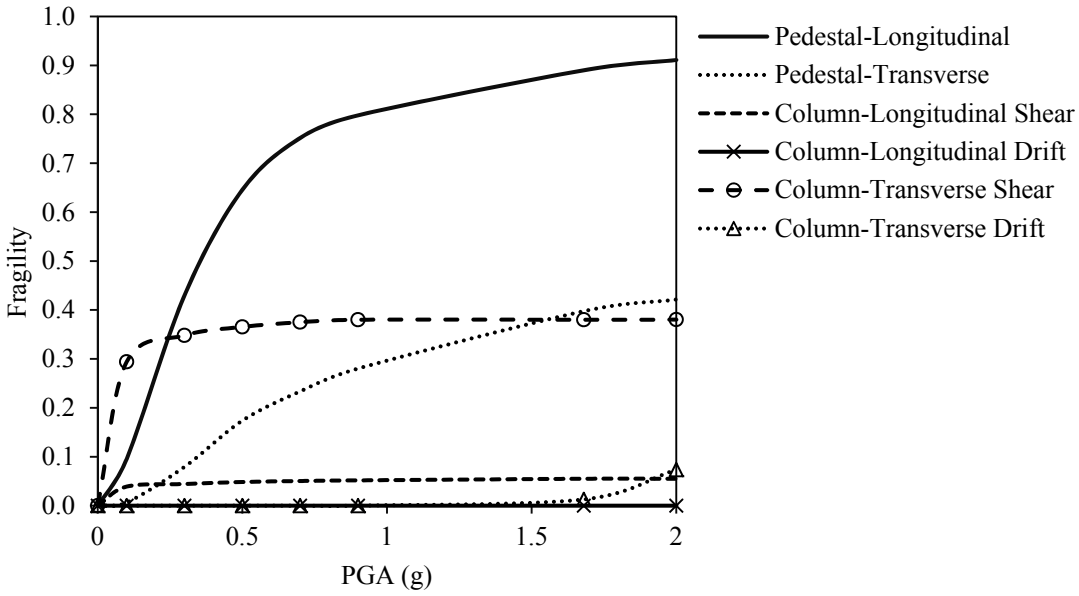

Figure 4-10. Fragility curves for different components of the example bridge for PGV=0.1 m/s

on AASHTO (2010) hazard maps for Region 4 of the United States (Southeastern United States), where the studied bridge is assumed to be located. The same spectrum is used for both longitudinal and transverse directions. Figure 4-10 shows the fragility curves for pedestals and columns in longitudinal and transverse directions for PGV=0.1 m/s. Figure 4-10 shows that pedestals of the studied bridge are more vulnerable in longitudinal direction than transverse direction, which is the result of the smaller concrete cover on the anchor bolts of the pedestals in the longitudinal direction than that value in the transverse direction. On the contrary, the columns are more vulnerable in the transverse direction due to their larger stiffness that results in more shear force. As Figure 4-10 illustrates, column failure for the studied bridge is mostly due to shear failure and failure probability due to deformation is close to zero.

Figure 4-11 shows the fragility contours for the studied bridge and its components (columns and pedestals). Fragility contours reveal that for the combination of small PGVs and large PGAs, pedestals have more contribution in bridge failure than columns but for the combination of large PGVs and small PGAs, columns have more contribution in bridge failure than pedestals. It is illustrated in Figure 4-11 by a solid grey line that separates the region governed by pedestal failure from the one governed by column failure. For example at PGV=0.1, columns have larger contribution in failure for PGA<0.22g, but pedestals have larger contribution in failure for PGA>0.22g. Considerable shear failure probability of columns shows that pedestals do not perform as seismic isolators and transfer demands to columns.

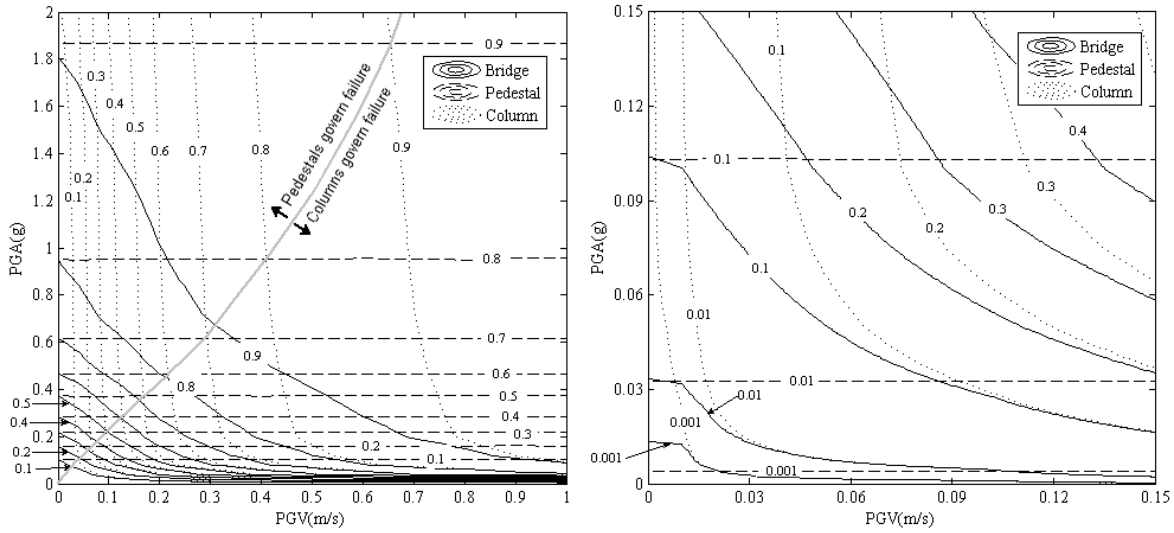

Figure 4-11. Fragility contours for the example bridge: (left) all PGAs and PGVs; and (right) small PGAs and PGVs

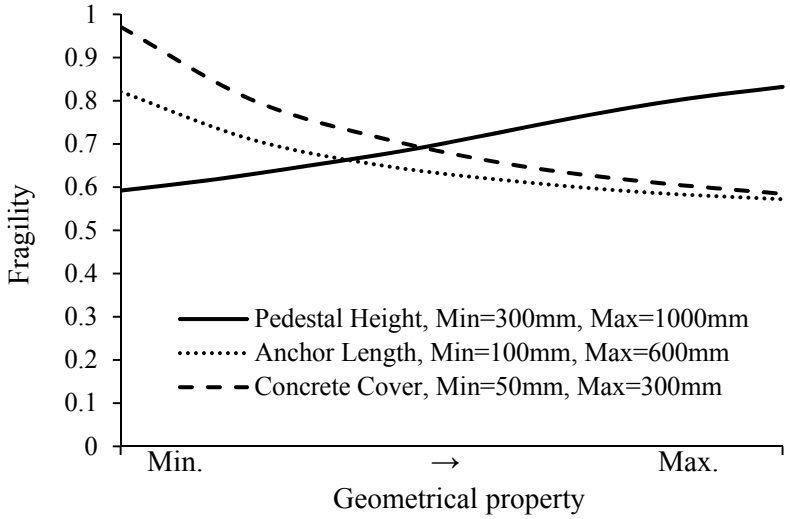

Figure 4-12. Sensitivity of the fragility to pedestal height, anchor length and concrete cover (Sensitivity of each quantity is computed while the other two quantities are fixed at values shown in Table 4-17)

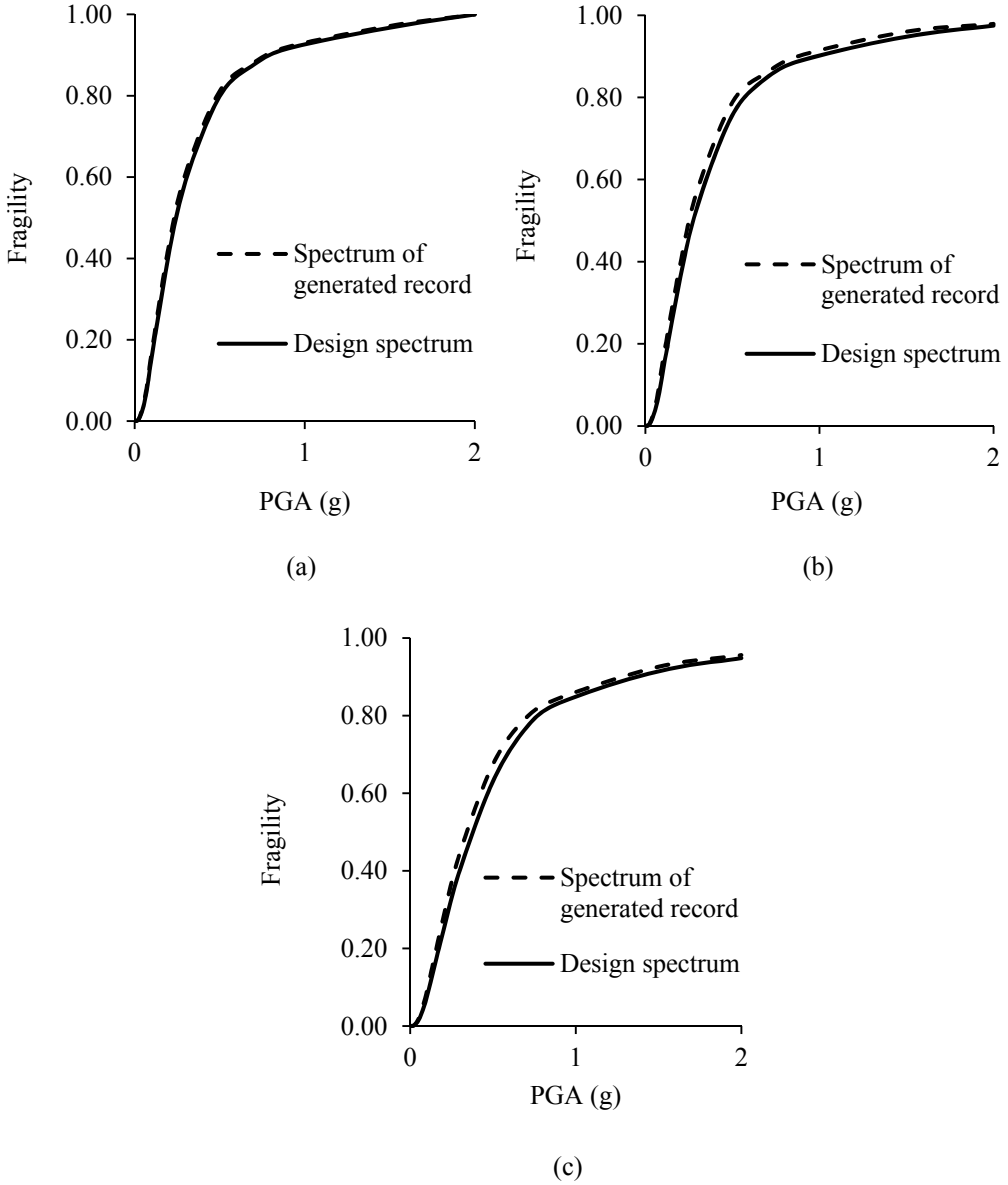

Figure 4-13. Comparison between the fragility curves using AASHTO design spectra and synthetic earthquake spectra for different locations for PGV=0.1m/s: (a) Liberty County, GA; (b) Lowndes County, GA; and (c) Charleston, SC

To investigate the effect of material and geometrical properties of the studied bridge on the probability of failure, a sensitivity analysis is conducted over all the properties used in capacity and demand models. Figure 4-12 shows the results of the

sensitivity analysis for the parameters that are more influential on the probability of failure than others, i.e. pedestal height, anchor length, concrete cover. According to Figure 4-12, decreasing pedestal height and increasing the length of anchor bolts and their concrete cover are effective ways to decrease the probability of failure. Therefore, for such a bridge, it is recommended that steel pedestals should not be used with heights more than required for bridge augmentation and maximum possible anchor length and concrete cover should be used to install them.

To check the accuracy of using design spectra instead of real earthquake spectra, the fragility curves of the example bridge are compared using AASHTO (2010) spectra and three earthquake spectra from synthetic earthquakes generated by Fernandez (2007) for Southeastern United States (Liberty and Lowndes Counties in Georgia and Charleston, South Carolina). Figure 4-13 shows the results of this comparison that implies that using the design spectra instead of real earthquakes does not have significant effects on fragility curves.

4.6 Conclusions

This section developed probabilistic seismic demand models for bridges elevated with steel pedestals. Failure due to lateral force for the pedestals and shear and deformation failure modes of columns were considered in longitudinal and transverse directions. An experimental design was conducted to generate 200 bridge configurations for generating detailed 3D finite element models used in nonlinear time history analyses. The results of nonlinear time history analyses were considered as virtual data to estimate parameters in

probabilistic models. To facilitate the use of the developed probabilistic models, they were constructed by adding correction terms to the modified N2 method, which is a nonlinear static analysis method and can be easily applied to all bridges. Correction terms were selected from a set of candidate explanatory functions using statistical model selection methods. Parameters in the probabilistic models were assessed by a Bayesian updating approach.

As an illustration, the fragility curves for a typical two-span simply supported bridge were estimated using developed probabilistic demand models and previously developed probabilistic capacity models. Importance Sampling was employed to estimate fragility curves. The studied bridge was not designed for seismic loads in order to represent the situation of a large number of bridges in Southeastern United States, where using steel pedestals to elevate bridges is more common. Fragility contours of the example bridge were provided over PGA and PGV. Also, the fragility curves for bridge components were provided versus pseudo acceleration of ground motion. Fragility curves showed that the studied bridge is vulnerable to seismic loads and has considerable failure probability even in small PGAs. Considerable failure probability of columns of the example bridge suggested that steel pedestals did not perform as seismic isolators and transformed the seismic loads from the deck to columns.

The results showed that the pedestals of the studied bridge are more vulnerable in longitudinal direction than transverse direction. It is because of the less concrete cover on the anchor bolts of pedestals in the direction of the load when the load is applied in longitudinal direction. As opposed to pedestals, columns of the studied bridge showed

larger failure probability in transverse direction than longitudinal direction, which is the effect of larger stiffness of the columns in transverse direction that produces larger shear forces. The results showed the pedestals of the studied bridge have more contribution in bridge failure than columns at the combination of small PGVs and large PGAs.

The sensitivity analysis of fragility to various design parameters showed that failure probability is more sensitive to pedestal height, anchor bolt length and concrete cover on anchor bolts. Therefore, decreasing the height of the pedestal, increasing anchor bolt lengths and concrete cover are recommended in the design of pedestals to decrease their failure probability. It should be noted that this section developed probabilistic demand models based on the load capacity of the steel pedestals. As the height of the pedestals increases, the stability of the pedestals becomes an important issue that should be investigated separately.

5. DECISION ANALYSIS FOR ELEVATING BRIDGE DECKS WITH STEEL PEDESTALS

5.1 Introduction

Deciding whether to elevate a bridge with steel pedestals and choosing the optimal height of the pedestals that should be used to elevate a bridge are challenging tasks for engineers because increasing the height of pedestals has relatively high construction costs and as shown in section 4, while it decreases the probability of vehicular impact to the bridge, it can also increase the probability of bridge damage or failure due to seismic loads. The answer is in the optimal tradeoff that minimizes the expected life-cycle cost that considers both vehicular impacts and seismic events. Therefore, there is still a need for a general framework that assists decision-makers determining if the installation of steel pedestals is beneficial and, if so, providing the optimum height of pedestals.

As such, this section develops a formulation for decision analysis for elevating bridges with steel pedestals. The proposed framework uses probabilistic models to estimate the expected costs associate to vehicular impacts and seismic loads, properly incorporating the relevant aleatory and epistemic uncertainties. As an illustration, the proposed approach is implemented considering different bridge locations to investigate the influence of the different seismological characteristics on the optimal solution.

This section is divided into six subsections. After this introduction, the following two subsections develop models for the estimation of the expected cost associated with vehicular impact and seismic loads, respectively. Then, based on the developed models

for expected costs, a framework is proposed for decision analysis. The last two subsections present the illustration of the developed approach and conclusions.

5.2 Expected Cost of Damage or Failure Due to Vehicular Impact to Bridge Decks

The annual probability that a specific bridge deck is impacted by an overheight vehicle , $P(VI)$, is needed to estimate the expected life-cycle cost of the bridge. Using the Total Probability Rule (Ang and Tang 2006), $P(VI)$ can be written as

$$P(VI) = \int_{h_v} P(VI|h_v) f(h_v)\, dh_v \tag{5-1}$$

where h_v = a random variable with probability density function $f(h_v)$ that represents the height of the vehicles passing underneath the bridge; and $P(VI \mid h_v)$ = the conditional probability of vehicular impact given the h_v that can be expressed as

$$\begin{aligned} P(VI|h_v) &= 0 \quad \text{if } h_v < h_b \\ &= 1 \quad \text{if } h_v \geq h_b \end{aligned} \tag{5-2}$$

where h_b = the vertical clearance of the bridge. Ideally, $f(h_v)$ should be defined using statistical data collected from the field. Fu et al. (2004) summarized data from the literature and their own investigation related to vehicle collisions for the bridge network in the state of Maryland. According to Fu et al. (2004), 20% of the bridges in the studied network are impacted by vehicles during their service life. Fu et al. (2004) also suggested that an increase of 0.3 m in h_b would halve the probability of vehicular impact

to bridge decks. In this section, to model the reduction in the $f(h_v)$ as h_v increases, we propose the following form for $f(h_v)$

$$\begin{aligned} f(h_v) &= f_0(h_v) && \text{if } h_v < h_{b\min} \\ &= \frac{a\lambda}{T}\exp\left[-\lambda\left(h_v - h_{b\min}\right)\right] && \text{if } h_v \geq h_{b\min} \end{aligned} \tag{5-3}$$

where $h_{b\min}$ = minimum bridge vertical clearance in the network; a = the fraction of the bridges in the studied network that are impacted by vehicles during their service life; λ = the parameter of the exponential distribution; and T = the service life of the bridge. The first part of Eq. (5-3) for $h_v < h_{b\min}$ describe the likelihood of passing of vehicles that are lower than $h_{b\min}$. However, by replacing Eq. (5-2) in Eq. (5-1), it can be seen that $f_0(h_v)$ does not contribute to $P(VI)$, because $f_0(h_v)$ is multiplied by zero. The second part of Eq. (5-3) defined for $h_v \geq h_{b\min}$ is the Probability Density Function (PDF) of a shifted exponential distribution that is constructed so that the probability of impact over the time T is equal to a. As per the observation in Fu et al. (2004), a should be equal to 0.2. By replacing Eqs. (5-2) and (5-3) into Eq. (5-1), the probability of vehicular impact can be written as

$$P(VI) = \int_{h_b}^{\infty} f(h_v)\, dh_v \tag{5-4}$$

In order to satisfy the conclusions made by Fu et al. (2004), that says the probability of vehicular impact for a bridge with height h_b is twice as the probability of vehicular impact for a bridge with height $h_b + 0.3$, the following equation can be written

$$\int_{h_b}^{\infty} f\left(h_v\right) dh_v = 2\int_{h_b+0.3}^{\infty} f\left(h_v\right) dh_v \tag{5-5}$$

Solving Eq. (5-5) results in a value of $\ln(2)/0.3 = 2.31$ for the parameter λ. The area under the second part of Eq. (5-3), is a/T that gives $P(VI) = a$.

The parameter λ can be updated in case any future study provides additional data about the impact of overheight vehicles. Following Box and Tiao (1992), the posterior PDF of λ, $f''(\lambda)$, can be obtained using the Bayesian updating rule as

$$f''\left(\lambda\right) = \Omega L\left(\lambda\right) f'\left(\lambda\right) \tag{5-6}$$

where Ω= a normalizing factor; $L(\lambda)$= the likelihood function that represents the information from the additional data; and $f'(\lambda)$= the prior distribution of λ (prior to obtaining the additional data). Conjugate distributions (Ang and Tang 2006) can be used to conveniently update the estimate of λ. If $f'(\lambda)$ is assumed to follow a Gamma distribution with mean k'/ν' and standard deviation $\sqrt{k'/\nu'^2}$, where k' and ν' are the parameters of the prior gamma distribution, at the presence of n_d new data for heights $(h_{v1}, h_{v2}, \ldots, h_{vn})$ then $f''(\lambda)$ follows again a gamma distribution with the following updated mean and standard deviation

$$\mu''\left(\lambda\right) = \frac{k' + n_d}{\nu' + \sum_{i=1}^{n_d}\left(h_{vi} - h_{b\min}\right)} \tag{5-7}$$

$$\sigma''\left(\lambda\right) = \sqrt{\frac{k' + n_d}{\left[\nu' + \sum_{i=1}^{n_d}\left(h_{vi} - h_{b\min}\right)\right]^2}} \tag{5-8}$$

Using a point estimate of parameter λ equal to its mean value and replacing Eq. (5-3) into Eq. (5-4), $P(VI)$ can be written as

$$P(VI) = \frac{a}{T}\exp\left[-\hat{\lambda}\left(h_b - h_{b\min}\right)\right] \tag{5-9}$$

where $\hat{\lambda}$ = point estimate of λ (e.g., its posterior mean). According to Fu et al. (2004), both the height of bridges and height of vehicles that pass under the bridges depend on the type of bridge network. For example, the minimum bridge height in a rural bridge network might be 4m and in an interstate highway bridge network might be 5m. Similarly, the height of vehicles that travel in an interstate highway network is also typically higher than in a rural bridge network. Therefore, the probability of vehicular impact is larger for a bridge in an interstate highway network than a bridge with the same height in a rural network. The term $h_{b\min}$ in Eq. (5-9) captures the effect of the bridge network type on the probability of vehicular impact.

According to Fu et al. (2004), 1/2 of the vehicular impacts to bridge decks result in superficial scrapes and gouges, 1/3 of them cause minor damage (minor bends, tears or cracks that do not need immediate repairs) and 1/6 of them result in severe damage (any damage for which repairs are necessary) or failure. Therefore the average cost of a vehicular impact can be written as

$$C_{VI} = \frac{1}{2}C_{SC} + \frac{1}{3}C_{MD} + \frac{1}{6}C_{SD} \tag{5-10}$$

where C_{SC} = the cost of repairing scrapes; C_{MD} = the cost of repairing minor damage; and C_{SD} = the cost of repairing severe damage or failure. Using Eqs. (5-9) and (5-10) along

with the equation proposed in NCHRP12-43 (2003) to compute the present value of the costs with constant annual values over time, the expected contribution to the life-cycle cost of a bridge that comes from the potential damage or failure associated with vehicular impacts can be expressed as

$$E\left[NPV\left(C_{VI}\right)\right]=\frac{1}{5T}\exp\left[-\lambda\left(h_b-h_{b\min}\right)\right]\left(\frac{1}{2}C_{SC}+\frac{1}{3}C_{MD}+\frac{1}{6}C_{SD}\right)\left[\frac{(1+r)^{(T-t_s)}-1}{r(1+r)^{(T-t_s)}}\right] \quad (5\text{-}11)$$

where, $E(\cdot)$ = the expected value; $NPV(\cdot)$ = the net present value; r = the discount rate; and t_s = the number of years of service completed. Therefore, $(T-t_s)$ is the time horizon in years (i.e., the remaining service life of the bridge.)

5.3 Expected Cost of Damage or Failure Due to Seismic Loads

Similar to the case of vehicular impact, the annual probability of damage or failure due to earthquakes (event indicated as FE) is expressed as follows

$$P\left(FE\right)=\int_{\mathbf{IM}}P\left(FE\middle|\mathbf{IM}\right)f\left(\mathbf{IM}\right)d\mathbf{IM} \quad (5\text{-}12)$$

where $\mathbf{IM}$ = vector of variables that represent intensity measures of the earthquake with distribution $f\left(\mathbf{IM}\right)$; and $P\left(FE\middle|\mathbf{IM}\right)$ = the probability of bridge damage or failure conditioned on $\mathbf{IM}$ generally known as fragility (Gardoni et al. 2002). The fragility of bridges elevated with steel pedestals can be estimated for given intensity measures peak ground acceleration (PGA) and peak ground velocity (PGV) using the models proposed in Section 4. The distributions of PGA and PGV depend on the location of the bridge. Annualized seismic hazard curves for different regions throughout the United States are

available from the United States Geological Survey (USGS), where past earthquakes, deformation of the earth crust, seismic attenuation relationships and geological site conditions are used to generate hazard curves for each location (Frankel et al. 2002). Alternatively, the open source program OpenSHA (Field et al. 2005) can be used for the hazard analysis.

The seismic hazard function of an intensity measure IM, $G(IM)$, is defined as the expected annual frequency of experiencing an intensity measure equal to or greater than IM. Using the hazard function for a location and assuming the occurrence of earthquakes follows a Poisson's process (Frankel et al. 2002), the annual probability density of IM at a bridge site, $f(IM)$ can be written as a function of $G(IM)$ as follows:

$$f(IM) = \exp\left[-G(IM)\right]\left[-\frac{dG(IM)}{dIM}\right] \tag{5-13}$$

Kumar and Gardoni (2012) proposed the Second-Order Logarithmic Formulation (SOLF) for hazard curves and also a closed-form approximation to the annual failure probability that can be used to compute $P(FE)$ without computing the integral in Eq. (5-12). However, the method developed by Kumar and Gardoni requires writing the limit state function in a closed-form. This is typically possible in component reliability analysis (i.e., when there is only one limit state function.) However, in this study, there are several limit state functions each capturing a possible mode of failure. Therefore, we cannot take advantage of the simplification offered by Kumar and Gardoni and the multi-fold integral in Eq. (5-12) should be computed numerically.

Eqs. (5-12) and (5-13) along with the present-value equation for the costs with constant annual values over time proposed by NCHRP12-43 (2003), are employed to estimate the expected present-value cost of bridge damage or failure due to seismic loads as follows

$$E\left[NPV\left(C_{FE}\right)\right] = P\left(FE\right)C_{FE}\left[\frac{(1+r)^{(T-t_s)}-1}{r(1+r)^{(T-t_s)}}\right] \tag{5-14}$$

where C_{FE} = the cost of bridge damage or failure subject to earthquake loads.

5.4 Decision Analysis Framework for Using Steel Pedestals to Elevate Bridges

Optimal decisions about whether to elevate a bridge using steel pedestals and the optimum height of the pedestals that should be used require conducting a life-cycle cost analysis (LCCA). There are several frameworks proposed for the LCCA of structures and optimization of management strategies. Studies conducted by Wen (2001), Stewart and Val (2003), Kong and Frangopol (2004), Val (2005), Kumar et al. (2009), Padgett et al. (2010) and Kumar and Gardoni (2012) provide examples of such frameworks. Following Kumar et al. (2009), the expected life cycle cost (LCC) of a bridge is expressed as

$$LCC = E\left[C_C\right] + E\left[NPV\left(C_{IN}\right)\right] + E\left[NPV\left(C_M\right)\right] + E\left[NPV\left(C_D\right)\right] \tag{5-15}$$

where C_C = initial construction cost; C_{IN} = cost of inspections; C_M = cost of routine maintenance; and C_D = cost of damage or failure that can be written as follows

$$E\left[NPV\left(C_D\right)\right] = E\left[NPV\left(C_{VI}\right)\right] + E\left[NPV\left(C_{FE}\right)\right] \tag{5-16}$$

where $E\left[NPV\left(C_{VI}\right)\right]$ and $E\left[NPV\left(C_{FE}\right)\right]$ can be obtained using Eq. (5-11) and Eq. (5-14), respectively. To find the optimum height of pedestals that results in the minimum expected life cycle cost of the bridge, it is assumed that the first three terms in Eq. (5-15) i.e. $E\left[C_C\right]$, $E\left[NPV\left(C_{IN}\right)\right]$ and $E\left[NPV\left(C_M\right)\right]$ do not depend on the height of pedestals. Therefore, the optimum height of pedestals is the height that minimizes $E\left[NPV\left(C_D\right)\right]$ in Eq. (5-15).

Once the optimum height of pedestals is obtained by minimizing Eq. (5-16), then its corresponding $E\left[NPV\left(C_D\right)\right]$ plus the installation cost of pedestals should be compared to the $E\left[NPV\left(C_D\right)\right]$ before the installation of pedestals to check if the installation of pedestals has financial justification or not. To make a fair comparison, the broader societal benefits of bridge elevation should also be considered. In other words installation of steel pedestals has financial justification if the following condition is satisfied

$$\zeta_p = \frac{E\left[NPV\left(C_D\right)\right]'}{E\left[NPV\left(C_D\right)\right]'' + E\left(C_{INST}\right) - E\left(B_{SB}\right)} > 1 \tag{5-17}$$

where $E\left[NPV\left(C_D\right)\right]'$ = expected cost of damage or failure before the installation of pedestals; $E\left[NPV\left(C_D\right)\right]''$ = expected cost of damage or failure after the installation of pedestals; $E\left(C_{INST}\right)$ = expected cost of installation; and $E\left(B_{SB}\right)$ = expected societal benefits of elevating bridge other than decreasing the probability of damage or failure

due to vehicular impacts. These broader societal benefits include eliminating the need for rerouting overheight vehicles and costly passive or active warning systems, and impact absorbers (Sharma et al. 2008). Murphy and Gardoni (2006) developed an approach to quantify the broader societal consequences of natural and man-made hazards. This approach could be used to determine the broader societal benefits of elevating the bridge. However, this is outside of the scope of this study. Next, the proposed framework is illustrated by applying it to a typical bridge.

5.5 Illustration of the Developed Framework

A typical two-span slab-on-girder bridge shown in Figure 4-8 is considered to illustrate the proposed framework. It is assumed that the lifetime of the bridge is $T = 75$ years from which 50 years are left ($t_s = 25$ years) and the bridge is a part of a network in which the minimum vertical clearance of bridges is $h_{b\min} = 4.3m$. The value of the discount rate, r, is needed to estimate the expected present-value cost of vehicular impact to the studied bridge using Eq. (5-11). Since there is not a generally accepted procedure for determining the discount rate for infrastructure systems, a typical discount rate of 0.05 is used in this study. Following Stewart and Val (2003) and Kumar et al. (2009), it is assumed that the cost of severe damage or failure of the bridge including all direct and indirect costs for the owner and users is 10 times the construction cost. Therefore, the value of $10C_C$ for both C_{SD} and C_{FE} is used in Eqs. (5-11) and (5-14), respectively. The cost of repairing scrapes, C_{SC}, is considered to be $0.001C_C$ and the cost

of repairing minor damage, C_{MD}, is considered to be $0.2C_C$. To investigate the effect of the location of the bridge on the optimal decision, eight different locations in the United States are considered. Table 5-1 shows the considered locations and their corresponding PGA with a return period of 1,000 years obtained, $PGA_{1,000}$, from USGS curves (Frankel et al. 2002). Five locations are considered in the Southeastern United States, where the use of steel pedestals to elevate bridges is more common and three locations are considered in the Western United States where the seismic hazard is the most important one compared to other hazards. For the considered locations in the Western United States, Los Angeles and San Francisco in California represent high seismic regions and Yuma in Nevada represents a moderate seismic region. The annual probability of failure of the example bridge due to earthquake is estimated using Eq. (5-12) for each location, where the seismic fragility of the bridges is obtained using the method presented in Section 4. Considering heights for the steel pedestals varying from 0.3 to 1.0m, Figure 5-1 compares the annual probability of damage or failure of the example bridge due to seismic loading in each location with the annual probability of damage or failure due to

Table 5-1. Locations considered for the studied bridge

Region	Location	PGA with return period of 1,000 years
Southeastern United States	Lowndes, GA	0.0322
	Bartow, GA	0.0714
	Liberty, GA	0.0755
	Fort Payne, AL	0.1109
	Charleston, SC	0.1934
Western United States	Yuma, NV	0.3992
	San Francisco, CA	0.6229
	Los Angeles, CA	0.6799

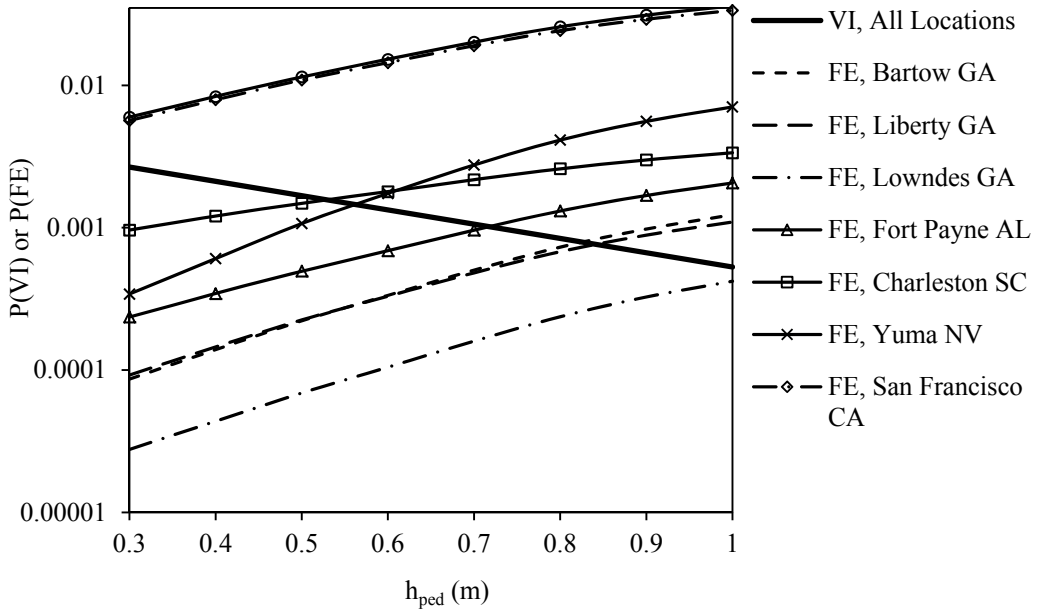

Figure 5-1. Annual probability of failure versus pedestal height

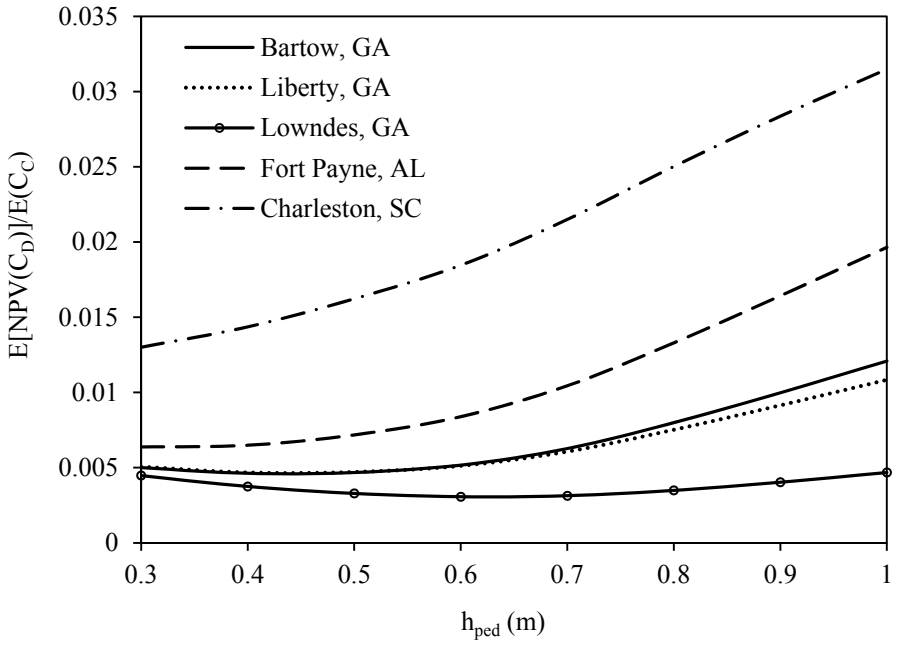

Figure 5-2. Normalized expected cost of failure versus pedestal height for the Southeastern United States

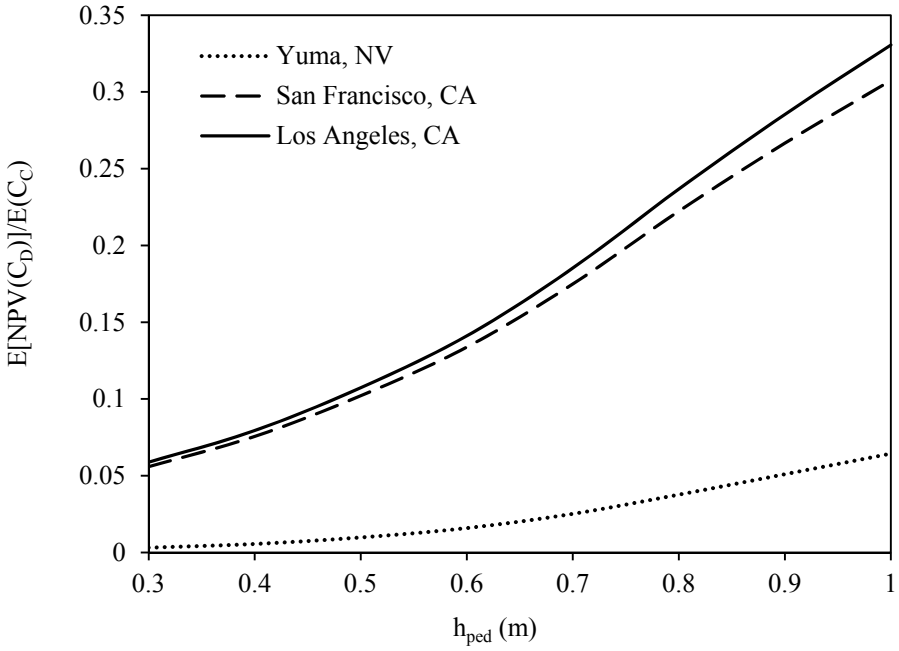

Figure 5-3. Normalized expected cost of failure versus pedestal height for the Western United States

vehicular impact, which is assumed to be the same for all the considered locations. As Figure 5-1 shows, $P(VI)$ decreases with the pedestal height, h_{ped}, but $P(FE)$ increases with h_{ped}. Figures 5-2 and 5-3 show $E[NPV(C_D)]/E(C_c)$ versus h_{ped} for the locations in the Southeastern and Western United States, respectively. These figures reveal that in low seismic regions such as Georgia, increasing the height of pedestals up to a certain height (about 0.5-0.6m) can be beneficial but after that increasing the height of pedestals raise the expected damage or failure cost. For moderate and high seismic zones such as South Carolina and California, the $E\left[NPV\left(C_{FE}\right)\right]$ in Eq. (5-16) governs the expected damage or failure costs and therefore the expected cost of damage or failure increases as a function of h_{ped}. Table 5-2 provides the optimum height of steel pedestals over the

considered range for the studied bridge at different locations. For moderate and high seismic regions, the smallest height in the considered range minimizes the expected cost of damage or failure. The smallest considered height in this study for steel pedestals is 0.3m because the height of pedestals should be larger than the height of previous bearings.

Table 5-2. Optimum height of pedestals for each location

Location	Optimum height of pedestals (m)
Lowndes, GA	0.63
Bartow, GA	0.44
Liberty, GA	0.44
Fort Payne, AL	0.30
Charleston, SC	0.30
Yuma, NV	0.30
San Francisco, CA	0.30
Los Angeles, CA	0.30

After obtaining the optimum height of pedestals based on the value of $E[NPV(C_D)]/E(C_c)$, it has to be checked if Eq. (5-17) is satisfied for each location. For the studied bridge, 0.3m rocker bearings are assumed to support the deck prior to installation of pedestals. Since the mechanism of transferring load for rocker bearings is through anchor bolts as for steel pedestals, the same probabilistic capacity and demand models are used for the rocker bearings. Figures 5-4 and 5-5 show the value of ζ_p from Eq. (5-17) versus $PGA_{1,000}$ for two cases. In the first case shown in Figure 5-4, it is assumed that there is no broader societal impact of elevating the bridge than decreasing

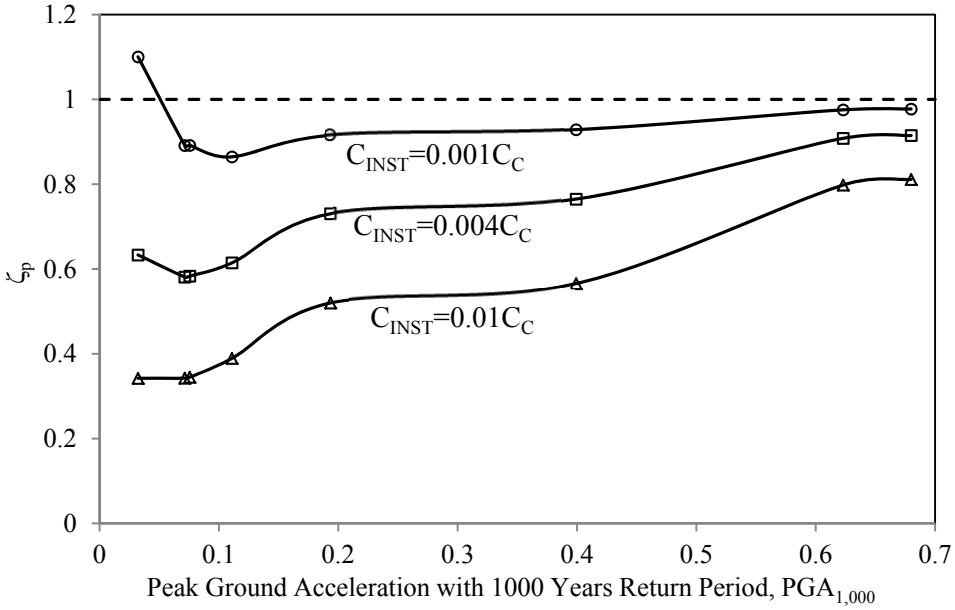

Figure 5-4. Ratio of expected cost of failure before elevation over expected cost of failure after elevation assuming the elevation of bridge has no societal benefits other than decreasing the probability of vehicular impact

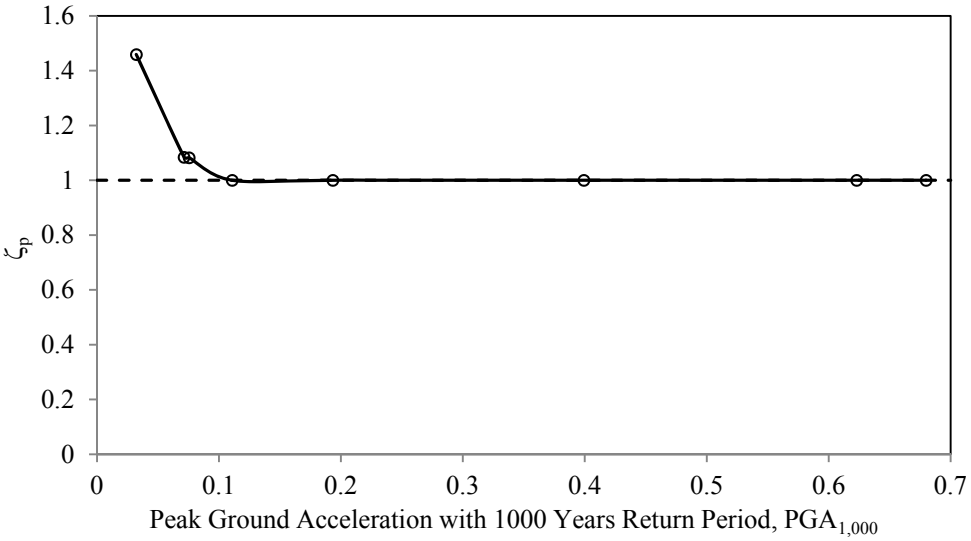

Figure 5-5. Ratio of expected cost of failure before elevation over expected cost of failure after elevation assuming the elevation of bridge has broader societal benefits other than decreasing the probability of vehicular impact

the probability of vehicular impact. In this case, Figure 5-4 reveals that even if the installation cost of steel pedestals is 0.001 times the construction cost, ζ_p is smaller than 1 for all the considered locations except Lowndes, GA. This means that the use of steel pedestals to elevate bridges has financial justification only for Lowndes, GA if the installation costs does not exceed 0.0014 times construction cost of the bridge. Hite et al. (2007) reported that in 1996, C_{INST} for a four-span bridge in Georgia was \$95,000. That is, in this case, C_{INST} was larger than 0.001 times the C_C. Therefore, it can be concluded that if elevating the bridge does not have any broader societal benefits, the installation of steel pedestals for the studied bridge is not a beneficial investment. In the second case, shown in Figure 5-5, it is assumed that the broader societal benefits of elevating the example bridge are such that they cover the installation cost. In this case, Figure 5-5 shows that the use of steel pedestals can be beneficial in low seismic regions such as Georgia. In Figure 5-5, ζ_p is equal to 1 for moderate and high seismic regions because the optimum height of pedestals for those regions is the same as the assumed bearing height before elevation that implies no elevation has to be done. Therefore, based on Figures 5-4 and 5-5, it is concluded that if the elevation of the studied bridge using steel pedestals has no broader societal benefits, it is not recommended in all the regions but if the broader societal benefits are such that they can at least cover the installation cost of pedestals, the use of steel pedestals to elevate the studied bridge can be beneficial in low seismic regions. It should also be noted that developing new technologies that decrease

the installation cost of pedestals can be helpful to satisfy Eq. (5-17) and make elevating bridges using steel pedestals more advantageous.

5.6 Summary and Conclusions

This study provided a framework to determine the financial benefit of elevating bridges using steel pedestals. Formulations to estimate the expected costs associated with vehicular impact and seismic loads were developed and used to estimate the total expected cost of damage or failure. Then the optimum height of steel pedestals was defined as the height that minimizes the total expected cost of damage or failure. To determine if the installation of the pedestals with the optimum height is beneficial, a ratio was defined that compares the expected cost of damage or failure before the installation of pedestals with the expected cost of damage or failure after the installation of pedestals accounting for installation cost and broader societal benefits.

The developed framework was applied on a typical two-span slab-on-girder bridge in different locations in Southeastern and Western United States. Investigations on a range of pedestal heights from 0.3m to 1.0m showed that the optimum height is 0.3m for all the considered regions except the state of Georgia, where the optimum height was found to be between 0.44m to 0.63m in different locations of this state depending on the local seismicity. Then the expected cost of damage or failure for the bridge before elevation is compared to the expected cost of damage or failure after elevation. Assuming rocker bearings for the bridge with similar behavior to steel pedestals before elevation, it was concluded that the elevation of the studied bridge using

steel pedestals does not have financial justification for all the considered locations in this study if the elevation of the bridge has no broader societal benefits. In other words, in this case benefits from decreasing the probability of vehicular impact to the bridge do not compensate for the installation cost and the additional expected cost due to increasing the probability of damage or failure due to earthquakes. Results showed that in the case the broader societal benefits for elevating the bridge can cover at least the installation cost of the pedestals, the use of pedestals has financial justification in low seismic regions. Although the framework developed in this section is general, the observations made in the illustration subsection are valid for the specific studied bridge, which is a typical two-span slab-on-girder bridge. Additional bridges can be investigated using the proposed framework to generalize these conclusions to other bridges.

6. CONCLUSIONS AND FUTURE WORK

6.1 Conclusions

This dissertation investigated the seismic effects of elevating bridges with steel pedestals in the Southeastern United States and developed probabilistic capacity and demand models for steel pedestals used to elevate bridges and probabilistic shear and deformation demand models for the columns of the elevated bridges. Probabilistic models were developed by adding correction and error terms to the commonly used deterministic models, which make them simple to use by engineering community. Developed models help engineers to include aleatory and epistemic uncertainties in the problem and estimate fragility of the elevated bridges with steel pedestals subjected to earthquake loads. Based on the developed probabilistic capacity and demand models, a decision analysis framework was proposed that helps designers and decision makers to determine if the elevation of a bridge has financial justification or not. The results of this study can be summarized as:

- For the three types of pedestals described in Section 2, some of the seismic responses of a studied bridge elevated with steel pedestals in low seismic regions such as pounding force, deck displacements and column demands were assessed to be less than the responses of the same bridge with elastomeric bearings while some of the responses such as transverse abutment force were found to be larger. Since there are stability issues if pedestals are used with two anchor bolts, the use of steel pedestals with four anchor bolts is recommended.

- Fragility curves for a typical bridge using developed capacity and demand models showed that elevated bridges with steel pedestals are vulnerable to earthquake loads. The results showed that steel pedestals are more vulnerable in longitudinal direction than transverse direction and columns of the elevated bridges are more vulnerable in transverse direction than longitudinal direction. The results also showed that at the combination of large PGAs and small PGVs, steel pedestals have more contribution in bridge failure than columns.
- Results of sensitivity analyses showed that decreasing the height of the pedestal, increasing anchor bolt lengths and concrete cover are the most effective ways to decrease the failure probability of steel pedestals.
- Increasing the height of pedestals results in increasing the probability of failure of the bridge subject to earthquake loads but decreases the probability of failure due to vehicular impact. A decision analysis framework was provided that computes the expected cost of failure considering failure probability due to vehicular impact and earthquake loads.
- Applying the developed decision analysis framework in this dissertation on a typical two-span bridge revealed that the use of steel pedestals to elevate bridges do not have financial justification in moderate and high seismic regions. In low seismic regions, it has financial justifications if the broader effects of installation of pedestals such as the effects on improving the economy can cover at least the installation cost of pedestals.

6.2 Unique Contributions

This dissertation provided for the first time, an analytical procedure to estimate the lateral capacity of and demand on steel pedestals. Although the developed models in this dissertation are probabilistic models but the point estimates of the models can be used to obtain deterministic values for the capacity and demand of steel pedestals. Point estimates of Eqs. (3-1) through (3-31) along with the procedure shown in Figure 3-3 would result in a deterministic capacity value for steel pedestals and point estimates of Eqs. (4-7) through (4-12) using the mean values of the parameters in Tables 4-6 through 4-11 provides deterministic values for the demands components of bridges

6.3 Future Work

Some suggestions for future work based on the progress of the research here include:

- Using the developed probabilistic models for transportation networks where several bridges might need to be elevated. In this case, the developed models in this dissertation can be applied to each individual bridge and then the probability of failure of the bridge network can be obtained using system reliability methods.
- Developing probabilistic demand models for bridges elevated with steel pedestals subject to other types of hazards such as flood loading. Such models can be used for bridges over rivers that do not have enough vertical clearance and installation of steel pedestals is an option to elevate them.
- Developing probabilistic capacity and demand models for other types of bridge bearings such as elastomeric bearings. Without such models comparisons

between the performance of steel pedestals and other types of bearings are not accurate enough to make general conclusions.

- Developing new methods for elevating bridges in moderate and high seismic regions where the installation of steel pedestals does not have financial justification or improving the design of steel pedestals such that they can be used in high seismic regions without considerable probability of failure.

REFERENCES

AASHTO. (2010). *AASHTO LRFD bridge design specifications*, 5th Ed., AASHTO, Washington, DC.

Abramhamson, N. A., and Silva, W. J. (2008). "Summary of the Abrahamson and Silva NGA ground-motion relations." *Earthquake Spectra*, 24(1), 67-97.

American Concrete Institute (ACI). (2008). *Building code requirements for structural concrete (ACI 318-08) and Commentary (318R-08)*, American Concrete Institute, Farmington Hills, MI.

Ang, A. H. S., and Tang, W. H. (2007). *Probability concepts in engineering: emphasis on applications to civil and environmental engineering*, Wiley, New York.

Astaneh-Asl, A., and Bergsma, G. (1993). "Cyclic behavior and seismic design of steel base plates." *Structural Engineering in Natural Hazards Mitigation*, Ang., A. H. S., Villaverde, R., eds., ASCE, New York, 409-414.

Baker, J. W., and Cornell C. A. (2005). "A vector-valued ground motion intensity measure consisting of spectral acceleration and epsilon." *Earthquake Eng. & Struct. Dyn.*, 34 (10), 1193-1217.

Bai, J. W., Gardoni, P., and Hueste, M. B. D. (2011). "Story-specific demand models and seismic fragility estimates for multi-story buildings." *Structural Safety*, 33(1), 96-107.

Bedi, A. K. (2000). "A Study of a bridge girder damaged by vehicle impacts." *Proc 2nd Forensic Engineering Congress*, American Society of Civil Engineers, Reston, VA, 263-272.

Bisadi, V., and Head, M. (2011). "Evaluation of combination rules for orthogonal seismic demands in nonlinear time history analysis of bridges." *J. Bridge Eng.*, 16(6), 711-717.

Box, G. E. P., and Cox, D. R. (1964). "An analysis of transformations." *J. R. Stat. Soc. Ser. B (Methodol.)*, 26, 211-246.

Box, G. E. P., and Tiao, G. C. (1992). *Baysian inference in statistical analysis*, Wiley, New York.

Buckle, I., Friedland, I., Mander, J., Martin, G., Nutt, R., et al. (2006). *Seismic retrofitting manual for highway structures: Part 1-Bridges*. MCEER and U.S. Department of Transportation Federal Highway Administration, Washington, DC.

Burnham, K. P., and Anderson, D. R. (2002). *Model selection and multimodel inference: a practical information-theoretic approach*, 2nd ed., Springer, New York.

Caltrans Seismic Design Criteria. (2006). Design manual version 1.4, Calif. Dept. of Transportation, Sacramento, CA.

Choe, D. E., Gardoni, P., and Rosowsky, D. (2007). "Closed-form fragility estimates, parameter sensitivity and Bayesian updating for RC columns." *J. Eng. Mech.*, 133(7), 833–843.

Choi, E. (2002). "Seismic analysis and retrofit of mid-america bridges." *Ph.D. Dissertation*, Georgia Institute of Technology, Atlanta, GA.

Cook, R. A., and Klingner, R. E. (1989). "Behavior and design of ductile multiple anchor steel to concrete connections." Rep. No. CTR1126-3, Univ. of Texas, Austin, TX.

DesRoches, R., Pfeifer, T., Leon, R. T., and Lam, T. (2003). "Full-scale tests of seismic cable restrainer retrofits for simply supported bridges." *J. of Bridge Eng.*, 8(4), 191–8.

DesRoches, R., Leon, R. T., Choi, E., Lam, T., Dyke, S., et al. (2000). "Response evaluation and modification of typical bridges in the central and southeastern United States", *Proc. 12th World Conf. on Earthquake Eng.*, Auckland, New Zealand, Jan. 30-Feb. 4.

Dewolf, J. T., and Sarisley, E. F. (1980). "Column base plates with axial loads and moments." *J. Struct. Div.*, 106(11), 2167–2184.

Ditlevsen, O., and Madsen, H. O. (1996). *Structural reliability methods*, Wiley, New York.

Douglas, B. M. (1979). "Experimental dynamic response investigations of existing highway bridges." *Proc. of a workshop on earthquake resistance of highway bridges*, National Science Foundation (U.S.), Applied Technology Council, Berkeley, CA. 497-523,

Eligehausen, R., and Fichtner, S. (2007). "Stiffness requirements for baseplates." *Proc. 6th Int. Conf. on Fracture Mechanics of Concrete and Concrete Structures*, RILEM, Catania, Italy, 945–949.

Eligehausen, R., Mallee, R., and Silva, J. (2006). *Anchorage in concrete construction*, Ernst & Sohn, Berlin.

Ermopoulos, J. C., and Stamatopoulos, G. N. (1996). "Analytical modelling of column-base plates under cyclic loading." *J. Constr. Steel Res.*, 40(3), 225-238.

Farrow, C. B., Frigui, I., and Klingner, R. E. (1996). "Tensile capacity of single anchors in concrete: Evaluation of existing formulas on an LRFD basis." *ACI Struct. J.*, 93(1), 128–137.

Feldman, L. R., Jirsa, J. O., and Kowal, E. S. (1998). "Repair of bridge impact damage." *Concrete International*, 20(2), 61-66.

Fernandez, J. A. (2007). "Numerical simulation of earthquake ground motions in the Upper Mississippi Embayment.", *PhD Dissertation*, Georgia Institute of Technology, Atlanta, GA.

Field, E. H., Gupta, N., Gupta, V., Blanpied, M., Maechling, P., et al. (2005). "Hazard calculation for the WGCEP-2002 earthquake forcast using OpenSHA and distributed object technologies." *Seismological Research Letters*, 76(2), 161-167.

Frankel, A. D., Peterson, M. D., Mueller C. S., Haller, K. M., Wheeler, R. L., et al. (2002). "Documentation for the 2002 update of the national seismic hazard maps." U.S. Geological Survey Open-File Report 02-20, USGS, Denver, CO.

Fu, C. C., Burhouse, J. R., and Chang, G. (2004). "Overheight vehicle collisions with highway bridges." *Transportation Research Record*, 1865, 80-88.

Fuchs, W., Eligehausen, R., and Breen, J. (1995). "Concrete capacity design (CCD) Approach for fastening to concrete." *ACI Struct. J.*, 92(1), 73–94.

Gardoni, P., Der Kiureghian, A., and Mosalam, K. M. (2002). "Probabilistic capacity models and fragility estimates for reinforced concrete columns based on experimental observations." *J. Eng. Mech.*, 128(10), 1024–1038.

Gardoni, P., Mosalam, K., and Der Kiureghian, M. A. (2003). "Probabilistic seismic demand models and fragility estimates for RC bridges." *J. Earthquake Eng.*, 7(Sp. Issue 1), 79–106.

Hadipriono, F. C. (1985). "Analysis of events in recent structural failures." *J. of Struct. Eng.*, 111(7), 1468-1481.

Hartik, I. E., Shaaban, A. M., Gesund, H., Valli, G. Y. S., and Wang, S. T. (1990). "United States bridge failures 1951-1988." *J. Performance of Construction Facilities*, 4(4), 272-277.

Hilton, M. H. (1973). "Some case studies of highway bridges involved in accidents." *Highway Research Board*, 432, 41-51.

Hite, M. (2007). “Evaluation of the performance of bridge steel pedestals under low seismic loads.”, *PhD Dissertation*, Georgia Institute of Technology, Atlanta, GA.

Hite, M., DesRoches, R., and Leon, R. T. (2006). “Evaluation of the performance of bridge steel pedestals under seismic loads.” Structural Engineering and Public Safety—Proc., ASCE 2006 Structures Congress, ASCE, Reston, VA, 171.

Hite, M., DesRoches, R., and Leon, R. T. (2008). “Full-scale tests of bridge steel pedestals.” *J. Bridge Eng.*, 13(5), 483–491.

Hsu, J. C. (1996). *Multiple comparisons: theory and methods*. 1st ed. Chapman and Hall/CRC, London.

Huer, T., and Eligehausen, R. (2007). “Splitting failure mode of bonded anchors.” *Proc., 6th Int. Conf. on Fracture Mechanics of Concrete and Concrete Structures*, RILEM, Catania, Italy, 753–760.

Hurvich, C. M., and Tsai, C. (1989). “Regression and time series model selection in small samples.” *Biometrika*, 76(2), 297-307.

Kelly, J. M. (1998). “The analysis and design of elastomeric bearings for application in bridges.” *Proc. U.S.–Italy workshop on seismic protective systems for bridges*, MCEER-98-0015, Friedland, I.M., Constantinou, M.C., eds., Buffalo, NY, 73-88.

Kong, J. S., and Frangopol, D. M. (2004). “Cost–reliability interaction in life-cycle cost optimization of deteriorating structures.” *J. Struct. Eng.*, 130(11), 1704-1712.

Kontoleon, M. J., Mistakidis, E. S., Baniotopoulos, C. C., and Panagiotopoulos, P. D. (1999). “Parametric analysis of the structural response of steel base plate connections.” *Computers and Structures*, 71(1), 87-103.

Krawinkler, H., and Nassar, A. A. (1992). “Seismic design based on ductility and cumulative damage demands and capacity.” *Nonlinear seismic analysis and design of*

reinforced concrete buildings, P. Fajfar and H. Krawinkler, eds., Elsevier Applied Science, New York, NY.

Kumar, R., and Gardoni, P. (2012). "Second order logarithmic formulation for hazard curves and closed-form approximation to annual failure probability." *J. Struct. Safety*, Submitted.

Kumar, R., Gardoni, P., and Sanchez-Silva, M. (2009). "Effect of cumulative seismic damage and corrosion on life-cycle cost of reinforced concrete bridges." *Earthquake Eng. Struct. Dyn.*, 38 (7), 887-905.

Maleki, S., and Bisadi, V. (2006). "Orthogonal effects in seismic analyses of skewed bridges." *J. Bridge Eng.*, 11(1), 122–130.

Mallows, C. L. (1973). "Some comments on CP". *Technometrics*, 15 (4), 661-675.

Mander, J. B., Kim, D. K., Chen, S. S., and Premus, G. J. (1996). "Response of steel bridge bearings to the reversed cyclic loading." Tech. Rep. NCEER 96-0014. NCEER, Buffalo, NY.

Mander, J. B., Priestley, M. J. N., and Park, R. (1988). "Theoretical stress strain model for confined concrete." *J. Struct. Eng.*, 114(8), 1804–1826.

McKay, M. D., Conover, W. J., and Beckman, R. J. (1979). "A comparison of three methods for selecting values of input variables in the analysis of output from a computer code." *Technometrics*, 22(2), 239-245.

McMackin, P. J., Slutter, R. G., and Fisher, J. W. (1973). "Headed steel anchor under combined loading." *AISC Eng. J.*, 10(2), 43–52.

Meinheit, D. F., and Heidbrink, F. D. (1985). "Behavior of drilled-in expansion anchors." *Concr. Int.*, 7(4), 62–66.

Melchers, R. E. (1992). “Steel baseplate-footing-soil behaviour.” *Connections in steel structures II: Behaviour, strength and design*, R. Bjorhovde et al., eds., AISC, Chicago, 132–139.

Michaltsos, G. T., and Ermopoulos, J. C. (2001). “Dynamic response of column bases.” *Engineering Structures*, 23(1), 58-71.

Montgomery, D. C., and Runger, G. C. (2006). *Applied Statistics and Probability for Engineers*, 4th ed., John Wiley & Sons, Inc., New York.

Muratli, H., Klingner, R. E., and Graves, H. L. III. (2004). “Breakout capacity of anchors in concrete—Part 2: Shear.” *ACI Struct. J.*, 101(6), 821–829.

Murphy, C., and Gardoni, P. (2006). “The role of society in engineering risk analysis: a capabilities-based approach.” *Risk Analysis*, 26(4), 1073-1083.

Muthukumar, S. A. (2003). “Contact element approach with hysteresis damping for the analysis and design of pounding in bridges.” *Ph.D. Dissertation*, Georgia Institute of Technology, Atlanta, GA.

Muthukumar, S., and DesRoches, R. (2006). “A Hertz contact model with non-linear damping for pounding simulation.” *Earthquake Eng. Struct. Dyn.*, 35(7), 811–828.

Naeim, F., and Kelly, J. M. (1999). *Design of seismic isolated structures: from theory to practice*, John Wiley & Sons, Inc., New York.

National Cooperative Highway Research Program (NCHRP) (2003). *Bridge Life-cycle Cost Analysis*, NCHRP Report 483, Washington, DC.

Nielson, B. G. (2005). “Analytical fragility curves for highway bridges in moderate seismic zones.” *Ph.D. Dissertation*, Georgia Institute of Technology, Atlanta, GA.

Nielson, B., and DesRoches, R. (2006). “Influence of modeling assumptions on the seismic response of multi-span simply supported steel girder bridges in moderate seismic zones.” *Eng. Struct.*, 28(8), 1083-1092.

Open System for Earthquake Engineering Simulation (OpenSees), *Version 2.2.2* [Computer software], Pacific Earthquake Engineering Research Center, Berkeley, CA.

Pacific Earthquake Engineering Research Center. (1999). “Pacific Earthquake Engineering Research Center: NGA Database.” ⟨http://peer .berkeley.edu/nga⟩, Accessed in Mar.-Apr. 2011.

Padgett, J. E., Dennemann, K., and Ghosh, J. (2010). “Risk-based seismic life-cycle cost-benefit (LCC-B) analysis for bridge retrofit assessment.” *Struct. Safety*, 32(3), 165-173.

Penserini, P., and Colson, A. (1989). “Ultimate limit strength of columnbase connections.” *J. Constr. Steel Res.*, 14, 301–320.

Ramamoorthy, S. K., Gardoni, P., and Bracci, J. M. (2006). “Probabilistic demand models and fragility curves for reinforced concrete frames.” *J. Struct. Eng.*, 132(10), 1563-1572.

Ramamoorthy, S. K., Gardoni, P., and Bracci, J. M. (2008). “Seismic fragility and confidence bounds for gravity load designed reinforced concrete frames of varying height.” *J. Struct. Eng.*, 134(4), 639-650.

SAS Jmp, Version 8.0.1 [Statistical discovery software], Cary, NC.

Shaikh, A. F., and Whayong, Y. (1985). “In-place strength of welded headed studs.” *J. Prestressed Concr. Inst.*, 30(2), 56–81.

Sharma, H., Hurlebaus, S., and Gardoni, P. (2008). “Development of a bridge bumper to protect bridge girders from overheight vehicle impacts.” *Computer-Aided Civil and Infrastructure Engineering*, 23(6), 415-426.

Shome, N., and Cornell, C. A. (1999). “Probabilistic seismic demand analysis of nonlinear structures.” Reliability of Marine Structures Rep. No. RMS-35, Dept. of Civil and Envir. Engineering, Stanford Univ., Palo Alto, CA.

Stamatopoulos, G. N., and Ermopoulos, J. C. (1997). “Interaction curves for column base-plate connections.” *J. Constr. Steel Res.*, 44(1–2), 69–89.

Stewart, M. G., and Val, D. V. (2003). “Multiple limit states and expected failure costs for deteriorating reinforced concrete bridges.” *J. Bridge Eng.*, 8(6), 405-415.

Subramanian, N., and Cook, R. A. (2004). “Behavior of grouted anchors.” *Ind. Concrete J.*, 78(4), 14–21.

Thambiratnam, D. P., and Paramasivam, P. (1986). “Base plates under axial load and moment.” *J. Struct. Eng.*, 112(5), 1166–1181.

Theil H. (1961). *Economic forcasts and policy*, North-Holland Pub. Co., Amsterdam, Holland.

Val, D. V. (2005). “Effect of different limit states on life-cycle cost of RC structures in corrosive environment.” *J. Infrastructure Systems*, 11(4), 231-240.

Wald F., Bauduffe N., and Muzeau J. P. (2001). “Preliminary prediction of the column-base stiffness.” In: *TU Graz papers*, Festschrift, Greiner R. et al., eds., Graz, Austria, 47-52.

Wardhana, K., and Hadipriono, F. C. (2003). “Analysis of recent bridge failures in the United States.” *Journal of Performance of Construction Facilities*, 17(3), 144-150.

Wen, Y. K. (2001). “Minimum lifecycle cost design under multiple hazards.” *Reliability Engineering & System Safety*, 73, 223-231.

Zamora, N. A., Cook, R. A., Konz, R., and Consolazio, G. R. (2003). “Behaviour and design of single, headed and unheaded, grouted anchors under tensile load.” *ACI Struct. J.*, 100(2), 222–230.

Zhong, J., Gardoni, P., Rosowsky, D., and Haukaas, T. (2008). “Probabilistic seismic demand models and fragility estimates for reinforced concrete bridges with two-column bents.” *J. Eng. Mech.*, 134(6), 495-504.

APPENDIX A

Table A.1. Ground motion records in Bin 1 (PEER NGA Database 1999)

#	Record ID	Earthquake	M	R	GM	Station
1	P0734	Loma Prieta 1989/10/18 00:05	6.9	21.8	A	57217 Coyote Lake Dam (SW Abut)
2	P0749	Loma Prieta 1989/10/18 00:05	6.9	17.9	A	58135 UCSC Lick Observatory
3	P0498	Nahanni, Canada 1985/12/23	6.8	16	A	6099 Site 3
4	P0885	Northridge 1994/01/17 12:31	6.7	26.8	A	127 Lake Hughes #9
5	P0915	Northridge 1994/01/17 12:31	6.7	22.7	A	90017 LA - Wonderland Ave
6	P0937	Northridge 1994/01/17 12:31	6.7	24.5	A	24047 Vasquez Rocks Park
7	P0059	San Fernando 1971/02/09 14:00	6.6	27	A	104 Santa Anita Dam
8	P0076	San Fernando 1971/02/09 14:00	6.6	24.2	A	126 Lake Hughes #4
9	P0077	San Fernando 1971/02/09 14:00	6.6	23.5	A	127 Lake Hughes #9
10	P0084	San Fernando 1971/02/09 14:00	6.6	19.1	A	266 Pasadena - Old Seismo Lab
11	P0090	San Fernando 1971/02/09 14:00	6.6	27.5	A	285 Santa Felita Dam (Outlet)
12	P0738	Loma Prieta 1989/10/18 00:05	6.9	19.9	B	57383 Gilroy Array #6
13	P0746	Loma Prieta 1989/10/18 00:05	6.9	24.2	B	57425 Gilroy Array #7
14	P0791	Loma Prieta 1989/10/18 00:05	6.9	18.1	B	15 UCSC
15	P0906	Northridge 1994/01/17 12:31	6.7	23.7	B	90015 LA - Chalon Rd
16	P0910	Northridge 1994/01/17 12:31	6.7	23.9	B	90016 LA - N Faring Rd
17	P0950	Northridge 1994/01/17 12:31	6.7	20	B	90059 Burbank - Howard Rd.
18	P0994	Northridge 1994/01/17 12:31	6.7	26.2	B	90049 Pacific Palisades - Sunset Blvd
19	P0056	San Fernando 1971/02/09 14:00	6.6	24.9	B	24278 Castaic - Old Ridge Route
20	P0078	San Fernando 1971/02/09 14:00	6.6	20.3	B	128 Lake Hughes #12
21	P0810	Cape Mendocino 1992/04/25 18:06	7.1	18.5	C	89324 Rio Dell Overpass - FF
22	P0817	Landers 1992/06/28 11:58	7.3	19.3	C	5071 Morongo Valley
23	P0889	Northridge 1994/01/17 12:31	6.7	20.8	C	90014 Beverly Hills - 12520 Mulhol
24	P0890	Northridge 1994/01/17 12:31	6.7	19.6	C	90013 Beverly Hills - 14145 Mulhol
25	P0891	Northridge 1994/01/17 12:31	6.7	24	C	90061 Big Tujunga, Angeles Nat F
26	P0916	Northridge 1994/01/17 12:31	6.7	22.3	C	90060 La Crescenta - New York
27	P0933	Northridge 1994/01/17 12:31	6.7	17.7	C	90058 Sunland - Mt Gleason Ave
28	P0975	Northridge 1994/01/17 12:31	6.7	22.8	C	24607 Lake Hughes #12A
29	P0058	San Fernando 1971/02/09 14:00	6.6	25.8	C	125 Lake Hughes #1
30	P0808	Cape Mendocino 1992/04/25 18:06	7.1	23.6	D	89486 Fortuna - Fortuna Blvd
31	P0814	Landers 1992/06/28 11:58	7.3	23.2	D	12149 Desert Hot Springs
32	P0818	Landers 1992/06/28 11:58	7.3	24.2	D	5070 North Palm Springs
33	P0865	Landers 1992/06/28 11:58	7.3	21.2	D	23 Coolwater
34	P0881	Landers 1992/06/28 11:58	7.3	24.9	D	22074 Yermo Fire Station
35	P0732	Loma Prieta 1989/10/18 00:05	6.9	28.2	D	1028 Hollister City Hall
36	P0737	Loma Prieta 1989/10/18 00:05	6.9	16.1	D	57382 Gilroy Array #4
37	P0742	Loma Prieta 1989/10/18 00:05	6.9	28.2	D	57066 Agnews State Hospital
38	P0743	Loma Prieta 1989/10/18 00:05	6.9	21.4	D	1652 Anderson Dam (Downstream)
39	P0884	Northridge 1994/01/17 12:31	6.7	25.5	D	24303 LA - Hollywood Stor FF
40	P0905	Northridge 1994/01/17 12:31	6.7	25.7	D	24389 LA - Century City CC North

Table A.2. Ground motion records in Bin 2 (PEER NGA Database 1999)

#	Record ID	Earthquake	M	R	GM	Station
1	P0880	Landers 1992/06/28 11:58	7.3	42.2	A	22161 Twentynine Palms
2	P0768	Loma Prieta 1989/10/18 00:05	6.9	30.6	A	1032 Hollister - SAGO Vault
3	P0771	Loma Prieta 1989/10/18 00:05	6.9	44.8	A	47377 Monterey City Hall
4	P0774	Loma Prieta 1989/10/18 00:05	6.9	36.3	A	1601 Palo Alto - SLAC Lab
5	P0926	Northridge 1994/01/17 12:31	6.7	36.1	A	24399 Mt Wilson - CIT Seis Sta
6	P0965	Northridge 1994/01/17 12:31	6.7	37	A	24592 LA - City Terrace
7	P0969	Northridge 1994/01/17 12:31	6.7	32.3	A	24611 LA - Temple & Hope
8	P0970	Northridge 1994/01/17 12:31	6.7	34.6	A	24605 LA - Univ. Hospital
9	P1011	Northridge 1994/01/17 12:31	6.7	41.7	A	90019 San Gabriel - E. Grand Ave.
10	P0731	Spitak, Armenia 1988/12/07	6.8	30	A	12 Gukasian
11	P0811	Cape Mendocino 1992/04/25 18:06	7.1	33.8	B	89530 Shelter Cove Airport
12	P0740	Loma Prieta 1989/10/18 00:05	6.9	43	B	57064 Fremont - Mission San Jose
13	P0750	Loma Prieta 1989/10/18 00:05	6.9	34.7	B	47189 SAGO South - Surface
14	P0763	Loma Prieta 1989/10/18 00:05	6.9	43.4	B	1686 Fremont - Emerson Court
15	P0793	Loma Prieta 1989/10/18 00:05	6.9	39.9	B	58127 Woodside
16	P0903	Northridge 1994/01/17 12:31	6.7	31.3	B	24157 LA - Baldwin Hills
17	P0923	Northridge 1994/01/17 12:31	6.7	35.2	B	24396 Malibu - Point Dume Sch
18	P0973	Northridge 1994/01/17 12:31	6.7	32.3	B	24469 Lake Hughes #4 - Camp Mend
19	P1014	Northridge 1994/01/17 12:31	6.7	43.4	B	24644 Sandberg - Bald Mtn
20	P0085	San Fernando 1971/02/09 14:00	6.6	38.9	B	269 Pearblossom Pump
21	P0907	Northridge 1994/01/17 12:31	6.7	32.8	C	90033 LA - Cypress Ave
22	P0918	Northridge 1994/01/17 12:31	6.7	36.3	C	24271 Lake Hughes #1
23	P0921	Northridge 1994/01/17 12:31	6.7	38.3	C	24055 Leona Valley #5 - Ritter
24	P0924	Northridge 1994/01/17 12:31	6.7	42	C	90046 Manhattan Beach - Manhattan
25	P0999	Northridge 1994/01/17 12:31	6.7	39.2	C	90095 Pasadena - N Sierra Madre
26	P0807	Cape Mendocino 1992/04/25 18:06	7.1	44.6	D	89509 Eureka - Myrtle & West
27	P0860	Landers 1992/06/28 11:58	7.3	36.1	D	23559 Barstow
28	P0773	Loma Prieta 1989/10/18 00:05	6.9	36.1	D	58264 Palo Alto - 1900 Embarc.
29	P0778	Loma Prieta 1989/10/18 00:05	6.9	32.6	D	47179 Salinas - John & Work
30	P0896	Northridge 1994/01/17 12:31	6.7	40.7	D	90079 Downey - Birchdale
31	P0904	Northridge 1994/01/17 12:31	6.7	30.9	D	90054 LA - Centinela St
32	P0912	Northridge 1994/01/17 12:31	6.7	37.9	D	24400 LA - Obregon Park
33	P0914	Northridge 1994/01/17 12:31	6.7	30	D	90091 LA - Saturn St
34	P0920	Northridge 1994/01/17 12:31	6.7	42.4	D	90045 Lawndale - Osage Ave
35	P0929	Northridge 1994/01/17 12:31	6.7	34.2	D	90047 Playa Del Rey - Saran
36	P0931	Northridge 1994/01/17 12:31	6.7	35.1	D	24401 San Marino, SW Academy
37	P0938	Northridge 1994/01/17 12:31	6.7	42.5	D	90099 Arcadia - Arcadia Av
38	P0942	Northridge 1994/01/17 12:31	6.7	35.7	D	24461 Alhambra - Fremont School
39	P0944	Northridge 1994/01/17 12:31	6.7	38.4	D	24576 Anaverde Valley - City R
40	P0946	Northridge 1994/01/17 12:31	6.7	44.2	D	90093 Arcadia - Campus Dr.

Table A.3. Ground motion records in Bin 3 (PEER NGA Database 1999)

#	Record ID	Earthquake	M	R	GM	Station
1	P0552	Chalfant Valley 1986/07/21 14:42	6.2	23	A	54424 Bishop - Paradise Lodge
2	P0359	Coalinga 1983/05/02 23:42	6.4	29.6	A	36438 Parkfield - Stone Corral 4E
3	P0370	Coalinga 1983/05/02 23:42	6.4	27.7	A	46175 Slack Canyon
4	P0165	Imperial Valley 1979/10/15 23:16	6.5	26.5	A	6604 Cerro Prieto
5	P0191	Imperial Valley 1979/10/15 23:16	6.5	26	A	286 Superstition Mtn Camera
6	P0448	Morgan Hill 1984/04/24 21:15	6.2	16.2	A	47379 Gilroy Array #1
7	P0538	N. Palm Springs 1986/07/08 09:20	6	25.8	A	12206 Silent Valley - Poppet F
8	P0612	Whittier Narrows 1987/10/01 14:42	6	26.8	A	108 Carbon Canyon Dam (L Abut)
9	P0341	Coalinga 1983/05/02 23:42	6.4	29.6	B	36449 Parkfield - Fault Zone 8
10	P0344	Coalinga 1983/05/02 23:42	6.4	28.4	B	36453 Parkfield - Fault Zone 11
11	P0347	Coalinga 1983/05/02 23:42	6.4	29.9	B	36445 Parkfield - Fault Zone 15
12	P0213	Livermore 1980/01/24 19:00	5.8	29.8	B	57064 Fremont - Mission San Jose
13	P0215	Livermore 1980/01/24 19:00	5.8	21.7	B	57134 San Ramon Fire Station
14	P0216	Livermore 1980/01/24 19:00	5.8	17.6	B	57187 San Ramon - Eastman Kodak
15	P0462	Morgan Hill 1984/04/24 21:15	6.2	22.7	B	57007 Corralitos
16	P0464	Morgan Hill 1984/04/24 21:15	6.2	16.2	B	47006 Gilroy Gavilan Coll.
17	P0606	Whittier Narrows 1987/10/01 14:42	6	23.3	B	951 Brea Dam (L Abut)
18	P0631	Whittier Narrows 1987/10/01 14:42	6	27	B	24157 LA - Baldwin Hills
19	P0639	Whittier Narrows 1987/10/01 14:42	6	28.5	B	90016 LA - N Faring Rd
20	P0697	Whittier Narrows 1987/10/01 14:42	6	29.3	B	90008 Sun Valley - Sunland
21	P0345	Coalinga 1983/05/02 23:42	6.4	29.5	C	36138 Parkfield - Fault Zone 12
22	P0346	Coalinga 1983/05/02 23:42	6.4	29.9	C	36456 Parkfield - Fault Zone 14
23	P0348	Coalinga 1983/05/02 23:42	6.4	28.1	C	36457 Parkfield - Fault Zone 16
24	P0361	Coalinga 1983/05/02 23:42	6.4	29.5	C	36448 Parkfield - Vineyard Cany 1W
25	P0520	N. Palm Springs 1986/07/08 09:20	6	15.8	C	5069 Fun Valley
26	P0525	N. Palm Springs 1986/07/08 09:20	6	29.8	C	22170 Joshua Tree
27	P0604	Whittier Narrows 1987/10/01 14:42	6	25.5	C	90061 Big Tujunga, Angeles Nat F
28	P0617	Whittier Narrows 1987/10/01 14:42	6	17.1	C	90068 Covina - S Grand Ave
29	P0625	Whittier Narrows 1987/10/01 14:42	6	19	C	90063 Glendale - Las Palmas
30	P0647	Whittier Narrows 1987/10/01 14:42	6	22.7	C	90060 La Crescenta - New York
31	P0698	Whittier Narrows 1987/10/01 14:42	6	27.5	C	90058 Sunland - Mt Gleason Ave
32	P0555	Chalfant Valley 1986/07/21 14:42	6.2	18.7	D	54428 Zack Brothers Ranch
33	P0323	Coalinga 1983/05/02 23:42	6.4	25.5	D	46314 Cantua Creek School
34	P0352	Coalinga 1983/05/02 23:42	6.4	29.2	D	36439 Parkfield - Gold Hill 3E
35	P0406	Coalinga 1983/07/22 02:39	5.8	17.4	D	1162 Pleasant Valley P.P. - yard
36	P0153	Coyote Lake 1979/08/06 17:05	5.7	15.6	D	1377 San Juan Bautista
37	P0154	Coyote Lake 1979/08/06 17:05	5.7	17.2	D	1492 SJB Overpass, Bent 3 g.l.
38	P0164	Imperial Valley 1979/10/15 23:16	6.5	23.8	D	5061 Calipatria Fire Sta
39	P0173	Imperial Valley 1979/10/15 23:16	6.5	15.5	D	5056 El Centro Array #1
40	P0450	Morgan Hill 1984/04/24 21:15	6.2	15.1	D	47380 Gilroy Array #2

Table A.4. Ground motion records in Bin 4 (PEER NGA Database 1999)

#	Record ID	Earthquake	M	R	GM	Station
1	P0550	Chalfant Valley 1986/07/21 14:42	6.2	33.4	A	54214 Long Valley Dam (L Abut)
2	P0559	Chalfant Valley 1986/07/21 14:42	6.2	40.6	A	54101 Tinemaha Res. Free Field
3	P0327	Coalinga 1983/05/02 23:42	6.4	38.4	A	36450 Parkfield - Cholame 3E
4	P0357	Coalinga 1983/05/02 23:42	6.4	34.4	A	36422 Parkfield - Stone Corral 2E
5	P0358	Coalinga 1983/05/02 23:42	6.4	31.8	A	36437 Parkfield - Stone Corral 3E
6	P0364	Coalinga 1983/05/02 23:42	6.4	32.3	A	36176 Parkfield - Vineyard Cany 3W
7	P0214	Livermore 1980/01/24 19:00	5.8	31	A	58219 APEEL 3E Hayward CSUH
8	P0477	Morgan Hill 1984/04/24 21:15	6.2	44.1	A	58135 UCSC Lick Observatory
9	P0537	N. Palm Springs 1986/07/08 09:20	6	43.8	A	5230 Santa Rosa Mountain
10	P0554	Chalfant Valley 1986/07/21 14:42	6.2	36	B	54T03 Lake Crowley - Shehorn Res.
11	P0325	Coalinga 1983/05/02 23:42	6.4	40.5	B	36230 Parkfield - Cholame 2E
12	P0353	Coalinga 1983/05/02 23:42	6.4	38.8	B	36420 Parkfield - Gold Hill 3W
13	P0354	Coalinga 1983/05/02 23:42	6.4	41	B	36433 Parkfield - Gold Hill 4W
14	P0355	Coalinga 1983/05/02 23:42	6.4	47	B	36434 Parkfield - Gold Hill 5W
15	P0365	Coalinga 1983/05/02 23:42	6.4	34.6	B	36446 Parkfield - Vineyard Cany 4W
16	P0456	Morgan Hill 1984/04/24 21:15	6.2	31.4	B	57064 Fremont - Mission San Jose
17	P0518	N. Palm Springs 1986/07/08 09:20	6	35.3	B	5157 Cranston Forest Station
18	P0522	N. Palm Springs 1986/07/08 09:20	6	34.9	B	5043 Hurkey Creek Park
19	P0694	Whittier Narrows 1987/10/01 14:42	6	32.6	B	90048 Santa Monica - Second St
20	P0705	Whittier Narrows 1987/10/01 14:42	6	30.1	B	90090 Villa Park - Serrano Av
21	P0328	Coalinga 1983/05/02 23:42	6.4	43.9	C	36410 Parkfield - Cholame 3W
22	P0340	Coalinga 1983/05/02 23:42	6.4	31	C	36431 Parkfield - Fault Zone 7
23	P0367	Coalinga 1983/05/02 23:42	6.4	41	C	36441 Parkfield - Vineyard Cany 6W
24	P0152	Coyote Lake 1979/08/06 17:05	5.7	31.2	C	57191 Halls Valley
25	P0217	Livermore 1980/01/24 19:00	5.8	37.7	C	57063 Tracy - Sewage Treatm Plant
26	P0535	N. Palm Springs 1986/07/08 09:20	6	32	C	12204 San Jacinto - Soboba
27	P0667	Whittier Narrows 1987/10/01 14:42	6	30.8	C	90009 N Hollywood - Coldwater Can
28	P0689	Whittier Narrows 1987/10/01 14:42	6	37.7	C	90044 Rancho Palos Verdes - Luconia
29	P0549	Chalfant Valley 1986/07/21 14:42	6.2	44.9	D	54099 Convict Creek
30	P0551	Chalfant Valley 1986/07/21 14:42	6.2	37.2	D	54100 Benton
31	P0324	Coalinga 1983/05/02 23:42	6.4	41.6	D	36452 Parkfield - Cholame 1E
32	P0337	Coalinga 1983/05/02 23:42	6.4	36.4	D	36408 Parkfield - Fault Zone 3
33	P0189	Imperial Valley 1979/10/15 23:16	6.5	31.7	D	5052 Plaster City
34	P0447	Morgan Hill 1984/04/24 21:15	6.2	32.5	D	1028 Hollister City Hall
35	P0455	Morgan Hill 1984/04/24 21:15	6.2	30.3	D	1377 San Juan Bautista
36	P0512	N. Palm Springs 1986/07/08 09:20	6	43.3	D	12331 Hemet Fire Station
37	P0527	N. Palm Springs 1986/07/08 09:20	6	38.2	D	22T13 Landers Fire Station
38	P0539	N. Palm Springs 1986/07/08 09:20	6	44.4	D	5038 Sunnymead
39	P0599	Whittier Narrows 1987/10/01 14:42	6	38.9	D	24087 Arleta - Nordhoff Fire Sta
40	P0623	Whittier Narrows 1987/10/01 14:42	6	35	D	90002 Fountain Valley - Euclid

Table A.5. Ground motion records in Bin 5 (PEER NGA Database 1999)

#	Record ID	Earthquake	M	R	GM	Station
1	P0806	Cape Mendocino 1992/04/25 18:06	7.1	8.5	A	89005 Cape Mendocino
2	P0873	Landers 1992/06/28 11:58	7.3	1.1	A	24 Lucerne
3	P0733	Loma Prieta 1989/10/18 00:05	6.9	11.2	A	47379 Gilroy Array #1
4	P0760	Loma Prieta 1989/10/18 00:05	6.9	10.3	A	13 BRAN
5	P0770	Loma Prieta 1989/10/18 00:05	6.9	6.1	A	16 LGPC
6	P0449	Morgan Hill 1984/04/24 21:15	6.2	0.1	A	57217 Coyote Lake Dam (SW Abut)
7	P0995	Northridge 1994/01/17 12:31	6.7	8	A	24207 Pacoima Dam (downstr)
8	P0996	Northridge 1994/01/17 12:31	6.7	8	A	24207 Pacoima Dam (upper left)
9	P0034	Parkfield 1966/06/28 04:26	6.1	9.9	A	1438 Temblor pre-1969
10	P0691	Whittier Narrows 1987/10/01 14:42	6	9	A	90019 San Gabriel - E Grand Av
11	P1043	Kobe 1995/01/16 20:46	6.9	0.6	B	0 KJMA
12	P0745	Loma Prieta 1989/10/18 00:05	6.9	5.1	B	57007 Corralitos
13	P0764	Loma Prieta 1989/10/18 00:05	6.9	11.6	B	47006 Gilroy - Gavilan Coll.
14	P0453	Morgan Hill 1984/04/24 21:15	6.2	11.8	B	57383 Gilroy Array #6
15	P0928	Northridge 1994/01/17 12:31	6.7	8.2	B	24088 Pacoima Kagel Canyon
16	P1021	Northridge 1994/01/17 12:31	6.7	14.6	B	90055 Simi Valley - Katherine Rd
17	P0032	Parkfield 1966/06/28 04:26	6.1	9.2	B	1015 Cholame #8
18	P0082	San Fernando 1971/02/09 14:00	6.6	2.8	B	279 Pacoima Dam
19	P0624	Whittier Narrows 1987/10/01 14:42	6	12.1	B	709 Garvey Res. - Control Bldg
20	P0706	Whittier Narrows 1987/10/01 14:42	6	10.5	B	90071 West Covina - S Orange
21	P0190	Imperial Valley 1979/10/15 23:16	6.5	11.1	C	6619 SAHOP Casa Flores
22	P0816	Landers 1992/06/28 11:58	7.3	11.6	C	22170 Joshua Tree
23	P0744	Loma Prieta 1989/10/18 00:05	6.9	4.5	C	47125 Capitola
24	P0454	Morgan Hill 1984/04/24 21:15	6.2	3.4	C	57191 Halls Valley
25	P0528	N. Palm Springs 1986/07/08 09:20	6	10.1	C	5071 Morongo Valley
26	P0541	N. Palm Springs 1986/07/08 09:20	6	7.3	C	5072 Whitewater Trout Farm
27	P0988	Northridge 1994/01/17 12:31	6.7	14.6	C	90009 N. Hollywood - Coldwater Can
28	P1005	Northridge 1994/01/17 12:31	6.7	7.1	C	77 Rinaldi Receiving Sta
29	P0636	Whittier Narrows 1987/10/01 14:42	6	11.4	C	90033 LA - Cypress Ave
30	P0648	Whittier Narrows 1987/10/01 14:42	6	13.5	C	90074 La Habra - Briarcliff
31	P0809	Cape Mendocino 1992/04/25 18:06	7.1	9.5	D	89156 Petrolia
32	P0553	Chalfant Valley 1986/07/21 14:42	6.2	9.2	D	54171 Bishop - LADWP South St
33	P0368	Coalinga 1983/05/02 23:42	6.4	8.5	D	1162 Pleasant Valley P.P. - bldg
34	P0006	Imperial Valley 1940/05/19 04:37	7	8.3	D	117 El Centro Array #9
35	P0160	Imperial Valley 1979/10/15 23:16	6.5	12.9	D	6618 Agrarias
36	P0736	Loma Prieta 1989/10/18 00:05	6.9	14.4	D	47381 Gilroy Array #3
37	P0451	Morgan Hill 1984/04/24 21:15	6.2	14.2	D	47381 Gilroy Array #3
38	P0452	Morgan Hill 1984/04/24 21:15	6.2	12.8	D	57382 Gilroy Array #4
39	P0530	N. Palm Springs 1986/07/08 09:20	6	8.2	D	5070 North Palm Springs
40	P0893	Northridge 1994/01/17 12:31	6.7	13	D	90057 Canyon Country - W Lost Cany